ANL--81-82

DE83 000921

Distribution Category:
Nuclear Waste Management
(UC-70)

ANL-81-82

ARGONNE NATIONAL LABORATORY
9700 South Cass Avenue
Argonne, Illinois 60439

FUEL CYCLE PROGRAMS
QUARTERLY PROGRESS REPORT

July-September 1981

by

M. J. Steindler, J. K. Bates, D. L. Bowers, R. E. Brock,
T. F. Cannon, D. L. Castelli, G. L. Chapman, R. A. Couture,
P. G. Deeken, J. E. Fagan, T. J. Gerding, D. G. Graczyk, R. R. Heinrich,
L. J. Jardine, R. W. Kessie, J. E. Kincinas, V. M. Kolba,
E. T. Kucera, Henry Lautermilch, N. M. Levitz, R. L. Malewicki,
W. J. Mecham, R. J. Meyer, R. E. Nelson, J. E. Parks, G. T. Reedy,
M. G. Seitz, L. E. Trevorrow, G. F. Vandegrift, Seymour Vogler,
C. G. Wach, and I. O. Winsch

Chemical Engineering Division

May 1982

Previous reports in this series

ANL-81-53	April-June 1981
ANL-81-35	January-March 1981
ANL-81-13	October-December 1980
ANL-80-114	July-September 1980

TABLE OF CONTENTS

TABLE OF CONTENTS (contd)

TABLE OF CONTENTS (contd)

LIST OF FIGURES

LIST OF FIGURES (contd)

LIST OF FIGURES (contd)

LIST OF TABLES

LIST OF TABLES (contd)

LIST OF TABLES (contd)

FUEL CYCLE PROGRAMS
QUARTERLY PROGRESS REPORT

July-September 1981

by

M. J. Steindler, J. K. Bates, D. L. Bowers, R. E. Brock,
T. F. Cannon, D. L. Castelli, G. L. Chapman, R. A. Couture,
P. G. Deeken, J. E. Fagan, T. J. Gerding, D. G. Graczyk, R. R. Heinrich,
L. J. Jardine, R. W. Kessie, J. E. Kincinas, V. M. Kolba,
E. T. Kucera, Henry Lautermilch, N. M. Levitz, R. L. Malewicki,
W. J. Mecham, R. J. Meyer, R. E. Nelson, J. E. Parks, G. T. Reedy,
M. G. Seitz, L. E. Trevorrow, G. F. Vandegrift, Seymour Vogler,
C. G. Wach, and I. O. Winsch

ABSTRACT

A program continues for the development of an interim waste form capable of being transported from facilities where waste is generated to terminal waste processing. Work on processes for converting high-level liquid waste to solids included the preparation of $NaNO_3/NaNO_2$ salt monoliths, phosphate-immobilized product, and silicate-agglomerated Fe_2O_3 pellets.

In experiments to measure the relative resistance to dissolution/disintegration, rates of dissolution (i.e., penetration rates) of various interim waste forms (pellets) in quiescent water were measured, and the pellets were found to be exceptionally stable.

A method of measuring rates of leaching from simulated waste glasses using radioactive spiking has been demonstrated. Leaching tests of glass samples irradiated with 3.5-MeV $^4He^{2+}$ ions indicated that the leach rates of irradiated samples were as little as one-fourth of the leach rates of nonirradiated glass leached under the same conditions.

Laboratory-scale impact tests of solid alternative waste forms are being performed to measure the BET surface areas of the fragments. From this, dispersion from mechanical impacts during normal and accidental conditions of transport can be determined. The surface areas increased smoothly with increasing impact energy. The probable accuracy of BET measurements was estimated to be about 10 to 30% on the basis of measurements of uniform glass microsphere samples having 0.1-0.3 m^2 total surface area. The precision of BET measurements of glass materials and ZnO was determined to be ±2% to ±6%.

A review of the methodology under development for the characterization of the impact behavior of brittle materials included the following topics: correlation of the values of several parameters obtained in standard impact tests on Pyrex and SRL 131 glass with energy densities, comparison of lognormal parameters for fragments of SRL 131 glass obtained by six measurement methods, and comparison of the effects on lognormal parameters of axial vs. diametral impact of 25-mm-OD x 25-mm specimens.

Logging techniques are being developed to measure the relative amount of residual oil in a depleted oil reservoir by injecting gamma-active solution into it. Some laboratory-scale experiments were completed that showed a 30% variation in gamma signal for oil-containing and oil-free rock cores.

In work to test the performance of proposed nuclear-waste repositories using laboratory-analog experiments, rock cores were obtained from basalt blocks, the engineered barrier material was tested for flow and leach properties, and laboratory treatments proposed for "aging" of repository components for use in the experiments.

The flow of groundwater through igneous rocks is of considerable interest in connection with geologic storage of high-level radioactive waste. Saline water and oil have been found in granite cores from the Illinois Basin. High chloride concentrations in the granite imply that communication with an overlying bed of sandstone by advection and diffusion is limited.

Testing and development of equipment for the destructive analysis of full-length irradiated fuel rods from the LWBR is in progress. This work is in support of the LWBR Proof-of-Breeding Project.

SUMMARY

Development of Interim Waste Forms

Several possible interim waste forms have been studied. These include the formation of a salt monolith from sodium nitrate-sodium nitrite simulated waste solution typical of that from a nuclear fuel reprocessing plant. Another waste form is prepared by the reaction of calcined sludge (usually found in neutralized waste tanks) with sodium silicate. Preliminary unsuccessful experiments were also carried out to evaluate phosphate and borate matrices as interim waste forms.

Irradiation experiments (using ^{60}Co as the irradiating agent) were carried out with sodium nitrate and sodium nitrate-sodium nitrite mixtures. With nitrate but no nitrite present, oxygen was the only gas detected after irradiation. Whenever nitrite was present in the system, N_2 and N_2O were the products.

Silicate/sludge pellets containing up to 75% sludge were prepared by cold pressing and then curing the samples for 24 h in a 90% relative humidity atmosphere at 25°C. Those pellets prepared with SS-65 sodium silicate were exceptionally stable in quiescent water, showing little or no weight loss after a three-week exposure.

Because $FePO_4$ is reported to be a constituent of the sludge in the waste tank at the Western New York Nuclear Service Center, its stability in caustic-sodium nitrate solutions was examined. The reaction upon mixing of

NaOH solutions with solid $FePO_4 \cdot 2H_2O$ is almost instantaneous. Except at extremely high ratios of $FePO_4$ to aqueous hydroxide, the hydrolysis reaction either goes to completion or continues until the supply of hydroxide is exhausted.

Results of the few phosphate-immobilization experiments performed thus far on high- and low-sodium-content wastes lead to the conclusion that solutions with a high sodium content yield a more consistent, higher density interim waste form.

Attempts to immobilize synthetic waste in B_2O_3 in a manner analogous to the phosphate technique were unsuccessful.

Neutron Activation and Tracer Studies

The method of measuring leach rates using radiotracer spiking has been demonstrated for modified Savannah River Laboratory (SRL) glass frits 131 and 211. The results indicate that by proper choice of the amount of each radiotracer added to the glass, the leach rates of four elemental groups can be measured simultaneously. The groups and the associated radiotracers are the alkali metals (^{137}Cs), the alkaline earth metals (^{85}Sr, ^{133}Ba), the rare earth metals ($^{139,141}Ce$, ^{152}Eu), and the noble metals (^{106}Ru).

Leach testing of glass samples irradiated by the Materials Science Division (MSD/ANL) has been completed. These tests indicate that the leach rates of irradiated SRL 131 and SRL 211 glasses, together with those of PNL 76-68 glass, are decreased to as little as one-fourth of those of nonirradiated glass leached under the same conditions.

Leach tests were concluded on samples of hot-pressed SYNROC, and the results have been given to the Materials Science Division, ANL.

Experiments to produce weathered samples of waste glass are continuing.

Brittle Fracture Studies

Impact tests were performed on three sizes of laboratory-scale specimens of SRL 131 simulated waste, PNL 76-68 glasses, alkoxide waste glass, SYNROC B, and Pyrex, to measure the BET surface areas of the fragments. The surface areas increased smoothly with increasing impact energy. The surface-area curves for Pyrex and SRL 131 glasses bounded all other surface-area curves. The SRL 131 glass surface area increases were about 20-30% less than those of Pyrex over an eightfold energy test range. Modest differences in surface area increases were observed for different specimen sizes, indicating a minor dependence on specimen size.

Uniform glass microspheres (50.7 μm and 120 μm) were used as quasi-standards to estimate the probable accuracy of BET measurements of surface areas as being ±10% to ±30% for glass samples of 0.1 m^2 to about 3 m^2 total surface area. The precision of BET measurements was determined to be ±2% to ±6%, using glass materials and ZnO material; the precision measurements included comparisons with measurements of one off-site independent laboratory.

Optical microscope observations of about 100-μm SRL 131 glass fragments showed small fragments (smaller than 10 μm) that were readily attached to the large particles by some type of bonding mechanism during or after impact.

For three laboratory-scale specimen sizes, the two lognormal parameters, the increases in surface area, respirable fractions, and other parameters obtained from standard impact tests on Pyrex and SRL 131 simulated waste glasses have been summarized and have been correlated with energy density over the range, 1-100 J/cm^3. The geometric mean diameter, D_g, varied inversely with energy density; the standard deviation was nearly invariant. The amount of respirable-size particles was directly proportional to energy density. For both glasses, d, the dimensionless surface area/volume shape factor (derived from the two lognormal distribution parameters and the measured BET surface areas), was also found to be nearly invariant at about 20.

Samples of impact fragments of SRL 131 glass smaller than 90 μm were sent to five different laboratories for size analyses by five different methods. The plots reported of size distributions were straight lines or lognormal graphical coordinates. There were some variations in the size distributions. However, the particle size distributions determined by our standard method approximately corresponded to the mean distribution of the several methods. Our standard method combines Coulter counter data and sieving data and determines the values of the two lognormal parameters (D_g and σ_g), which characterized the size distribution completed. From this result, it is concluded that several standard methods of performing small-particle analysis are adequate for the characterization of fracture particulates.

Standard impact tests at an energy density of 10 J/cm^3 were used to compare diametral impacts with axial impact of 25-mm-OD by 25-mm specimens. The standard deviation of the lognormal distribution for axial impact was about 10 to 20% smaller than those for diametral impacts. This result is consistent with stresses being more uniformly distributed in axial impacts than in diametral impacts.

Impact tests of SYNROC B, SYNROC D, and SRL 131 glass were made at the very severe test conditions of 141 J/cm^3 used in Australia on approximately 13-mm-OD by approximately 13-mm specimens. The size distributions of fragments were lognormal. The respirable sizes measured in our tests agreed with those reported in Australia in which different analysis methods and types of SYNROC were used.

Rock-Water Interactions

Work in the program on nuclear logging of depleted oil reservoirs consisted of core flood-experiments to test the possibility of logging an oil reservoir by the use of gamma-active fluid. The experiments indicate that the gamma signals from cores injected with radioactive solution varied by up to 36%, depending on the presence or absence of oil in the cores. This signal is substantial, but whether it is sufficient to overcome uncertainties inherent in field operations remains to be explored.

Work was also performed on the Laboratory Analog program. This work included the cutting of cores from blocks of Pomona basalt, the testing of bentonite clay for leachable constituents, and the choosing of laboratory procedures to "age" components of a nuclear waste repository. Procedures were selected to give one aged state for each material (waste form, engineered barrier rock) out of a myriad of possible aged states.

Trace-Element Transport in Lithic Material by Fluid Flow

Pore fluids in granite and sandstone from Northern Illinois drill hole UPH-3 have been sampled by displacement ("elution") and by washing of crushed rock with water and with benzene. Both saline water and oil are present.

The salinity is low in sandstone and just below the contact with granite but increases downward. The chloride concentration increases to 0.1M in a fracture zone 6 m below the contact, and reaches 2.4M in a lower fracture zone, 664 m below the contact.

Paraffin-base oil is present in the sandstone and to depths of at least 516 m below the contact. In unfractured granite at 176 m below the contact, oil occupies most of the pore space.

The oil and brine are believed to be derived from the overlying sediments.

The high chloride concentrations in the granite imply that communication with the sandstone by advection and diffusion is limited. The lower salinity at higher levels of the granite is not necessarily due to advection, but may be due to diffusion.

Light Water Breeder Reactor Proof-of-Breeding Analytical Support Project

This Project is responsible for the destructive analysis of full-length irradiated fuel rods from the LWBR. The results will be used by the Bettis Atomic Power Laboratory (BAPL) in support of their nondestructive assay of the end-of-life (EOL) core to determine the extent of breeding.

Activity is reported on four main subactivities of this Project: (1) the full-scale shear (FSS), (2) the single-unit or prototype dissolver (SUD), (3) multiple dissolvers needed for the destructive analyses of full-length (about 3-m) irradiated fuel rods for the EOL campaign, and (4) scrap/waste disposal. In addition, current work in support of this Project by the Analytical Section is being done in the areas of planning and procurement. Development of an integrated computer/data acquisition system for the entire Project is also in progress.

I. DEVELOPMENT OF INTERIM HIGH-LEVEL WASTE FORMS

(Seymour Vogler, G. F. Vandegrift, E. T. Kucera,* T. J. Gerding, G. Bandyopadhyay,† D. Castelli,* I. M. Galvin,† J. E. Slattery,† and R. B. Poeppel†)

A. Introduction

High-level liquid radioactive wastes (HLLW) are often produced at facilities where terminal processing of the waste is not practical because of the high cost or hazards of such an operation. Under these circumstances, the waste could be incorporated into a interim solid waste form for shipping to a processing site and conversion to a terminal waste form. The interim form should be prepared by simple processing methods so that extensive additional facilities will not be required at the originating site. Additionally, the interim waste form must satisfy shipping criteria, particularly in relation to transportation accidents; should be mechanically and chemically stable in the ambient environment; and should be readily compatible with the terminal-waste-form processes. From this research, a technology should evolve for preparing interim waste forms compatible with transportation requirements and with subsequent terminal waste form processing.

Support for this program was terminated at the end of fiscal year 1981. The experimental effort to date is summarized in this report. Some of the information presented may not be as complete as desired.

The information to date indicates that interim waste forms can be prepared from neutralized high-level wastes consisting of two phases, a concentrated sodium nitrate solution and a precipitated oxide such as that stored in the waste tank at the Western New York Service Center. In one instance, a portion of the total waste (salt plus sludge) is heated to a high-enough temperature to remove the water, yielding a molten salt with dispersed sludge. Upon cooling, the solidified salt is the waste form. In a second case, separated sludge can be calcined and agglomerated with sodium silicate to form a suitable interim waste form.

Phosphate and borate matrices were also examined to determine their suitability as interim waste forms. Acceptable phosphate interim waste forms have been prepared using a single preparative technique. Undoubtedly, there are other preparative techniques that require examination. Borates were difficult to prepare and are subject to phase separation when prepared with mixtures of cations of differing charge and coordination number.

---

*Member of the Analytical Chemistry Laboratory, Chemical Engineering Division.

†Member of the Materials Science Division, Argonne National Laboratory.

B. Experimental Results

(Seymour Vogler, G. F. Vandegrift, T. J. Gerding, E. T. Kucera,* and D. L. Castelli*)

1. Fused Salts

a. Radiation Results

(T. J. Gerding)

(1) Introduction

One technique for isolating the high-level liquid waste stored at the Western New York Service Center yields a salt monolith consisting of sodium nitrate and sodium nitrite. The solidified waste would be stored for some time in sealed canisters before being converted to a final form. Radiation levels associated with the interim solid, and the existing information on the radiolytic decomposition of nitrates to form nitrites and oxygen, suggested that additional experiments be performed to estimate the quantity of gases produced in this system by self-irradiation. Pressure buildup from this process, if excessive, is a potential path by which containers might be breached.

Previous work dealing with the irradiation of solid inorganic nitrates [JOHNSON] indicates that nitrite and oxygen are the stable products of this reaction and that nitrite concentration is often used to measure the reactivity of the system. The stoichiometry of the room temperature radiolytic decomposition can be represented by

$$NaNO_3 \longrightarrow NaNO_2 + 1/2\ O_2$$

For this reaction carried out at room temperature using cobalt-60 gammas as the energy source, $G(NO_2^-)$ values of 0.20 to 0.27 are given in the literature [CUNNINGHAM, HOCHANADEL].

The addition of certain materials to the nitrate system is reported to increase the decomposition rate, at least during the initial radiation exposure. For example, upon exposure to radiation, initial decomposition rates of nitrate in a mixture of potassium bromide and potassium nitrate in pellet form are higher than in potassium nitrate by itself [JONES]. However, after a dose of about 10^{21} eV/g was absorbed, enhanced energy transfer was no longer observed. The same effect was observed when low concentrations of calcium ion (0.1 to 0.2 mol % Ca^{2+}) were present in the sodium nitrate system [KAUCIC]. The addition of Ca^{2+} is reported to increase the initial $G(NO_2^-)$ approximately 50%; the $G(NO_2^-)$ value reaches a maximum and then becomes constant.

In addition to the nitrite ion formed by gamma irradiation of the inorganic nitrate solid, gas phase analyses (generally mass spectrometry) show oxygen to be the only gaseous species present. Efforts to find nitrogen and oxides of nitrogen in the gas phase have been unsuccessful.

---

*Member of the Analytical Chemistry Laboratory, Chemical Engineering Division.

The nitrite product is described as being very stable; no decomposition of nitrite ion occurs during irradiation of nitrate [JOHNSON, TINGEY].

(2) Experimental Procedure

The salt mixture presented in Table 1 was used to simulate NFS (Nuclear Fuel Services, Inc.) solid waste. The salt mixture is principally $NaNO_3/NaNO_2$ (85 wt %), with the balance being sulfate, hydroxide, phosphate, and various metal oxides to represent fission products and fuel hardware materials. No actinides are included in this mixture.

Table 1. Simulated NFS Fused Salt/Sludge Composition Used for Gamma-Irradiation Studies

Constituent	Weight, g	Constituent	Weight, g
$NaNO_3$	59.09	NiO	0.10
$NaNO_2$	25.09	Nd_2O_3	0.10
Na_2SO_4	6.98	MnO_2	0.20
NaOH	1.29	SrO	0.04
KCl	0.23	RuO_2	0.04
Fe_2O_3	4.51	ZrO_2	0.11
CrO_3	0.41	$Na_3PO_4 \cdot 12H_2O$[a]	6.77

[a] It appeared that the water of hydration was boiled away when the mixture was heated to 275°C in a dry box.

The salt mixture was prepared by melting the salts in a high-purity alumina crucible in an inert dry environment. Two similar salt mixes were prepared, one with $NaNO_3$ absent and the other with $NaNO_2$ absent. Also included in these experiments was a melt consisting of $NaNO_3$ (68 wt %) and $NaNO_2$ (32 wt %).

Pyrex tubes with break seals were used for sample containment. Crushed salt samples (1-3 g) were heated under vacuum and cooled; then argon cover gas was added prior to flame-sealing of the tubes. The break seal provided access to the sample for subsequent analytical work. Samples were irradiated to a total dose of 4.89×10^8 rad using a ^{60}Co source. Dosimetry was done with cobalt glass.

Mass spectrometric methods were used to determine gas phase composition. For gas analysis, the samples were melted in order to separate gaseous material from the solids. A conventional colorimetric determination of nitrite was done by a modified Shinn [SHINN] procedure.

(3) Experimental Results and Discussion

The $G(NO_2^-)$ for $NaNO_3$ is well established in the literature; therefore, samples of $NaNO_3$ were irradiated to provide a check on the anticipated performance of the total system. The value for $G(NO_2^-)$ was 0.2 in these $NaNO_3$ irradiation experiments, in good agreement with literature values. The results of the oxygen analyses yielded $G(O_2)$ values that were consistently low, and the data were scattered extensively. The lack of reproducibility of the data precludes making quantitative statements regarding gas yields. The quantities of gas produced in these tests ranged from 0.5 to 50 μmol; however, most yields were in the range, 5 to 25 μmol.

Gas products of the reactions were identified, and a brief summary of the results for the various experiments is presented below. The $NaNO_3$ test was done in triplicate; the others represent the results of duplicate experiments.

$NaNO_3$--Irradiation of pure, dry sodium nitrate with an argon cover gas yielded O_2 gas only. This is in agreement with other studies.

$NaNO_3 + NaNO_2$--Irradiation of dry $NaNO_3$-$NaNO_2$ with an argon cover gas produced N_2 and N_2O; no O_2 gas was detected.

$NaNO_3$ + sludge simulates (SS)--Irradiation of dry $NaNO_3$ and SS with an argon cover gas produced O_2 gas only.

$NaNO_2$ + SS--Irradiation of dry $NaNO_2$ and SS with an argon cover gas produced N_2 and N_2O; no oxygen gas was present.

$NaNO_3 + NaNO_2$ + SS--Irradiation of this dry mix with an argon cover gas produced N_2 and N_2O; again, no O_2 gas was found.

$NaNO_3 + NaNO_2$ + SS--Irradiation of an identical mix, but with a cover gas of 25 vol % O_2-Ar, yielded N_2 and N_2O products, accompanied by complete depletion of the O_2.

The irradiation of pure $NaNO_3$ or $NaNO_3$ mixed with several metal oxides produced a gas phase that contained only oxygen. This was expected and agrees with similar studies. The gamma irradiation of samples containing $NaNO_3$ and $NaNO_2$, with and without other metal oxides present, yielded N_2 and N_2O. The same products were formed when oxygen was added to the cover gas. Nitrogen and N_2O were produced by irradiating $NaNO_2$ mixed with several metal oxides. These experiments showed that whenever NO_2^- was present in the system, the gas formed from gamma irradiation was a mix of N_2 and N_2O; in no experiment with N_2 and N_2O products was oxygen present.

(4) Differential Thermal Analysis Studies on Irradiated Salts

(G. F. Vandegrift and D. L. Castelli*)

We were concerned that during the sample melting step in the analytical technique for measuring gaseous decomposition products from gamma irradiation, there might be decomposition of the simulated NFS fused

*Member of the Analytical Chemistry Laboratory, Chemical Engineering Division.

salt form. We examined this potential problem by performing simultaneous differential thermal analysis (DTA) and thermal gravimetric analysis (TGA) on samples of fused salt with and without sludge prior to and following ^{60}Co gamma-irradiation. The samples were heated to 400°C, then cooled to 150°C at the rate of 5°C/min. This temperature profile was repeated over several cycles. During these experiments, the endothermic melting of the sample was monitored by DTA, as was the freezing curve. The melting curve was a nondescript, broad hump; the freezing curve on the recording chart showed a fine structure of multiple peaks in the freezing range. The freezing curve of the simulated NFS fused salt/sludge composition described in Table 1 and the $NaNO_3/NaNO_2$ curves had one extremely sharp peak near the initiation of freezing and trailed off to a group of minor peaks at lower temperatures.

Table 2 is a compilation of the DTA data for the four samples tested. These results and the TGA results, which show that none of the four samples lost weight during temperature cycling, lead to the conclusion that no thermal decomposition occurred during the melting of these samples. For samples of each material, the differences in the five temperature points observed after a temperature cycle (Table 2) are all within measurement error. Although the differences in melting and freezing points of irradiated and nonirradiated samples may be significant, they most likely are the result of sampling variation.

Table 2. Differential Thermal Analysis Data Obtained by Cycling the Material from 150 to 400°C

	Melting Point, °C		Freezing Peak, °C		
Material	Initiated	Finished	Initiated	Maximum Peak Height	Finished
Nonirradiated	224	258	250	246	206
70 wt % $NaNO_3$	223	259	248	245	205
30 wt % $NaNO_2$					
Irradiated	228	268	260	258	218
$NaNO_3/NaNO_2$	226	269	260	259	218
	227	268	260	259	218
Nonirradiated	219	254	243	241	199
70 wt % $NaNO_3$	215	255	245	241	198
30 wt % $NaNO_2$	214	254	245	240	199
+ sludge components					
Irradiated	221	257	243	242	203
$NaNO_3/NaNO_2$	221	255	244	243	203
+ sludge	222	257	245	243	204
components					

Contrary to these results are the results obtained on a sample of 20 wt % simulated NFS sludge/fused salt prepared by members of ANL Materials Science Division (MSD); the composition of the simulated sludge used in this preparation was reported earlier [STEINDLER-1980]. The differences in this preparation compared to the Chemical Engineering Division preparation were: (1) $FePO_4 \cdot 2H_2O$ was used in conjunction with Fe_2O_3 to produce the necessary iron content and (2) Cr_2O_3 was used instead of CrO_3 to produce the necessary chromium content.

Figure 1 shows the dramatic effect of cycling the MSD sample between 150 and 400°C. Although the loss in weight tended to subside after the eighth cycle, the changes in the freezing curve did not. The fairly narrow melting range of the first cycle (9°C) had expanded to 72°C by the 15th cycle. Because this sludge/salt had been stored for six months in the atmosphere, these changes in melting range may be attributable to water loss during this heat treatment. There is also a possibility that the melt composition changed due to the reaction:

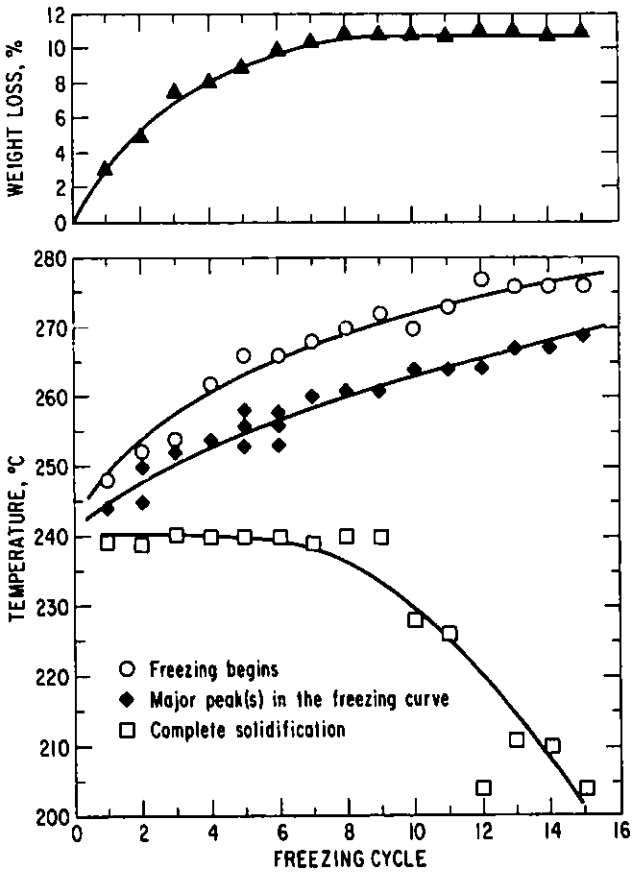

Fig. 1. Freezing Behavior of Materials Science Division Sample during Fifteen Freezing and Melting Cycles

$$2FePO_4 + 6NaOH \rightleftharpoons Fe_2O_3 + 2Na_3PO_4 + 3H_2O$$

or perhaps due to the slow dissolution of sludge components (e.g., SrO) in the salt melt.

b. Solubility of Sludge Components in the Nitrate/Nitrite Melt
(G. F. Vandegrift, E. T. Kucera,* and T. J. Gerding)

One potential problem of a fused salt interim waste form is that it is not homogeneous; another is its low melting point (220-260°C). If the fused salt should become molten, those fission product hydroxides/oxides not solubilized in the melt and having a density greater than that of the salt would drop to the bottom of the canister and form a hot spot. Since the density of molten $NaNO_3/NaNO_2$ in the canister would be between 1.9 and 1.7 g/cm^3 and the density of strontium salts is in the range of 3.0-3.7 g/cm^3, this situation is of real concern This same problem could arise during the original casting of the salt, necessitating positive steps to ensure that there is a homogeneous slurry at the time of solidification.

The following measurements were made to gain some indication of the solubility of some of the sludge components in the $NaNO_3/NaNO_2$ fused salt. The composition of the sodium nitrate, sodium nitrite/sludge mixture is given in Table 1. This composition differs in at least two important respects from the fused salt/sludge composition reported earlier [STEINDLER-1980]. CrO_3 was used as a source of chromium instead of Cr_2O_3 and phosphate was added as the sodium salt, while all iron was added as Fe_2O_3.

The mixture given in Table 1 was heated to approximately 275°C in a dry box and then poured, as it was swirled, onto a glass slab where it solidified. A part of that material was ground and analyzed by energy dispersive X-ray fluorescence spectroscopy (EDXRF). Part of the remaining material was again heated to about 275°C for 19 h. After this heating period, the molten salt was decanted from the solid constituents, cooled, ground, and analyzed by EDXRF as previously. Table 3 shows the comparable concentrations of some elements in the sludge plus fused salt and in the molten salt alone. Because only one sample of each was tested and the sample of fused salt may not have been completely representative, it is best merely to view a large percentage of dissolved material as indicating high solubility in the salt for that constituent and a low percentage as indicating little solubility.

2. Phosphate Immobilization
(G. F. Vandegrift and T. J. Gerding)

HLLW converted to a phosphate solid appears to be an attractive interim waste form. Phosphate, pyrophosphate, and metaphosphate ions form strong bonds with most metal ions, and their salts with multivalent metal cations have low aqueous solubilities. (Phosphate and acid phosphate cements, used as dental cements, have low leachability and high compressive strengths.) Two more experiments were performed to prepare a phosphate-immobilized product from a nitric acid solution of simulated Purex waste (its composition was described previously [STEINDLER-1981A]).

---

*Member of the Analytical Chemistry Laboratory, Chemical Engineering Division.

Table 3. Percentages of Elements in the Sludge/Fused Salt Mixture (Table 1) Dissolved in the $NaNO_3/NaNO_2$ Fused Salt

Element	Sludge + Salt, cps	In Molten Salt after 19-h Heating,[a] cps	% Dissolved in Salt
Cr	71.7	65.4	91
Fe	1655	20.3	1
Zr	63.9	0	0
Ni	32.2	2.6	8
K	4.2	3.3	79
Sr	45.3	2.7	5
S	6.2	4.5	72

[a]Measured count rate was multiplied by the factor 96.05/100.97, which is the weight ratio of salt-soluble species to total sludge plus salt soluble species.

The first experiment was a replicate of one reported earlier [STEINDLER-1981A], where twice the amount of phosphoric acid needed to neutralize all metal cations as PO_4^{3-} was added to the simulated acid waste solution. In the previous experiment, the temperature was allowed to rise above 400°C. After it became impossible to stir the material (about 160°C), continued heating turned the material in the pot into a low-density spongy mass. In the repeat experiment, heating was stopped when stirring became impossible. The translucent white-green product was more like stiff taffy than glass; it would dent with pressure but pieces could also be cracked away from the bulk; its density was 1.73 g/cm^3.

In the second experiment, the ratio of phosphoric acid to acidic metal solution was increased so that 3.5 times the metal cationic equivalent was neutralized as PO_4^{3-}. This mixture was heated and the distillate was separated until a pot temperature of 400°C was reached. The material cooled to a hard glassy material that was extremely hygroscopic; sitting overnight in contact with the atmosphere turned this product into a viscous liquid.

The few experiments performed thus far on high- and low-sodium-content wastes lead to the conclusion that solutions with a high sodium content yield a more-consistent, higher-density interim waste form. A large excess of phosphoric acid does provide the chance to prepare a glassy, high-density, homogeneous product from low-sodium-content wastes, but unfortunately one that is extremely hygroscopic.

3. Preparation of a Borate-Immobilized Interim Waste Form
(G. F. Vandegrift and T. J. Gerding)

Two experiments were performed this quarter to test boric anhydride as a reagent for solidifying HLLW. One experiment was performed to test the capability of B_2O_3 to immobilize simulated NFS waste (salt plus sludge), the

other to test its ability to solidify the acid waste solution. The compositions of simulated-NFS waste and the acid waste solution were described previously [STEINDLER-1980]. The equipment, basically a stirred reaction kettle, distillation apparatus, was also described previously [STEINDLER-1981A].

The attempt to immobilize simulated NFS waste (Table 1) under the same conditions as were used for immobilization with H_3PO_4 was a complete failure. As the amount of solid boric anhydride needed to balance 300% of the cationic charge as BO_3^{3-} was slowly added to the kettle, nitrogen oxides began to evolve due to decomposition of nitrous acid. An extremely stable foam formed during gas evolution. As gas evolution increased during heating of the reaction kettle, so did foam formation. In less than one minute, the foam completely filled the reaction kettle, the Vigreux column, the water-cooled condenser, and receiving vessel before it forced the glass stoppers out of the top of the reaction kettle and oozed out of the kettle to be caught in the porcelain pan below. This foam was very rigid and did not break by mechanical means. The addition of water enhanced its ability to flow but did not change the rigidity of the foam.

Two hundred milliliters of suspension became perhaps 2000 mL of rigid foam. Such a situation, even if predictable, would be untenable in a remote operation and, therefore, is not acceptable for immobilizing NFS waste.

In the second experiment, there was no problem when B_2O_3 was added to the acid waste solution; no nitrous acid was present to decompose. Enough boric anhydride was added to balance 300% of the cationic charge as BO_3^{3-}. The distillation went very smoothly, but it appeared that most of the excess B_2O_3 distilled away as HBO_2. There were white crystals on the sides and top of the reaction vessel and on other parts of the apparatus. The product was not homogeneous, was not glassy, and showed a larger degree of disintegration in water. It is thus not an acceptable product.

4. Rates of Disintegration/Dissolution of Candidate Interim Waste Forms for NFS Waste
(G. F. Vandegrift and T. J. Gerding)

Experiments designed to measure the relative resistance to dissolution/disintegration of candidate interim waste forms in stagnant water were continued. Samples studied were several specimens of (1) simulated fused salt containing 10 and 20 wt % sludge and (2) silicate-agglomerated calcine pellets of various compositions. Results of previous studies and an experimental procedure were reported last quarter [STEINDLER-1981B].

Dissolution/disintegration rate experiments were performed on pellets (fused salt containing 10 and 20 wt % of a simulated sludge) that were prepared several months previously by members of MSD. The results of this study were not as satisfactory as results of earlier studies [STEINDLER-1981B]. Figure 2 compares the rates of dissolution/disintegration of the current measurements with the rates obtained previously for samples prepared at CEN and consisting of fused salt samples with and without simulated sludge. The CEN data showed a convincing linear correlation of the dissolution/disintegration rate with the initial surface area not only for the sample for the fused salt samples prepared here, but also for five other materials.

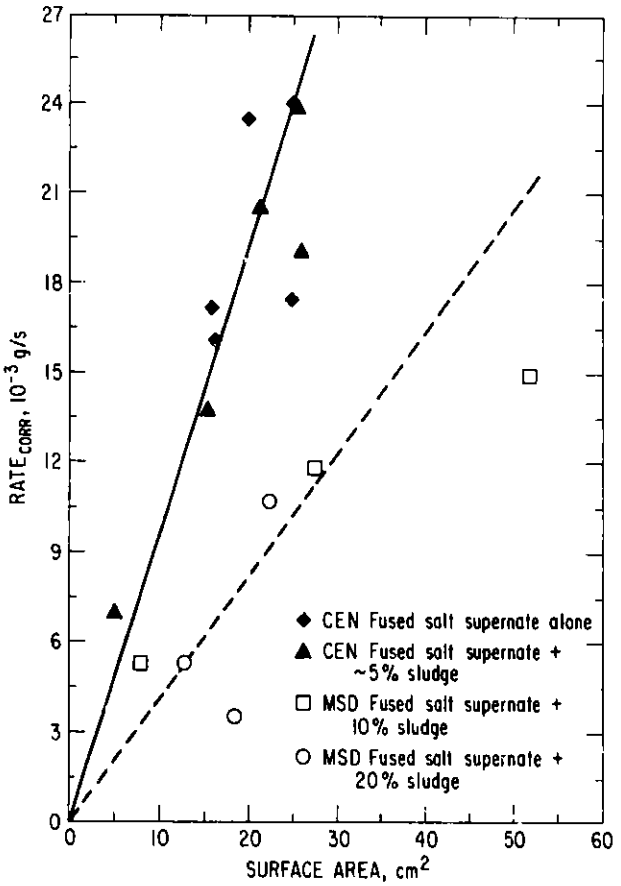

Fig. 2. Dissolution/Disintegration Rates vs. Surface Area for NFS Simulated Waste Fused Salt

For the MSD results, this correlation is far from convincing. Examination of the data in Table 4 shows a large scatter for the measured density (a reflection of the lack of homogeneity of the MSD-prepared material). For CEN samples of similar material, the measured densities of the various samples agreed within 2% in all cases. The MSD samples obviously dissolve more slowly than the CEN samples do (Fig. 2). This difference may be due to the long standing times of the MSD samples in ambient conditions and/or to a difference in composition of the CEN and MSD fused salts. Although these differences are real, insufficient time remains to resolve the issue.

The dissolution/disintegration rates in quiescent water of two other silicate-agglomerated Fe_2O_3 pellets prepared by MSD were measured. These two pellets, prepared as described previously [STEINDLER-1980], were composed of 2/1 and 6/1 weight ratios of SS-65 to Fe_2O_3. (SS-65 is a silicate powder with a 3.22 weight ratio of SiO_2/Na_2O.) The SS-65 agglomerated pellets were even more resistant to water attack than the SS-C pellets studied earlier. (SS-C is a 2/1 weight ratio of SiO_2/Na_2O silicate powder.) The induction period of initial weight gain was two hours for these materials, compared with 20 min for the SS-C pellets. The results of these experiments and, for comparison, those reported previously on SS-C samples are presented in Table 5. The SS-65 pellets were more resistant to attack by water, as might be expected because of their higher silicon content.

Table 4. Results of Dissolution/Disintegration Experiments on MSD-Prepared Fused Salt/Simulated Sludge Samples

Sludge Content, %	ρ, g/cm^3	Dissolution Rate, g/s	Initial Area, cm^2	Rate Constant	
				g/cm^2-s	cm/s
10	2.13	5.24×10^{-3}	8.0	6.6×10^{-4}	3.1×10^{-4}
	2.20	1.18×10^{-2}	27.4	4.3×10^{-4}	2.0×10^{-4}
	2.08	1.49×10^{-2}	52.1	2.9×10^{-4}	1.4×10^{-4}
20	2.34	5.29×10^{-3}	12.3	4.3×10^{-4}	1.8×10^{-4}
	1.88	3.53×10^{-3}	18.4	1.9×10^{-4}	1.0×10^{-4}
	2.17	1.07×10^{-2}	22.2	4.8×10^{-4}	2.2×10^{-4}
Avg	2.13	8.58×10^{-3}		4.1×10^{-4}	1.9×10^{-4}

Table 5. Rate of Dissolution/Disintegration of Silicate-Agglomerated Fe_2O_3 Pellets in Stagnant Water

Material	Density, g/cm^3	Rate Constant	
		g/cm^2-s	cm/s
SS-65/Fe_2O_3 6/1	2.49	4.8×10^{-7}	1.9×10^{-7}
SS-65/Fe_2O_3 2/1	2.50	7.9×10^{-6}	3.2×10^{-6}
SS-C/Fe_2O_3 6/1	2.48	1.6×10^{-5}	6.4×10^{-6}
SS-C/Fe_2O_3 2/1	2.48	5.3×10^{-5}	2.1×10^{-5}

The other simulated silicate-agglomerated calcine samples tested this quarter were all highly loaded with simulated sludge whose composition was reported previously [STEINDLER-1980]. These samples, prepared by a new technique, are called ambient-temperature silicate/sludge waste forms. Because of the high loading of insoluble material, our method of studying the dissolution/disintegration rate was ineffectual. A short description of that procedure is as follows: samples to be tested are placed in a wide-mesh stainless steel basket suspended by a Teflon cord from the bottom hook of a

top-loading balance. The basket is then suspended in 4000 mL of stagnant water. As soluble material dissolves, the insoluble portion falls away, through the basket, onto the bottom of the beaker. The weight loss is therefore a measure of loss of total sample; at completion, essentially no material is left in the basket.

When the fraction of soluble material is very small, its dissolution does not cause the insoluble component to become loose and fall out of the basket. Because of this, the rate of weight loss from these samples cannot be compared with that for samples with smaller fractions of solids. The compositions studied are given in the following paragraphs, along with comments on their behavior. When a salt was used in pellets, it was a mixture of $NaNO_3$, $NaNO_2$, Na_2SO_4, and KOH. These samples were produced by the ambient-temperature technique.

75% sludge/20% SS-C/5% $Ca(OH)_2$--An initial weight gain was followed by a slow weight loss over fifteen days. The sample was partially soft and crumbly after removal from the water.

75% sludge/20% SS-65/5% $Ca(OH)_2$--An initial weight gain was followed by an extremely small weight loss over twelve days. The sample showed no signs of crumbling to the touch after three weeks of immersion in water.

75% sludge/25% SS-65--The disintegration rate was too small to measure. After the pellet was in water three weeks, its surface was still hard and shiny.

70% sludge/5% salt/25% SS-C--A noticeable crack began to form in the pellet 5 h after contact with water. The pellet crumbled completely as it was removed from the basket five days later.

70% sludge/5% salt/25% SS-65--Flux lines were noticed near the bottom of the pellet during the first 15 min of contact with water, indicating dissolution of the salt component of the pellet. Three weeks later, the pellet's surface was still hard and shiny.

50% sludge/50% SS-C--A rate of disintegration/dissolution was measured for this sample but, for the reasons stated above, the measured value is far lower than it should be. Rate constant = 1×10^{-6} g/cm^2-s = 4×10^{-7} cm/s.

50% sludge/50% SS-65--In the same exposure interval that resulted in the disintegration of the SS-C sample (24 h), no signs of disintegration of this pellet were visible.

Two important bits of information that were discussed earlier [STEINDLER-1980, 1981A] are exemplified in these data: (1) pellets with high sludge loadings are more water-resistant than are pellets with low sludge loadings and (2) high-ratio SiO_2/Na_2O silicate powders (e.g., SS-65) are superior to low-ratio silicate powders (e.g., SS-C) as binders.

C. Stability of $FePO_4$

(G. F. Vandegrift and E. T. Kucera)

Literature references concerning the hydrolysis of ferric phosphate led us to question the validity of the estimates of $FePO_4$ (30 wt %) in West Valley sludge in Tank 8D2 [WNYNSCS, STEINDLER-1981A]. Because of this concern, we have studied the reaction of solid $FePO_4$ in contact with caustic-sodium nitrate solutions:

$$2FePO_{4(s)} + 6OH^-_{(aq)} + (m - 3)H_2O \rightleftharpoons Fe_2O_3 \cdot mH_2O + 2PO^{3-}_{4(aq)} \quad (1)$$

The extent of this reaction has been estimated by measuring the concentrations of iron and phosphorus dissolved in the aqueous phase and in the solid residue after contact. Energy dispersive X-ray fluorescence (EDXRF) was used to measure both elements in both phases.

The data from these experiments lead to the following conclusions.

- The reaction of NaOH solutions and solid $FePO_4 \cdot 2H_2O$ is almost instantaneous upon mixing.
- Except when there are extremely high ratios of $FePO_4$ to aqueous hydroxide, reaction 1 either goes to completion or continues until the supply of $FePO_4$ or $OH^-_{(aq)}$ is exhausted.
- Surface area, at least over the narrow range examined, had no significant effect on the rate or extent of reaction 1.

However, when high ratios of $FePO_4 \cdot 2H_2O$ to aqueous solution were used, less PO_4^{3-} was lost from the solid residue than would ordinarily be expected. This may only be an indication of the experimental error associated with measuring leachate phosphorus concentrations, but also could be explained by adsorption of Na_3PO_4 on the surface of $FePO_4$. Another explanation is that with a large excess of $FePO_4$, reaction 1 does not go to completion; rather, the first intermediate species, a mixed salt--$NaFe(PO_4)(OH)$, may be formed on the surface so that no hydroxide remains in solution to drive the reaction further.

In NFS Tank 8D2, the estimated ratio of solid $FePO_4$ in the sludge to supernate solution is 16.6 g/L of supernate [WNYNSCS]. In terms of these experiments, this is 500 mg $FePO_4 \cdot 2H_2O$/25 mL of supernate. The equilibrium NaOH concentration of the supernate is 0.18M. Based on the current experiments, there should be no $FePO_4$ in the sludge under the conditions estimated for Tank 8D2; all ferric iron should be present as $Fe_2O_3 \cdot xH_2O$.

The experimental details for these experiments follow.

1. Experimental Procedure

a. Sample Preparation

(1) Leach solutions of various NaOH concentrations in 6M $NaNO_3$ were prepared from reagent grade NaOH pellets and solid $NaNO_3$. Typical leach solutions were 25-mL volumes of 6M $NaNO_3$ and 0.18M NaOH. Solutions having other NaOH concentrations in 6M $NaNO_3$ were also prepared.

(2) High-purity $FePO_4 \cdot 2H_2O$ was sieved to obtain working amounts of various particle sizes, viz, 90 μm (+90 μm -180 μm) and 45 μm (+45 μm -90 μm). Sample weights were 10 mg to 8.0 g (0.053 to 42.7 mmol).

(3) A solid sample and 25 mL of the leaching solution were placed in a 50-mL plastic-screw-cap centrifuge tube. Slurrying of the samples to promote leaching was accomplished by rotating the sample suspensions at a preferred angle of 45° at 28 cycles/min for time periods of 1 h to as much as 120 h.

(4) The test samples were then centrifuged, the phases separated, and the residues ($FePO_4$ or Fe_2O_3) were water-washed. The residue portions were dried and the supernates were evaporated to dryness in an 85°C oven.

b. Analysis of Samples

Pressed discs containing dried products of the leached material, the leaching solution, and cellulose binder were prepared for analysis by energy dispersive X-ray fluorescence spectroscopy (EDXRF).

The oven-dried sample products, evaporated leachates, and residues were each powdered along with cellulose binding material (microcrystalline, Baker Reagent) by means of a tungsten carbide ball-milling device (Wiggle-bug). Great care was exercised in reproducing the grinding and disc-making procedure for all samples. The discs were produced using a 0.75-in. stainless steel (polished) die compressed at 8.28×10^4 kPa (12,000 psi). The bulk of the prepared discs consisted of cellulose binder--99% for the residue samples and 25% to 50% for the leachate samples.

Working standards were prepared for (1) unleached $FePO_4 \cdot 2H_2O$ and (2) an appropriate salt concentration of the leaching materials plus cellulose binder. Corrections were made for volume changes and the different densities of the dried leaching solutions.

Analyses for phosphorus and iron were completed by the EDXRF method. In this study, a Kevex 0700 spectrometer was interfaced with a 7000 series analyzer. Secondary targets were used for each of the element analyses. The Kd lines (2.02 keV for P and 6.40 for Fe) were used.

A titanium (unfiltered) secondary target was used for the phosphorus determination. Measurement conditions were 30 kV and 2.0 mA, vacuum, dead time of about 10%, and line counting times from 100 s to 4000 s. The 1.9-cm (0.75-in.) diameter discs were placed on aluminum holders.

A nickel (unfiltered) secondary target was used for the iron determination, using 25 kV and 2.0 mA. Counting line times seldom exceeded 100 s. Blank discs were also examined at the same operating conditions to determine background.

2. Results

Tables 6 and 7 are a compilation of the data collected in this study. For sample sizes of 10-1000 mg of $FePO_4 \cdot 2H_2O$, the ratio of Fe to P in the residue was used to measure the amount of PO_4^{3-} exchanged via reaction 1. Changes of PO_4^{3-} content in sample sizes between 300 and 8000 mg were measured by determining the concentration of phosphorus in the leachate solutions. Because the Fe/P ratio in the residual solid was much more reproducible and accurate than measurements of phosphorus in the leachate, the residue ratio results of the 300-mg and 1000-mg samples, which were measured by both techniques, were used to normalize leachate results for 3000- and 8000-mg samples. Iron concentrations in the leachate solutions were found to be inconsequential compared to those of P; $[Fe]/[P] \sim 3 \times 10^{-3}$.

Table 6. Reaction of $FePO_4 \cdot 2H_2O$ in Alkaline Solutions[a]

Conditions	Weight of $FePO_4 \cdot 2H_2O$, mg	PO_4^{3-} available for exchange, meq	PO_4^{3-} exchanged, meq	PO_4^{3-} exchanged, %
+90 μm	10	0.16	0.16	99
-180 μm	30	0.48	0.47	98
particle	100	1.60	1.6	99
size, 120 h	300	4.80	4.6	95
	1000	16.0	3.7	23
	3000	48	1.4	3
	8000	128.4	1.3	1
+45 μm	100	1.60	1.6	99
-90 μm	300	4.8	4.3	89
particle	1000	16.0	4.0	25
size, 60	3000	48.0	4.3	9
min				
+90 μm	10	0.16	0.15	94
-180 μm	30	0.48	0.48	100
particle	100	1.6	1.6	100
size, 145	300	4.8	4.8	100
min	1000	16.0	4.8	30
	3000	48	3.8	8

[a] 25 mL of 6M $NaNO_3$-0.18M NaOH (4.8 meq NaOH).
T = 19 to 24°C.

Table 7. Effect of Hydroxide Concentration Upon Reaction of $FePO_4 \cdot 2H_2O$ in Alkaline Solution[a]

Initial $[OH^-]$, M	$[OH^-]$ available for exchange reaction, meq	$[PO_4^{3-}]$ exchanged, meq	PO_4^{3-} exchanged, %	% of OH^- Utilized
0.05	1.25	0.91	19	73
0.08	2.00	2.0	42	100
0.12	3.00	3.2	66	107
0.18	4.50	4.6	95	102
0.20	5.00	4.8	100	96
0.50	12.5	4.8	100	38

[a]Solution 6M $NaNO_3$, varying [NaOH], 300 mg $FePO_4 \cdot 2H_2O$ (4.8 meq), 25 mL of solution, T = 19-24°C.

D. Interim Waste Form Development: Materials Studies

(G. Bandyopadhyay, T. M. Galvin, J. E. Slattery, and R. B. Poeppel)*

1. Preparation of Silicate/Sludge Pellets

Earlier experiments had shown that sodium silicate/sludge pellets pressed at 70 MPa (10,000 psi) and sintered at 600°C lost much of their strength as the sludge loading was increased. Recent experiments with silicate/sludge specimens have shown that substantially stronger pellets can be prepared by exposing the specimens to a high humidity at 35°C for 24 h.

SS-65 and SS-C sodium silicates† were mixed with as much as 75 wt % synthetic sludge and cold-pressed at 70 MPa (10,000 psi); chemical bonds were then formed by curing the cold-pressed samples at 90% relative humidity and 35°C for 24 h. For several compositions, 5 wt % $Ca(OH)_2$ powder was added to form a cementitious bond during curing. The presence of excess water was avoided by using a controlled-humidity environment.

Some of the compositions that were considered are listed in Table 8. The addition of salt (sodium nitrate-sodium nitrite) to the sludge/silicate pellet represented the case of incomplete separation of the sludge from the supernatant salt solution.

During curing in the high-humidity environment, specimens containing SS-C sodium silicate absorbed substantially larger quantities of water than did those containing SS-65. As a result, SS-C/sludge specimens exhibited extensive cracking after curing. However, the presence of $Ca(OH)_2$,

*Materials Science Division, ANL.

†SS-65 and SS-C are anhydrous, amorphous sodium silicate powders with SiO_2:Na_2O ratios of 3.22 and 2.0, respectively.

Table 8. Water Absorption, Sample Quality, and Fracture Strength of the Silicate/Sludge Specimens[a] Prepared at Ambient Temperature

Composition					Water Absorption, wt %	Sample Quality	Fracture Strength,[b] MPa
Sludge, wt %	Silicate Type	Silicate wt %	$Ca(OH)_2$, wt %	Salt, wt %			
75	SS-65	25	-	-	2.4	Good	1.13
75	SS-C	25	-	-	11.6	Cracked	Cracked
70	SS-65	25	-	5	9.44	Good	1.74
70	SS-C	25	-	5	16.72	Slight tendency to slump	1.28
75	SS-65	20	5	-	3.2	Good	1.85
75	SS-C	20	5	-	9.8	Fair	3.24
70	SS-65	20	5	5	9.8	Good	1.98
70	SS-C	20	5	5	12.8	Good	2.44

[a]Cold-pressed at 70 MPa (10,000 psi), then cured for 24 h in 90% relative humidity atmosphere at 35°C.

[b]Standard deviation: ±20%.

salt, or both inhibited cracking in the samples and improved the quality of the specimens. Samples containing SS-65 were of good quality and remained intact with $Ca(OH)_2$ and/or salt present or absent. Samples prepared by this technique are termed ambient-temperature silicate/sludge waste forms.

2. Properties

a. Physical and Chemical Stability

Ambient-temperature silicate/sludge waste forms show excellent physical and chemical stability in the ambient environment. To simulate exposure to a hot-fire condition, several cured silicate/sludge* and silicate/sludge/$Ca(OH)_2$ specimens with and without 5 wt % salt were heated to 800°C. The specimens containing salt showed no visible changes after the heat treatment; the samples containing no salt, on the other hand, exhibited a limited amount of cracking. The reasons for this behavior are not currently understood. However, the results clearly show that particularly in the presence of residual salt, the specimens would be stable under hot-fire conditions.

b. Rate of Dissolution/Disintegration of Silicate/Sludge Pellets

These results are discussed in Section B.4.

*SS-C/sludge samples containing no salt and/or $Ca(OH)_2$ were unstable (Table 8) and therefore were not considered.

c. Fracture Strength

The fracture strengths of several compositions cured in high-humidity environments are shown in Table 8. The samples prepared from compositions containing SS-65/sludge/$Ca(OH)_2$ were slightly stronger than those prepared from SS-65/sludge. The small differences in strength indicate that the addition of silicates alone may provide adequate bonding between the sludge particles by the formation of hydrated silicates and/or by the formation of cementitious bonds due to reaction of one or more of the sludge components with the silicates. The presence of 5 wt % salt in the pellet did not significantly influence the mechanical strength.

d. Impact Properties

Controlled crushing-type impact tests were performed on cylindrical ambient-temperature silicate/sludge specimens, using a Dynatup instrumented impact testing machine (Dynatup Model 8000, Effects Technology, Inc., Santa Barbara, CA), to determine the impact behavior and to estimate the generation of respirable fines (defined as particles <10 μm). The crushed specimens from the impact experiments were subjected to sieve analysis. Figure 3 shows a lognormal plot [MECHAM] of the particle size distribution data for two silicate/sludge/$Ca(OH)_2$ compositions for impacts with an energy density of about 12 J/cm^3. Particle sizes smaller than 44 μm (325 mesh) could not be distinguished by means of the sieve analysis.

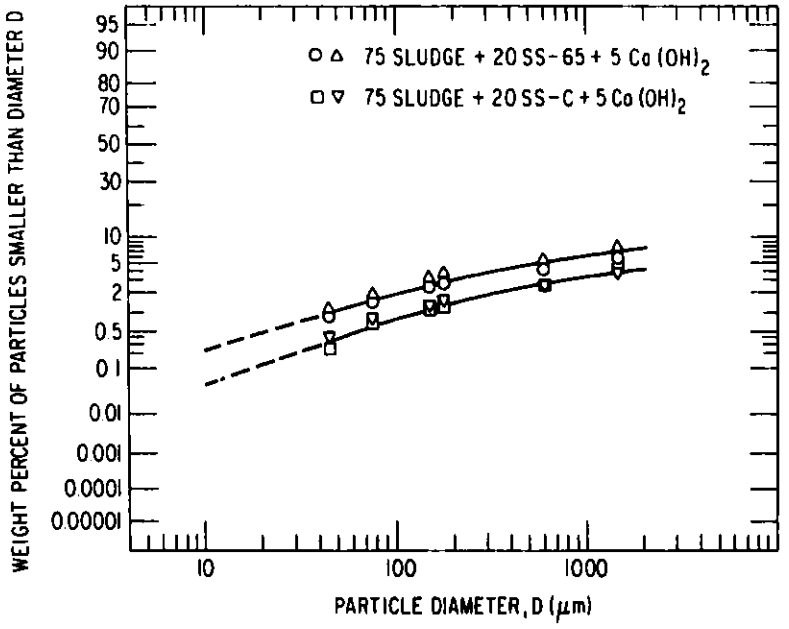

Fig. 3. Size Distribution of Fracture Particles Generated by the Instrumented Impact Testing of Ambient-Temperature Silicate/Sludge Samples. Impact energy density, about 12 J/cm^3.

However, extrapolation of the straight-line portions of the curves to D = 10 μm provided a conservative estimate of the fractions of fines generated. In these cases, the sample containing SS-65 yielded about 0.2 wt % fines and SS-C sample yielded about 0.04 wt % fines.

II. NEUTRON ACTIVATION AND TRACER STUDIES
(L. J. Jardine, J. K. Bates, and J. E. Kincinas)

A. Introduction

Dispersion of wastes into the biosphere is the principal potential hazard of nuclear waste disposal. Characterization of waste forms requires the use of sensitive analytical methods to obtain dispersion data for low-rate phenomena. Neutron activation analysis (NAA) has been shown to be one method applicable for measuring leach rates. Alternatively, radioactive tracers can provide sensitive methods for applications in which NAA is not possible or practical. Both methods are likely to be useful also for characterization measurements other than leach rates.

The general objective of this program is to develop techniques and to qualify methods that utilize neutron activation analysis and radioactive tracers for characterizing simulated waste forms. From comparisons of characterization test results obtained using these two methods with other existing characterization data, conditions can be specified under which such tests and the resulting data may be extrapolated to fully radioactive specimens. The current focus is on leach-rate characterizations of simulated waste glasses and, to a lesser extent, advanced waste forms.

Major accomplishments of this program include development of the NAA method for leach-rate determination, definition of the accuracy, sensitivity, and limitations of NAA, and establishment of the applicability of the test results to larger-scale waste forms. These results are presented in a topical report [BATES-1982A].

Similar goals exist for the development of methods utilizing radioactive tracers. The experimental tests qualifying the use of radioactive tracers have been completed and are described in this report. A topical report on this subject is under preparation and will be completed by December 1981.

B. Qualification of Radioactive Tracer Method

1. Introduction

A series of experiments have been completed which qualify the use of NAA and radioactive tracers in the measurement of leach rates from SRL frit 131 and SRL frit 211 simulated waste glasses. Four classes of chemical elements present as minor (<5 wt %) elements in SRL defense wastes and of concern in radioactive waste management were the focus of the measurements. The four classes are alkali metals (Cs), alkaline earths (Sr and Ba), rare earths (Ce, Eu), and noble metals (Ru). Simulated waste glass containing radioactive tracers was prepared; this glass was leached directly and also was submitted for neutron activation prior to leaching. Leach rates were measured wherever possible, using four different techniques: (1) conventional chemical solution analysis (ICP,* AA,† DCP,‡ flame emission)

*Inductively-coupled plasma emission spectroscopy.

†Atomic absorption.

‡Direct current plasma emission spectroscopy.

of leachates from nonneutron-activated glass, (2) gamma-ray spectroscopy analysis of leachate solutions from neutron-activated glass specimen (A), (3) gamma-ray spectroscopy analysis of leachate solutions from spiked glass specimens containing radioactive tracers (S), (4) gamma-ray spectroscopy analysis of leachate solutions from neutron-activated glass specimens containing radioactive tracers (S/A).

The objective of these measurements was to obtain comparative leach rate data in order to define the reproducibility, sensitivity, limitations, and precision of leach-rate measurements by the various methods.

2. Radioactive Glass Preparations and Source Counting

Gamma-ray analyses of the current series of samples were done by (1) R. Malewicki of the Analytical Chemistry Laboratory (ACL/CEN), (2) the University of Missouri (U of M), and (3) the Fuel Cycle Section (FCS/CEN). To ensure that the results from each laboratory are consistent, careful documentation and calibration of each procedure have been done [STEINDLER-1981B]. Results obtained from the University of Missouri and from ACL/CEN could be reproduced by FCS/CEN to within 10% accuracy.

3. Leaching Characterizations

To qualify the spike/leach methods, tests are being done on four different glasses, SRL 211**, SRL 211***, SRL 131, and SRL 131* (Table 9). For each type of glass, the leach rates obtained with spiked glass will be compared with leach rates obtained by another method. The following tests have been completed.

a. SRL 211**

Leach testing of SRL 211** glass has been done using cold, activated, spiked, and spiked/activated samples. Leachate analysis and test conditions for each leach test are given in corrected and updated Tables 10 and 11. Consolidated results for each glass type are depicted graphically in Figs. 4 through 6.

Cold samples L-154 to L-165 have been leached for 182 days, and a further test is in progress that will terminate at 364 days. Leachate analysis was done by ACL/CEN using atomic absorption or flame emission for Cs, Na, and Li; DC plasma spectroscopy was used by TEI Analytical for 18 other elements. Leach tests on cold samples were done to establish a base leaching behavior for the glass type, including leach rates for both waste and nonwaste elements in the glass.

Cesium, sodium, lithium, and boron leach from SRL 211** glass at the highest rate. The $(NL)_i$ values for each element are nearly the same and increase with time. The value of $(NL)_{Si}$ also increases with time, but at a slower rate. Aluminum and calcium values in solution actually decrease after 42 days while manganese and iron have small constant $(NL)_i$ values. The overall leaching behavior of cold SRL 211** glass is shown in Fig. 4.

Table 9. Nominal Compositions[a] of Simulated SRL Waste Glasses Used in this Work

	wt %					
	SRL 211[a]	SRL 211*	SRL 211**	SRL 211***	SRL 131	SRL 131*
Element						
Si	20.34	20	19.65	19.60	19.9	19.4
Na	11.5	11.15	11.04	11.08	9.9	9.7
Fe	10.28	10.08	9.75	9.91	9.7	9.5
B	2.48	2.43	2.40	2.39	3.3	3.2
Ca	3.78	3.78	3.66	3.64	0.9	0.9
Mn	2.46	2.41	2.38	2.37	2.3	2.2
Al	2.01	1.96	1.94	1.94	1.8	1.7
Li	1.48	1.47	1.44	1.44	1.9	1.8
Ni	1.34	1.31	1.29	1.29	1.3	1.3
Mg	-	-	-	-	0.9	0.9
Ti	-	-	-	-	0.4	0.4
Zr	-	-	-	-	0.3	0.3
La	-	-	-	-	0.3	0.3
Additive						
Cs	-	0.19	0.12	0	-	0
Sr	-	0.07	0.30	0.32	-	0.3
Ba	-	0.10	0.05	0.29	-	0.3
Ce	-	0.52	0.73	0.74	-	0.7
Nd	-	0.63	0.79	0.81	-	0.8
Eu	-	0.003	0.01	0.11	-	0.1
Ru	-	-	0.51	0.41	-	0.4
Mg	-	0.11	-	0	-	0
K	-	-	-	0.05	-	0

[a] [SRL].

Table 10. Summary of Current Test Conditions, Analytical Results of Leachate Analyses, and Weight Loss Rates for SRL 211** Glass

Sample	Sample No. L-	Test Conditions: Temp, °C	Time, days	Initial Mass, g	Δ Mass, g×10^{-4}	SA, m^2×10^{-4}	Final pH	Final Leachate Volume, mL	Δ Mass/SA, g/m^2	Leachate Analysis Element Concentration, µg/mL: ACL[a] Si	ACL Na	ACL Li	ACL Cs	TEI[b] Si	TEI B	TEI Mn	TEI Ca	TEI Al	TEI Fe	TEI Ba
SRL 211** (activated)	134	90	3.6	0.5874	30	3.69	9.8		8.1											
	135	90	7.0	0.5746	38	3.64	9.7	50.6	10.5	21.48										
	136	90	14.6	0.4573	43	3.61	9.6		11.9											
	137	90	14.6	0.5839	48	3.67	9.6		13.1											
	138	90	14.6	0.5525	40	3.67	9.8		10.9											
	139	90	28.0	0.6276	55	3.80	9.7		14.5											
	140	90	42.7	0.5273	60	3.87	9.8		15.5											
	141	90	42.7	0.5824	57	3.73	9.7		15.3											
	142	90	42.7	0.6174	62	3.74	9.8		16.6											
	143	90	98.8	0.5750	62	3.91	9.7		15.9											
	144	90	182	0.6396	60	4.10	9.5	42.6	14.6	31.0			0.17							
	145	90		0.6098		3.94														
	146	90		0.7473		4.18														
SRL 211**	154	90	3	0.3655	32	4.21	9.8	spilled	7.6											
	154a	90	3	0.3866	31	4.22	9.7	42.2	7.4		12.1	1.40	0.12	20	2.6	0.05	2.4	1.8	0.28	<0.05
	155	90	5	0.3776	33	4.19	9.6	43.0	7.9		13.5	1.60	0.12	18	2.8	<0.05	2.5	1.6	0.05	<0.05
	156	90	7	0.3833	38	4.20	9.7	43.8	9.1		15.8	1.88	0.14	19	3.3	<0.05	2.4	1.8	0.09	<0.05
	157	90	14	0.3735	40	4.20	9.7	41.5	9.5		19.1	2.28	0.17	21	4.0	<0.05	2.6	1.9	0.12	<0.05
	158	90	14	0.3889	39	4.19	9.7	41.2	9.3		18.7	2.22	0.17	21	3.9	0.06	2.6	1.8	0.17	<0.05
	159	90	14	0.3576	40	4.18	9.6	42.5	9.6		18.1	2.14	0.16	21	3.8	0.05	2.6	1.9	0.12	<0.05
	160	90	28	0.3760	48	4.20	9.6	40.5	11.4		21.5	2.72	0.19	23	4.5	0.06	2.7	1.8	<0.05	<0.05
	161	90	42	0.3817	51	4.20	9.5	42.5	12.1		23.6	2.93	0.21	26.2	4.76	0.05	2.48	1.87	0.09	<0.05
	162	90	42	0.3634	45	4.19	9.5	41.2	10.7		22.2	2.71	0.19	25.2	4.54	0.05	2.65	1.85	0.08	<0.05
	163	90	42	0.3803	48	4.20	9.5	41.5	11.4		24.7	2.82	0.20	25.5	4.59	0.06	2.61	1.88	0.13	<0.05
	164	90	94.7	0.4200	50	4.24	9.7	40.5	11.8		26.1	3.44	0.26	29.8	5.46	0.05	2.33	1.45	0.08	<0.05
	165	90	182	0.3775	56	4.19	9.2	40.1	13.4				0.27	34.4	6.79	0.05	2.05	1.41	<0.05	<0.05
	166	90		0.3661		4.18														

(contd)

Table 10 (contd)

Sample	Sample No. L-	Test Conditions: Temp,	Time, days	Initial Mass, g	Δ Mass, g×10^{-4}	SA, m^2×10^{-4}	Final pH	Final Leachate Volume, mL	Δ Mass / SA, g/m^2	Leachate Analysis Element Concentration, µg/mL: ACL[a] Si	ACL Na	ACL Li	ACL Cs	TEI[b] Si	TEI B	TEI Mn	TEI Ca	TEI Al	TEI Fe	TEI Ba
SRL 211** (spiked and acti-vated)	222	90	3	0.4393	23	3.90	9.5	39.7	5.9											
	223	90	7	0.4505	35	3.93	9.7	38.0	8.9											
	224	90	14	0.4577	42	3.93	9.4	37.5	10.7											
	225	90	14	0.4537	46	3.86	9.4	37.9	11.2											
	226	90	14	0.4528	42	3.91	9.4	38.1	10.7											
	227	90	28	0.4532		3.97	9.3	35.3												
	228	90	42	0.4542	46	3.95	9.7	32.3	11.7	35.5										
	229	90	42	0.4504	49	3.95	9.5	32.4	12.4	35.4										
	230	90	42	0.4572	47	3.97	9.7	33.0	11.8	34.4										
	231	90	95	0.4526	47	3.97	9.7	23.2	11.8	37.2										
SRL 211** (spiked)	257	90	3	0.4194	25		9.5	39.0	6.7											
	258	90	7	0.4549	38	3.91	9.5	38.9	9.7											
	259	90	14	0.4297	44	3.74	9.4	37.5	11.8											
	260	90	28	0.4152	44	3.94	9.4	37.0	11.2											
	261	90	28	0.4493	41	3.99	9.4	37.9	10.3											
	262	90	28	0.5513			9.4	35.8												
	263	90	42	0.4597	45	3.98	9.6	32.6	11.3	36.2										
	264	90	42	0.4432	44	3.98	9.6	33.1	11.1	35.3										
	265	90	42	0.4483	47	3.92	9.4	32.8	12.0	37.2										
	266	90	95	0.4424	42	3.89	9.6	25.6	10.8	51.4										
	234	90	182	0.4741	69	3.97	9.1	36.2	17.4	43.1			0.18							

(contd)

Table 10 (contd)

Sample	Sample No. L-	Element Concentration ($A_I/A_O \times 10^3$) NAA by either ACL or University of Missouri									
		^{51}Cr	^{59}Fe	^{85}Sr	^{124}Sb	^{131}Ba	^{134}Cs	^{137}Cs	^{141}Ce	^{147}Md	^{152}Eu
SRL 211** (spiked and activated)	222	0.5			3.32	0.31	4.86	5.57	0.025		0.026
	223	2.11			4.61	0.21	7.55	8.82	ND		ND
	224	1.55			5.04	0.15	7.62	8.87	0.028		ND
	225	1.22			6.65	0.22	8.49	9.93	0.037		0.021
	226	2.41			6.45	0.26	8.62	10.1	ND		ND
	227	1.77			7.04	0.19	9.28	12.0	ND		0.033
	228	4.66			9.51	0.16	12.4	14.3	ND		ND
	229	3.22			8.64	0.14	11.2	13.0	ND		0.009
	230				4.41	0.16	10.6	12.4	ND		0.010
	231										
SRL 211** (spiked)	257					0.05		6.27			
	258					0.20		7.41			
	259					0.19		9.69			
	260					0.22		10.50			
	261					0.23		9.93			
	262					0.14		8.82			
	263					0.15		12.60			
	264					0.15		12.90			
	265					0.14		13.40			
	266										
	234										

[a] Analyses done by the Analytical Chemistry Laboratory, Argonne National Laboratory.

[b] Analyses done by Trace Elements, Inc.

Table 11. Summary of Normalized Leach Rates Calculated from Data in Table 10 for SRL 211** Glass

Sample	Sample No. L-	Time, days	Normalized Elemental Loss, $(NL)_i$, g/m^2										
			ACL[a] Si	ACL Na	ACL Li	ACL Cs	TEI[b] Si	TEI B	TEI Mn	TEI Ca	TEI Al	TEI Fe	TEI Ba
SRL 211** (activated)	134	3.6											
	135	7.0	15.3										
	136	14.6											
	137	14.6											
	138	14.6											
	139	28.0											
	140	42.7											
	141	42.7											
	142	42.7											
	143	98.8											
	144	182	16.5			17.7							
	145												
	146												
SRL 211**	154	3											
	154a	3		11.1	11.2	11.4	10.3	10.7	0.2	7.0	9.9	0.3	
	155	5		12.8	13.1	11.5	9.5	11.9	<0.2	7.5	9.0	0.06	
	156	7		15.3	15.7	13.7	10.2	14.2	<0.2	7.3	10.3	0.1	
	157	14		17.4	18.0	16.0	10.7	16.3	<0.2	7.5	10.3	0.1	
	158	14		17.0	17.5	16.1	10.6	15.8	0.3	7.5	9.7	0.2	
	159	14		17.0	17.4	16.1	11.0	16.0	0.2	7.7	10.6	0.2	
	160	28		19.1	21.0	17.6	11.4	17.9	0.3	7.6	9.5	<0.06	
	161	42		21.8	23.4	20.0	13.5	19.7	0.2	7.2	10.3	0.1	
	162	42		20.2	21.3	18.1	12.7	18.4	0.2	7.6	10.0	0.1	
	163	42		22.5	22.3	18.8	12.9	18.7	0.3	7.5	10.2	0.2	
	164	94.7		23.0	26.3	23.7	14.6	21.6	0.2	6.5	7.6	0.1	
	165	182				25.8	16.9	26.9	<0.2	5.7	7.3	<0.06	
	166												

(contd)

Table 11. (contd)

Sample	Sample No. L-	Time, days	Normalized Elemental Loss, $(NL)_i$, g/m^2										
			ACL[a] Si	ACL Na	ACL Li	ACL Cs	TEI[b] Si	TEI B	TEI Mn	TEI Ca	TEI Al	TEI Fe	TEI Ba
SRL 211** (spiked and acti-vated)	222	3											
	223	7											
	224	14											
	225	14											
	226	14											
	227	28											
	228	42	14.9										
	229	42	14.9										
	230	42	14.7										
	231	95	11.2										
SRL 211** (spiked)	257	3											
	258	7											
	259	14											
	260	14											
	261	14											
	262	28											
	263	42	15.2										
	264	42	15.1										
	265	42	16.0										
	266	95	17.4										
	234	182	20.0			16.4							

(contd)

Table 11. (contd)

Sample	Sample No. L-	Time, days	Normalized Elemental Loss, $(NL)_i$, g/m^2													
			^{51}Cr	^{59}Fe	^{85}Sr	^{103}Ru	^{106}Ru	^{131}Ba	^{133}Ba	^{134}Cs	^{137}Cs	^{139}Ce	^{141}Ce	^{147}Nd	^{152}Eu	^{154}Eu	^{124}Sb
SRL 211** (activated)	134	3.6															
	135	7.0															
	136	14.6															
	137	14.6															
	138	14.6															
	139	28.0								20.1							
	140	42.7															
	141	42.7															
	142	42.7															
	143	98.8								12.9					0.1		
	144	132								11.1			0.4		0.4		
	145																
	146																
SRL 211** (spiked and activated)	222	3	<0.85						0.72	11.4	13.2		0.01		0.06		7.8
	223	7	4.4						0.44	16.0	18.7		ND		ND		9.7
	224	14	3.7						0.36	18.7	21.7		0.01		ND		12.1
	225	14	2.8						0.49	19.3	22.4		0.02		0.05		15.0
	226	14	5.2						0.55	18.8	21.6		ND		ND		13.9
	227	28	3.5						0.38	21.0	24.3		ND		0.07		14.1
	228	42	8.1						0.28	22.0	25.3		ND		ND		16.5
	229	42	5.9						0.25	21.0	24.3		ND		0.02		15.8
	230	42	ND						0.30	20.4	23.8		ND		0.02		8.7
	231	95	ND						0.25	16.6	18.0		ND		0.01		15.7

(contd)

Table 11. (contd)

Sample	Sample No. L-	Time, days	Normalized Elemental Loss, $(NL)_i$, g/m^2													
			^{51}Cr	^{59}Fe	^{85}Sr	^{103}Ru	^{106}Ru	^{131}Ba	^{133}Ba	^{134}Cs	^{137}Cs	^{139}Ce	^{141}Ce	^{147}Nd	^{152}Eu	^{154}Eu	^{124}Sb
SRL 211** (spiked)	257	3							0.92		14.3				<0.09		
	258	7							0.48		18.1				<0.09		
	259	14							0.43		22.7				0.06		
	260	14							0.44		21.4				<0.04		
	261	14							0.48		21.1				0.10		
	262	28							0.34		22.1				ND		
	263	42							0.29		23.8				<0.10		
	264	42							0.28		24.2				<0.10		
	265	42							0.26		24.6	0.02			0.10		
	266	95							0.25		24.7	0.17			0.19		
	234	182							0.41		11.7				ND		

[a]Analyses done by the Analytical Chemistry Laboratory, Argonne National Laboratory.

[b]Analyses done by Trace Elements, Inc.

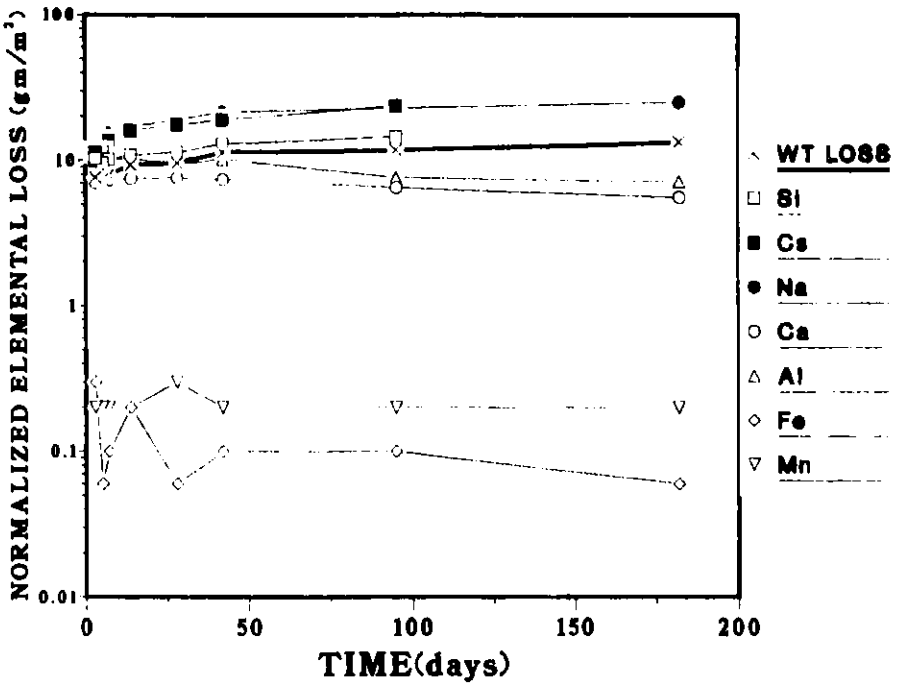

Fig. 4. Leach Results for Cold SRL 211** Glass. MCC-1 test. 90°C.

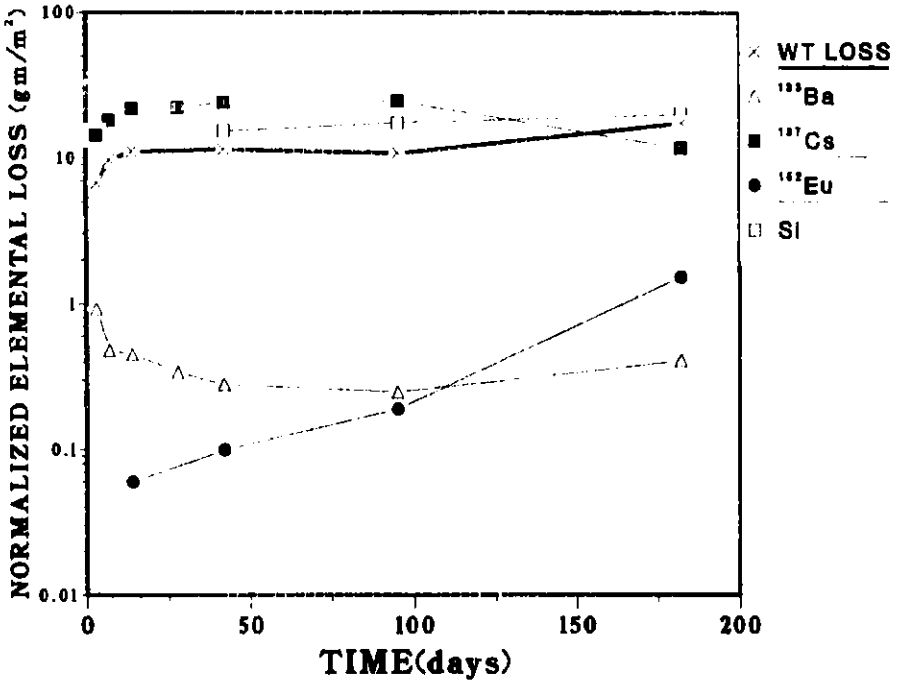

Fig. 5. Leach Results for Spiked SRL 211** Glass. MCC-1 test. 90°C.

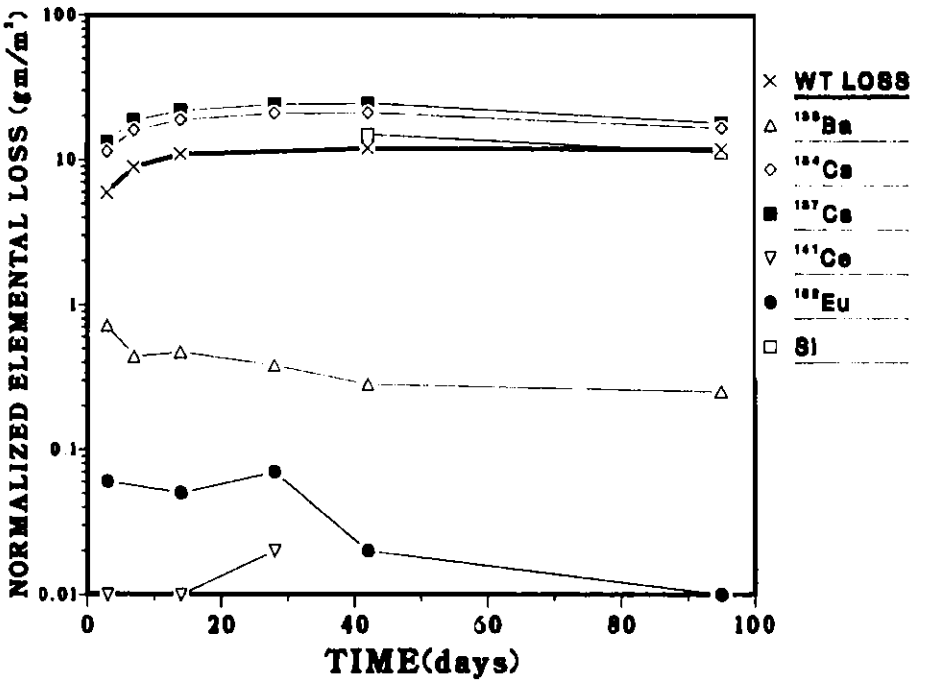

Fig. 6. Leach Results for SRL 211** Spiked and Activated Glass. MCC-1 test. 90°C.

Leaching of activated samples (L-134 to L-146) for 182 days has been completed, and experiments are in progress that will continue for one year. Leachate analysis was done using gamma-ray spectroscopy. For tests through 42.7 days, only ^{134}Cs could be detected. Since cesium leach rates were being obtained for cold 211** glass, analyses for cesium in activated glass were not planned. However, for leachates starting at 98.8 days, both ^{152}Eu and ^{141}Ce can also be detected; thus, complete gamma-ray analyses of samples L-143 (98.8 days) and L-144 (182 days) were done. No systematic solution analysis of this glass was performed.

Other tests (spiked and spiked/activated leach tests) were run concurrently to ensure temperature equalization. These tests have been completed, 95 days for spiked/activated glass and 182 days for spiked glass. Gamma-ray analysis for the radionuclides and analysis for silicon matrix element are complete for the entire series of tests. The leaching behavior is shown in Figs. 5 and 6.

Two major issues are involved in relation to the data presented for 211** glass: (1) Does radiotracer spiking allow reliable measurement of leach rates from simulated nuclear waste glasses and, if so, what are the optimized experimental conditions? (2) What inferences can be drawn about the leaching behavior of the waste glass? The first point is of greater concern in this program and will be developed fully. The second point is being studied by correlating surface analysis with analyses of leachates.

To address the first point, observations can be made pertaining to the various types of SRL 211** glass:

Any effect that radiotracer spiking may have on the leaching of the glass matrix would be reflected in the rates at which silicon is leached. Updated observations are as follows:

1. The silicon leach rates at 42 days have been determined for each glass except activated glass. Triplicate samples were analyzed, and within experimental error, no difference in $(NL)_{Si}$ was observed. $(NL)_{Si}$ was also determined for longer time periods; through 182 days, no significant difference in the silicon leach rates of activated, spiked, and cold glass was observed. These data indicate that the matrix for each type of glass is leaching at the same rate.

2. Cesium leach rates have been determined for each type of glass. For the spiked glass, ^{137}Cs was measured, while for glasses that were neutron-activated, ^{134}Cs was also measured. Agreement of ^{137}Cs leach rates in spiked and spiked/activated glass is excellent. In spiked activated glass, ^{134}Cs leaches about 10% slower than ^{137}Cs, which is about the counting accuracy for different radioisotopes. The leaching trends for both cesium isotopes are the same--an increasing $(NL)_{Cs}$ through 91 days and then a significant decrease in $(NL)_{Cs}$ over the next 91 days. For cold SRL 211** glass, the cesium leach rates are about the same as for the radioactive glasses through 91 days, but the leaching trend continues to increase through 182 days. This difference in trend may be a solution effect reflecting the substantially smaller leachate volume for the radioactive glasses.

3. Barium-133 leach rates were measured in both spiked and spiked/activated glasses, and no significant differences in the $(NL)_{Ba}$ values are observed. Barium released from cold SRL 211** glass could not be detected by the use of DC plasma spectroscopy.

The experiments were successful in demonstrating that cesium and barium leach rates can be measured successfully using radiotracer spiking, but they also demonstrate the care that must be taken when loading the glass. For SRL 211** glass, none of the other spikes were observed in the leachate due to the low leach rates of these elements and the high background produced by the large amount of cesium in the leachate.

b. SRL 211***

Since SRL 211** glass contains so much cesium that most other gamma-emitters cannot be detected, SRL 211*** glass was made which contains nominally no added cesium. Tests were done on cold, activated, and spiked (^{137}Cs, ^{141}Ce, ^{152}Eu, and ^{106}Ru) samples of this glass. Results on all samples are complete, and the data (Tables 12 and 13) indicate that the leach

Table 12. Summary of Current Test Conditions, Leachate Analytical Results, and Weight Loss Rates for SRL 211*** Glass

Sample	Sample No. L-	Test Conditions: Temp, °C	Time, days	Initial Mass, g	Δ Mass, $g \times 10^{-4}$	SA, $m^2 \times 10^{-4}$	Final pH	Final Leachate Volume, mL	Δ Mass / SA, g/m^2	Leachate Analysis Element Concentration, µg/mL: ACL[a] Si	ACL Na	ACL Li	ACL Cs	TEI[b] Si	TEI B	TEI Mn	TEI Ca	TEI Al	TEI Fe	TEI Ba
SRL 211***	276	90	3	0.4056	33	4.13	9.7	44.4	8.0		11.5	1.49		15.4	2.56	0.06	2.43	1.54	0.12	0.07
	277	90	7	0.3974	36	4.22	9.7	41.7	8.5		16.4	2.03		20.2	3.45	0.06	2.47	1.86	0.11	0.06
	278	90	14	0.3970	43	4.24	9.7	41.9	10.1		18.0	2.23		22.0	3.91	0.05	2.73	1.76	0.13	0.06
	279	90	28	0.4048	47	4.28	9.8	44.7	11.0		19.2	2.53		21.4	4.50	0.06	2.76	1.82	0.16	0.05
	280	90	28	0.3835	49	4.17	10.0	44.1	11.8		19.8	2.60		24.3	4.49	0.05	2.66	1.76	0.09	<0.05
	281	90	28	0.4129	48	4.27	9.8	44.8	11.2		19.6	2.52		24.3	4.01	0.06	2.23	1.95	0.12	0.05
	282	90	42	0.3748	51	4.21	9.5	44.2	12.1		21.4	2.81		27.0	4.76	0.06	2.68	1.53	0.11	<0.05
	283	90	91	0.3621	59	4.15	9.7	42.5	14.2		ND	ND		30.2	5.60	<0.05	2.00	1.41	0.06	<0.05
	284	90	182	0.3698	62	4.21	9.2	42.2	14.7		38.6	4.9		47.0	8.59	<0.05	1.51	1.15	0.14	<0.05
	285	90		0.3917		4.21														
SRL 211*** (spiked)	287	90	3	0.4541	24	4.11	9.6	39.9	5.8											
	288[c]	90	7	0.4430	36	4.08	9.8	39.4	8.8											
	289	90	14	0.4482	35	4.09	9.5	36.5	8.6											
	290	90	28	0.4501	39	4.09	9.5	34.9	9.5											
	291	90	28	0.4618	41	4.12	9.0	37.9	10.0											
	292	90	28	0.4607	38	4.11	9.4	34.6	9.3	30.8										
	293	90	42	0.4407	40	4.08	9.5	31.4	9.8											
	294	90	91	0.4496	ND	4.09	9.7	23.0	ND											
	295	90	182	0.4458	41	4.08	9.7	23.9	10.1											
	296	90		0.4946		4.15														

(contd)

Table 12 (contd)

Sample	Sample No. L-	Test Conditions: Temp, °C	Time, days	Initial Mass, g	Δ Mass, g×10^{-4}	SA, m^2×10^{-4}	Final pH	Final Leachate Volume, mL	Δ Mass / SA, g/m^2	Leachate Analysis Element Concentration, µg/mL: ACL[a] Si	ACL Na	ACL Li	ACL Cs	TEI[b] Si	TEI B	TEI Mn	TEI Ca	TEI Al	TEI Fe	TEI Ba
SRL 211*** (activated)	237	90	3	0.4194	ND	4.30	9.4	39.5	ND											
	238	90	7	0.3878	36	4.28	9.4	38.7	8.4											
	239	90	14	0.3993	58	4.36	9.6	37.1	13.3											
	240	90	28	0.3712	53	4.26	9.6	39.5	12.4	NS										
	241	90	28	0.4119	49	4.30	9.6	35.0	11.4	32.5										
	242	90	28	0.3694	85	4.30	9.6	34.3	19.8	33.2										
	243	90	43.1	0.4054	112	4.34		32.5	25.8											
	244	90	91	0.3945	73	4.28	9.4	77.9	17.1	18.7										
	245	90	182	0.3680	51	4.29	9.0	47.6	11.9	24.8										
	246	90		0.4098		4.36														

Sample	Sample No. L-	Element Concentration (A_1/A_0×10^3) NAA by either ACL or University of Missouri: ^{51}Cr	^{59}Fe	^{85}Sr	^{124}Sb	^{131}Ba	^{134}Cs	^{137}Cs	^{141}Ce	^{147}Md	^{152}Eu
SRL 211*** (spiked)	288						18.9				1.001
SRL 211*** (activated)	237	0.63	0.058	0.97	3.97	0.46	2.22		0.022	0.036	0.019
	238	1.14	0.056	1.02	7.27	0.29	3.12		0.024	0.032	0.018
	239	1.71	0.038	1.14	7.20		3.72		0.020		0.017
	240	5.20	0.069		16.0						0.023
	241	3.60	0.140		13.0						–
	242	5.30	0.049		14.0						0.027

[a] Analyses done by the Analytical Chemistry Laboratory, Argonne National Laboratory.

[b] Analyses done by Trace Elements, Inc.

Table 13. Summary of Normalized Leach Rates Calculated from Data in Table 12 for SRL 211*** Glass. Temp = 90°C.

Sample	Sample No. L-	Time, days	Normalized Elemental Loss, $(NL)_i$, g/m^2										
			ACL[a] Si	ACL Na	ACL Li	ACL Cs	TEI[b] Si	TEI B	TEI Mn	TEI Ca	TEI Al	TEI Fe	TEI Ba
SRL 211*** (spiked)	287	3											
	288	7											
	289	14											
	290	28											
	291	28											
	292	28	13.3										
	293	42											
	294	91											
	295	182											
	296												
SRL 211*** (activated) (contd below)	237	3											
	238	7											
	239	14											
	240	28											
	241	28	13.6										
	242	28	13.6										
	243	43.1											
	244	91	17.5										
	245	182											
	246												
SRL 211***	276	3		11.4	12.8		8.5	11.4	0.3	7.6	9.1	0.2	2.6
	277	7		15.0	16.1		10.2	14.1	0.3	7.1	10.1	0.2	2.0
	278	14		16.4	17.6		11.2	16.0	0.2	7.8	9.6	0.2	2.0
	279	28		18.5	21.1		11.5	19.5	0.2	8.4	10.4	0.2	<1.7
	280	28		19.3	22.0		13.2	19.7	0.2	8.2	10.2	0.1	<1.7
	281	28		19.0	21.2		13.1	17.5	0.3	6.8	11.2	0.2	<1.7
	282	42		20.8	23.6		14.6	20.8	0.3	8.2	8.8	0.2	<1.7
	283	91		ND	ND		15.8	24.0	<0.2	5.6	8.0	0.1	<1.7
	284	182		35.7	39.3		24.2	35.6	<0.2	4.4	6.3	0.2	<1.7

(contd)

Table 13 (contd)

Sample	Sample No. L-	Time, days	Normalized Elemental Loss, $(NL)_i$, g/m^2													
			^{51}Cr	^{59}Fe	^{85}Sr	^{103}Ru	^{106}Ru	^{131}Ba	^{133}Ba	^{134}Cs	^{137}Cs	^{139}Ce	^{141}Ce	^{147}Nd	^{152}Eu	^{154}Eu	^{124}Sb
SRL 211*** (spiked)	287	3					ND				9.3	ND	0.002		0.002		
	288	7					ND				18.5	ND	0.003		0.004		
	289	14					ND				10.7	ND	ND		0.003		
	290	28					0.01				8.9	0.19	0.11		0.09		
	291	28					0.08				11.3	0.11	0.10		0.08		
	292	28					ND				11.2	ND	ND		0.005		
	293	42					0.02				12.0	ND	0.02		0.02		
	294	91					0.09				15.8	0.17	0.15		0.15		
	295	182					0.06				20.7	ND	ND		0.02		
	296																
	475	3					0.008				13.5				0.008		
	476	7					0.006				17.7				0.004		
	477	14					0.002				16.4				0.005		
	478	28					0.002				19.9				0.011		
	479	28					0.004				34.2				0.009		
	480	28					0.02				20.3				0.004		
	481	42					0.02				22.7				0.008		
SRL 211*** (acti-vated)	237	3	1.3	0.12	1.9			0.9		ND			0.04	0.07	0.04		7.9
	238	7	1.6	0.09	1.9			0.5		ND			0.04	0.05	0.03		12.4
	239	14	2.9	0.06	1.9					ND			0.03		0.03		12.0
	240	28	7.2	0.12	1.4					22.1			0.04		0.04		20.2
	241	28	5.3	0.21	1.1	0.03				20.9			0.15		0.12		18.1
	242	28	7.3	0.07	0.13	0.02				21.9			0.04		0.04		18.2
	243	43.1		0.18	0.9					20.6			0.08		0.08		17.0
	244	91		0.21						35.5			0.06		0.08		20.2
	245	182		0.50						18.2			0.50		0.15		
	246																

[a] Analyses done by the Analytical Chemistry Laboratory, Argonne National Laboratory.

[b] Analyses done by Trace Elements, Inc.

rates of all spikes plus more than ten activated isotopes can be detected. Results for these tests are shown in Figs. 7 through 9.

For cold glass leached up to 182 days, analyses are complete; experiments are in progress that will extend through 364 days. For activated samples, which are being run simultaneously with the cold samples, all analyses have been completed for experiments through 182 days. Experiments on activated-glass samples are planned to continue through 364 days. Spiked-glass experiments are also complete through 182 days, and experiments will extend to 364 days.

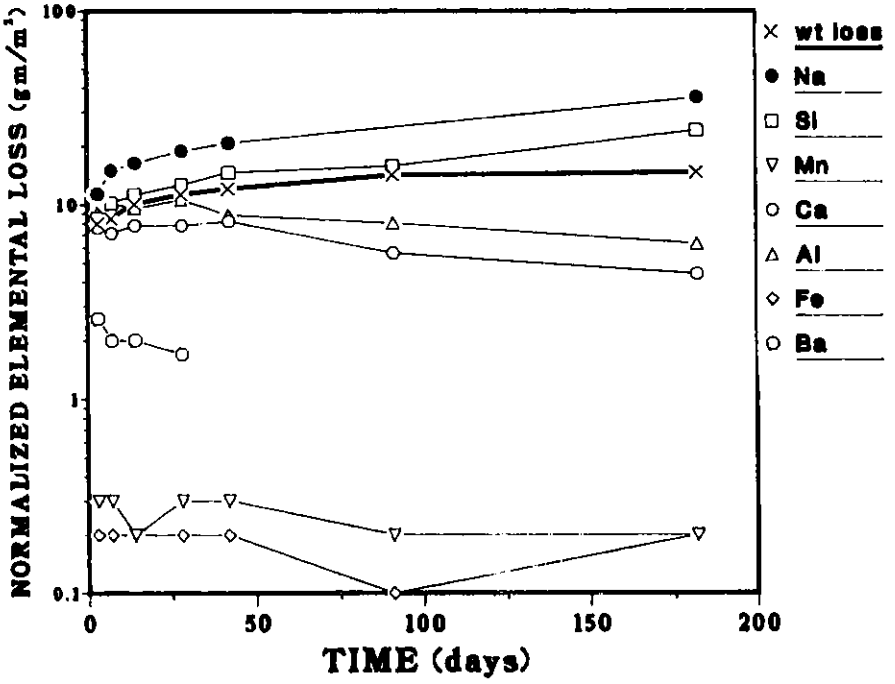

Fig. 7. Leach Results for Cold SRL 211*** Glass. MCC-1 test. 90°C.

c. SRL 131 and 131* Glass

SRL 131 glass is the current SRL reference frit glass. Leach tests have been completed that show the leaching behavior of both this frit glass and this glass containing about 3 wt % waste additives of minor elements (SRL 131*) as shown in Table 9. Tests are being done on cold glass, activated glass, and glass spiked with ^{85}Sr, ^{137}Cs, ^{133}Ba, ^{141}Ce, and ^{152}Eu. The tests have been completed through 91 or 182 days, and the updated results (Tables 14 and 15) are also depicted in Figs. 10 through 13.

d. Conclusion

From the previously described leach tests, the usefulness of radioisotopic tracers in measuring leach rates will be qualified. Additionally, the behavior of several types of glasses when contacted with water will be determined. This behaviorial information can be used to demonstrate

elemental release from a glass and to study the mechanism by which the glass is attacked. Conclusions and qualifications of the spike/leach method are being described in a topical report [BATES-1982B].

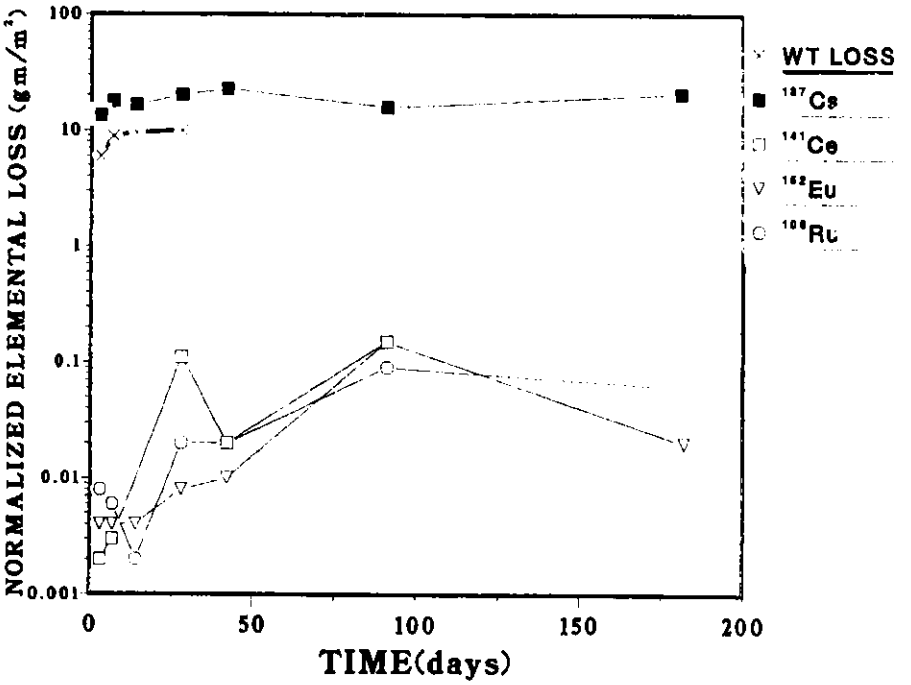

Fig. 8. Leach Results for Spiked SRL 211*** Glass. MCC-1 test. 90°C.

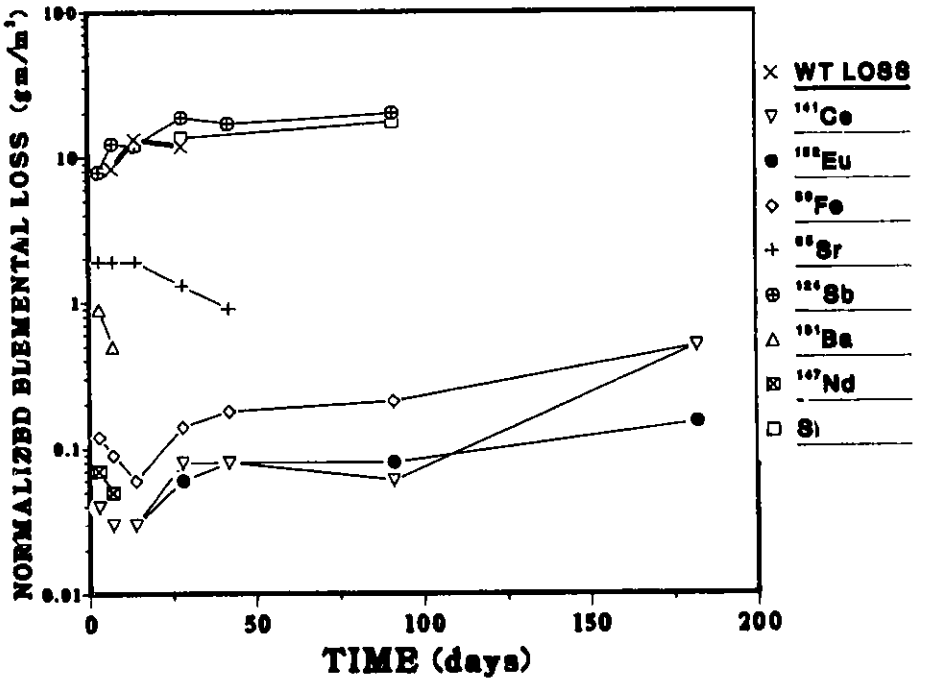

Fig. 9. Leach Results for SRL 211*** Activated Glass. MCC-1 test. 90°C.

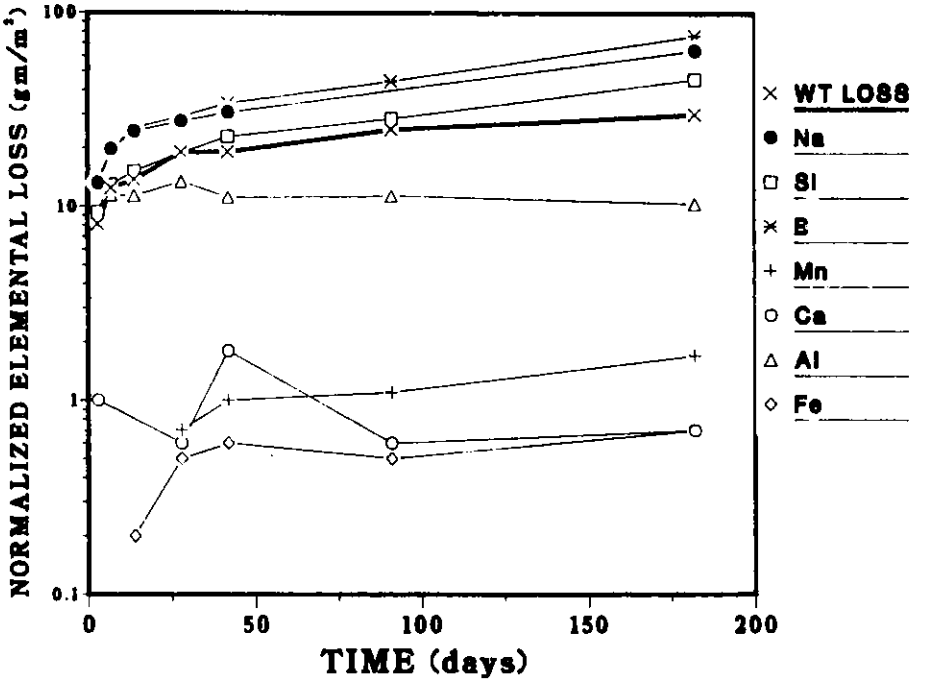

Fig. 10. Leach Results for Cold SRL 131 Glass. MCC-1 test. 90°C.

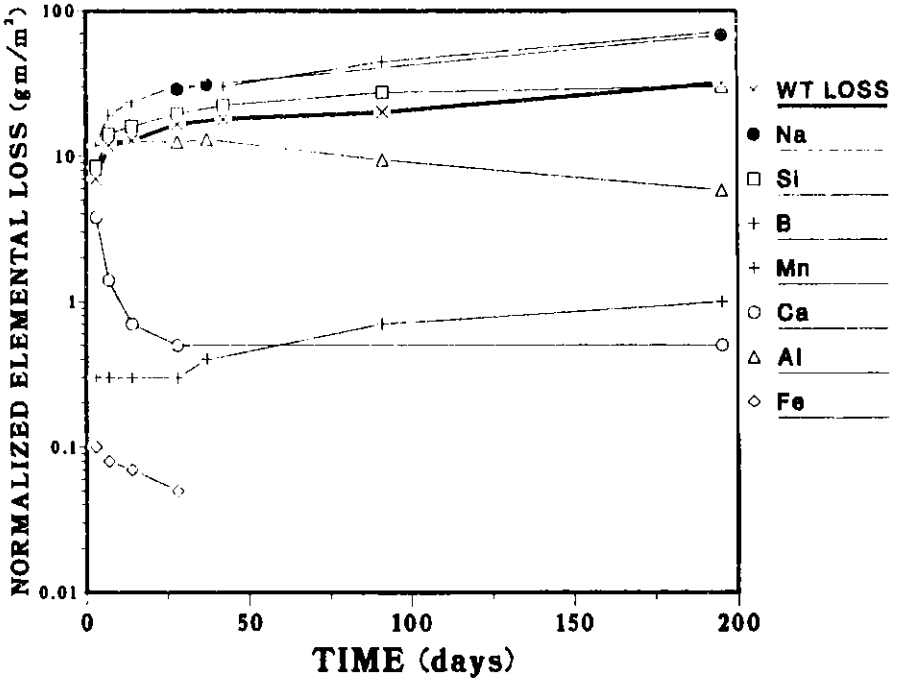

Fig. 11. Leach Results for Cold SRL 131* Glass. MCC-1 test. 90°C.

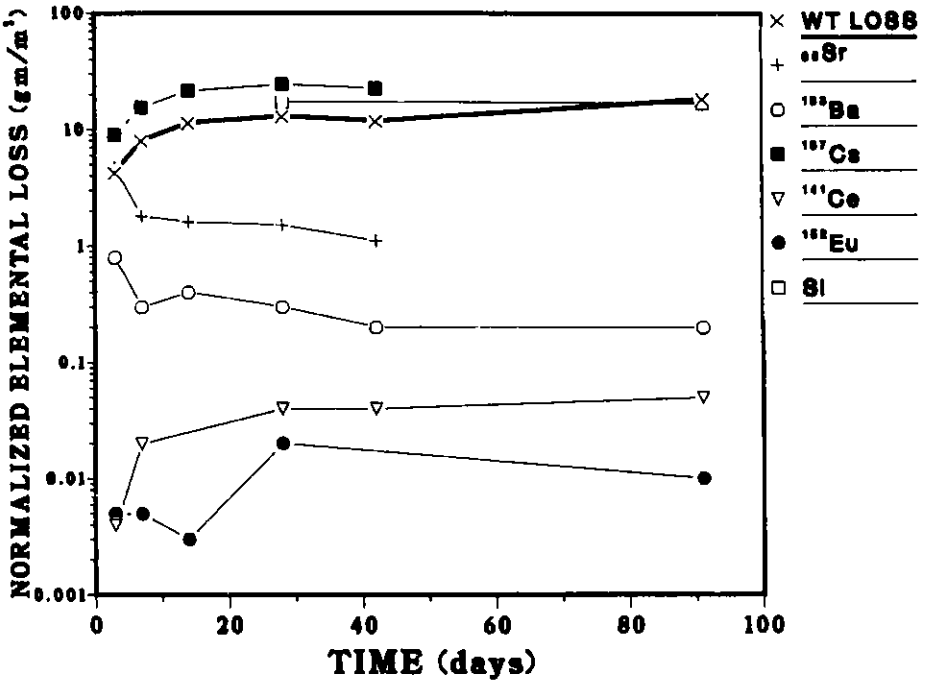

Fig. 12. Leach Results for Spiked SRL 131* Glass. MCC-1 test. 90°C.

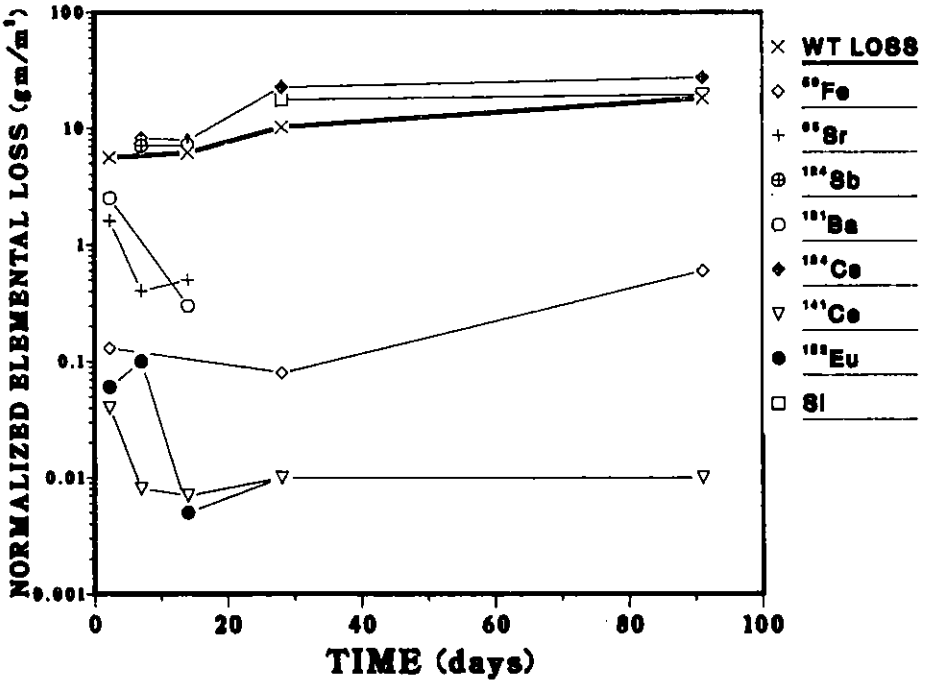

Fig. 13. Leach Results for Activated SRL 131* Glass. MCC-1 test. 90°C.

Table 14. Summary of Current Test Conditions, Leachate Analytical Results, and Weight Loss Rates for SRL 131 Glass

Sample	Sample No. L-	Test Conditions: Temp, °C	Time, days	Initial Mass, g	Δ Mass, $g \times 10^{-4}$	SA, $m^2 \times 10^{-4}$	Final pH	Final Leachate Volume, mL	Δ Mass / SA, g/m^2
SRL 131	298	90	3	0.4393	33	4.08	9.8	41.4	8.1
	299	90	7	0.4854	51	4.13	9.8	42.4	12.4
	300	90	14	0.5093	57	4.16	9.8	45.1	13.7
	301	90	28	0.4917	75	4.17	9.8	43.0	18.0
	302	90	28	0.4624	75	4.10	9.8	43.9	18.3
	303	90	28	0.5066	86	4.16	9.8	43.5	20.7
	304	90	42	0.3893	77	4.02	9.4	44.6	19.1
	305	90	91	0.4769	103	4.13	9.8	41.8	24.9
	306	90	182	0.4259	123	4.09	9.3	41.5	30.1
	307	90	182	0.4978	123	4.15	9.3	40.8	29.6
	308	90		0.5308		4.18			
	309	90		0.4925		4.15			
SRL 131*	311	90	3	0.4527	29	4.15	9.7	42.5	7.0
	312	90	7	0.3030	39	3.32	9.7	38.0	11.8
	313	90	14	0.4025	55	4.29	9.7	46.4	12.8
	314	90	28	0.3697	67	4.14	0.8	44.9	16.2
	315	90	28	0.4887	69	4.43	9.8	44.9	15.6
	316	90	28	0.3891	65	3.64	9.8	45.9	17.9
	317	90	37	0.4556	74	4.12	9.6	45.5	18.0
	318	90	91	0.4987	80	4.01	9.6	40.2	20.0
	319	90	195	0.4699	135	4.27	9.7	39.9	31.6
	320	90	195	0.4799	139	4.35	9.7	41.5	32.0
	321	90		0.4125		4.11			
	322	90		0.4851		4.38			
	323	90		0.4919		4.29			

(contd)

Table 14 (contd)

Sample	Sample No. L-	Test Conditions: Temp, °C	Time, days	Initial Mass, g	Δ Mass, $g \times 10^{-4}$	SA, $m^2 \times 10^{-4}$	Final pH	Final Leachate Volume, mL	Δ Mass / SA, g/m^2
SRL	327	90	2.25	0.3112	21	3.77	9.5		5.6
131*	328	90	7	0.3986	15	3.90			3.9
(acti-	329	90	14	0.3989	24	3.86			6.2
vated)	330	90	28	0.4595	39	4.33	9.2	35.4	9.0
	331	90	28	0.4067	49	4.21	9.2	34.0	11.6
	333	90	91	0.4794	79	4.34	9.2	30.9	18.2
SRL	339	90	3	0.5174	17	4.35	9.5	39.5	3.9
131*	340	90	7	0.4869	32	4.26	9.3	39.0	7.5
(spiked)	341	90	14	0.4842	54	4.27	9.4	37.7	12.7
	342	90	28	0.4772	56	4.28	9.2	34.0	13.1
	343	90	28	0.4866	50	4.29	9.0	34.2	11.7
	344	90	28	0.4965	58	4.29	9.3	34.5	13.5
	345	90	42	0.4733	51	4.27	9.2	31.9	11.9
	346	90	91	0.4651	79	4.26	9.5	33.4	18.5

(contd)

Table 14 (contd)

Sample	Sample No. L-	Leachate Analysis Element Concentration, µg/mL													
		ACL[a] Si	ACL Na	ACL Li	ACL Cs	TEI[b] Si	TEI B	TEI Mn	TEI Ca	TEI Al	TEI Fe	TEI Ba	TEI Ti	TEI Mg	TEI Mo
SRL 131	298		12.9	2.32		18.5	4.15	<0.05	0.09	1.55	<0.05	<0.05			
	299		19.0	3.52		25.0	6.22	<0.05	<0.05	1.99	0.05	<0.05			
	300		22.3	4.02		27.9	7.77	<0.05	<0.05	1.88	0.15	<0.05			
	301		26.2	5.09		37.0	9.44	0.16	0.05	2.50	0.54		0.09		
	302		26.0	4.89		35.6	9.12	0.16	0.06	2.35	0.48		0.08		
	303		25.7	4.81		34.6	8.92	0.12	0.05	2.03	0.28		<0.05		
	304		27.4	5.42		41.2	9.85	0.20	0.15	1.71	0.52	<0.05	0.08		
	305		ND	ND		55.9	14.4	0.25	0.05	2.00	0.49		0.08		
	306		62.4	11.7		87.7	22.8	0.33	<0.05	1.96	0.78		0.09	0.16	
	307		64.4	12.0		93.8	27.6	0.43	0.10	1.74	0.56		0.08	0.11	
	308														
	309														
SRL 131*	311					16.0	3.68	0.05	0.33	1.39	0.09	0.05			
	312					24.1	5.36	0.05	0.11	1.91	0.07	0.05			
	313					28.7	6.88	0.05	0.06	1.98	0.05	0.05			
	314		25.5	4.87		34.2	8.96	0.06	<0.05	4.14	<0.05	<0.05			
	315		25.2	4.91		34.6	8.96	0.06	<0.05	1.87	<0.05	<0.05			
	316		24.5	4.51		32.6	8.42	0.07	<0.05	1.77	<0.05	<0.05			
	317		27.2	5.22		39.2	8.79	0.08	<0.05	2.00	<0.05	<0.05			
	318		ND	ND		53.2	14.2	0.15	<0.05	1.59	<0.05	<0.05			
	319		71.3	13.7		50.8	25.1	0.20	0.06	0.99	<0.05	<0.05	<0.05	0.07	0.09
	320		68.3	13.2		72.0	23.6	0.22	<0.05	1.09	<0.05	<0.05	<0.05	0.06	0.07
	321														
	322														
	323														

(contd)

Table 14 (contd)

Sample	Sample No. L-	Leachate Analysis Element Concentration, μg/mL													
		ACL[a] Si	ACL Na	ACL Li	ACL Cs	TEI[b] Si	TEI B	TEI Mn	TEI Ca	TEI Al	TEI Fe	TEI Ba	TEI Ti	TEI Mg	TEI Mo
SRL 131* (activated)	327														
	328														
	329														
	330	41.2													
	331	43.2													
	333	53.2													
SRL 131* (spiked)	339														
	340														
	341														
	342	43.3													
	343	36.2													
	344	46.5													
	345	ND													
	346	41.5													

[a]Analyses done by the Analytical Chemistry Laboratory of the Chemical Engineering Division.

[b]Analyses done by Trace Elements, Inc.

Table 15. Summary of Normalized Leach Rates Calculated from Data in Table 14 for SRL 131 Glass

Sample	Sample No. L-	Time, days	Normalized Elemental Loss, $(NL)_i$, g/m^2												
			ACL[a] Si	ACL Na	ACL Li	ACL Cs	TEI[b] Si	TEI B	TEI Mn	TEI Ca	TEI Al	TEI Fe	TEI Ba	TEI Ti	TEI Mg
SRL 131	298	3		13.2	12.4		9.4	12.8	<0.2	1.0	8.7	<0.05			
	299	7		19.7	19.0		12.9	19.4	<0.2	<0.6	11.4	<0.05			
	300	14		24.4	22.9		15.2	25.5	<0.2	<0.6	11.3	0.2			
	301	28		27.3	27.6		19.2	29.5	0.7	0.6	14.3	0.6		2.3	
	302	28		28.1	27.6		19.2	29.6	0.7	0.7	14.0	0.5		2.1	
	303	28		27.2	26.5		18.2	28.3	0.6	0.6	11.8	0.3			
	304	42		30.6	31.6		22.9	34.1	1.0	1.8	11.1	0.6			
	305	91		ND	ND		28.4	44.2	1.1	0.6	11.3	0.5			
	306	182		64.0	62.5		44.7	70.1	1.5	<0.6	11.1	0.8		2.3	1.8
	307	182		64.0	62.1		46.3	82.2	1.8	1.1	9.5	0.6		2.0	1.2
	308														
	309														
SRL 131*	311	3					8.5	11.8	<0.2	3.8	8.4	0.1	<1.7		
	312	7					14.2	19.2	0.3	1.4	12.9	0.08	<1.7		
	313	14					16.0	23.3	0.3	0.7	12.6	0.07	<1.7		
	314	28		28.5	29.3		19.1	30.0	0.3	<0.5	26.4	<0.06	<1.7		
	315	28		26.3	27.7		18.1	28.4	0.3	<0.5	11.1	<0.06	<1.7		
	316	28		31.8	31.6		21.2	33.2	0.4	<0.5	13.8	<0.06	<1.7		
	317	37		31.0	32.0		22.3	30.3	0.4	<0.5	13.0	<0.06	<1.7		
	318	91		ND	ND		27.5	44.5	0.7	<0.5	9.4	<0.06	<1.7		
	319	195		68.7	71.1		24.5	73.3	0.9	0.6	5.4	<0.06	<1.7	<1.2	0.7
	320	195		67.2	70.0		35.4	70.4	1.0	<0.5	6.1	<0.06	<1.7	<1.2	0.6
	321														
	322														
	323														

(contd)

Table 15 (contd)

Sample	Sample No. L-	Time, days	Normalized Elemental Loss, $(NL)_i$, g/m^2												
			ACL[a] Si	ACL Na	ACL Li	ACL Cs	TEI[b] Si	TFI B	TEI Mn	TEI Ca	TEI Al	TEI Fe	TEI Ba	TEI Ti	TEI Mg
SRL 131* (activated)	327	225													
	328	7													
	329	14													
	330	28	17.4												
	331	28	18.0												
	332	28	19.5												
	333	91													
SRL 131* (spiked)	339	3													
	340	7													
	341	14													
	342	28	17.7												
	343	28	14.9												
	344	28	19.3												
	345	42													
	346	91	16.8												
	468	3													
	469	7													
	470	14													
	471	28													
	472	28													
	474	42													

(contd)

Table 15 (contd)

Sample	Sample No. L-	Time, days	Normalized Elemental Loss, $(NL)_i$, g/m^2													
			^{51}Cr	^{59}Fe	^{85}Sr	^{103}Ru	^{106}Ru	^{131}Ba	^{133}Ba	^{134}Cs	^{137}Cs	^{139}Ce	^{141}Ce	^{147}Nd	^{152}Eu	^{154}Eu	^{124}Sb
SRL	327	225	1.5	0.13	1.6			2.5		17.9			0.04		0.06		17.6
131*	328	7	1.1		0.4					8.2			0.008		0.10		7.1
(acti-	329	14	3.2		0.5			0.3		7.9			0.007		0.005		7.2
vated)	330	28	3.8	0.07						22.0			0.01		0.01		
	331	28	3.0	0.08						23.4			0.01		0.01		
	333	91	9.9	0.6						27.4			0.01		0.01		
SRL	339	3			4.1				0.8		4.2		0.004		0.01		
131*	340	7			1.5				0.2		7.4		0.02		0.02		
(spiked)	341	14			1.8				0.5		9.9	0.5	0.52		0.43		
	342	28			1.4				0.3		13.9	0.05	0.06		0.05		
	343	28			2.5				0.4		9.0	0.18	0.18		0.16		
	344	28			1.3				0.6		9.7	0.61	0.54		0.46		
	345	42			1.1				0.4		11.6	0.13	0.12		0.11		
	346	91							0.2				0.05		0.02		
	468	3			5.3				0.8		9.0				0.002		
	469	7			2.1				0.3		15.5				0.008		
	470	14			1.1				0.2		21.6				0.003		
	471	28			-				0.1		-		0.02		0.01		
	472	28			1.0				0.1		24.4		0.03		0.01		
	474	42							-		-		-		-		
									0.08		22.5		0.01		0.004		

[a]Analyses done by the Analytical Chemistry Laboratory of the Chemical Engineering Division.

[b]Analyses done by Trace Elements, Inc.

4. Auxiliary Leach Tests

a. Irradiated Glass

Recently, it has been suggested that radiation damage in nuclear waste glasses may be simulated by ion-beam (Pb^{+}, Ar^{+}, H^{2+}, etc.) bombardment. Some evidence indicates that such treatment of the glass surface increases leaching from the irradiated region and that the effect seems to be smaller for waste glasses than for simple glasses. Within experimental uncertainty, results on simulated waste glass PNL 76-68 agree with curium-loading experiments [PNL]. Other results suggest that there is no difference in the leaching behaviors of irradiated (Xe^{2+}, 160 keV) and nonirradiated glass. These different observations may result from the different experimental techniques used to measure leaching. Here we present preliminary results of leach tests conducted on samples of PNL 76-68 (Material Characterization Center, MCC), SRL 211***, and SRL 131 glasses that have been irradiated with He^{2+} ions by the Materials Science Division (MSD/ANL).

The glass samples (1 × 1 × 0.1 cm) were irradiated with 3.5-MeV $^{4}He^{2+}$ ions from the ANL Dynamitron in an ultrahigh vacuum target chamber at about 75-100°C. During irradiations, an infrared pyrometer was used to monitor surface temperature. Samples were each clamped in a holder such that almost all of the sample surface area (top and bottom) could be subjected to ion bombardment. In addition, the samples were rotated with respect to the ion beam to ensure uniform damage production/implantation throughout the irradiated volume (which was about 20 μm thick).

The leach tests were done by the MCC-1 static leach test procedure [MCC] except that the same samples were leached several times by the IAEA (International Atomic Energy Agency) method. The leach tests were done in Teflon containers containing deionized water (DIW), with the sample attached to the lid of the container by means of a Teflon filament. The sample was disturbed as little as possible. To change the leachate, the lid and the sample from the test in progress were transferred to a new container filled with fresh, preheated DIW. Leachate remaining in a used container was analyzed. Only after the last leaching period was the sample dried for weight loss measurement.

Since the effect of irradiation on leaching was not known prior to the experiments, time periods were chosen for best observation of any effect. Control samples of nonirraidated glasses were leached to allow comparison with leaching of irradiated glasses.

The leaching process may be monitored by pH changes, weight loss per unit surface area, and complete analysis of the solution. Results for PNL 76-68, SRL 131, and SRL 211 glasses are shown in Table 16. Also included for comparison are MCC tests on the same glasses. The main observations are:

1. The measured leachate pH indicates that for each type of irradiated glass, some retardation of pH increase occurs (although there are some inconsistencies for certain time periods). This pH effect is most dramatic for SRL 131 and SRL 211*** glasses at time periods of less than one week. No obvious acceleration in the leaching process is indicated by the pH changes.

Table 16. Leach Results for Control and Irradiated Glass Samples[a]

Sample[b]	Test No.	Leaching Period,[c] days	Δ Mass, SA g/m²	Final pH	$(NL)_i$ Cs	Ca	Ba	Al	Mo	Si	B	Zn	Fe	Ni	Mg	Mn
PNL 76-68 (MCC)[d]	445	1		3.8	4.9	3.4	3.2		0.6	2.5	2.9	2.3	0.14	3.0		
I 500 μC	446	2		3.8	5.8	4.3	4.2		0.7	3.5	3.6	2.8	0.13	3.0		
	447	25	12.7	6.6	17.0	10.5	9.6		4.4	7.9	9.2	3.2	<0.05			
PNL 76-68 (MCC)	449	1		4.3	3.3	2.7	2.4		0.6	1.7	2.0	1.5	<0.05			
Control	450	2		4.8	3.8	3.3	2.9		0.9	2.4	2.5	1.9	<0.05			
	451	25	15.4	9.4	47.6	2.2	<1.1		23.2	17.0	29.0	<0.05	<0.05			
PNL 76-68 (MCC)		3	4.1	9.2						6.3						
Round		7	5.9	9.3						9.6						
Robin		14	9.3	9.3						12.4						
		28	12.3	9.3	51.7	2.4	3.1		21.7	18.1	46.1	0.3	0.06			
SRL 211*** (IAEA)[e]	452	1		4.1		2.1	2.9	<0.4		1.2	2.9			0.09		2.2
I 500 μC	453	2		4.3		2.2	2.9	<0.4		2.6	2.4			0.14		2.2
	454	4		6.3		1.5	<2.4	0.6		1.7	1.5			0.08		1.2
	455	21	11.5	9.2		6.7	3.6	6.6		9.3	6.7			<0.05		<0.3
SRL 211*** (IAEA)	456	1	4.6	9.2		3.8	1.5	4.3		4.8	4.5			<0.05		<0.3
Control																
SRL 211*** (IAEA)	457	1/4		6.1		1.1	<1.7	1.0		1.1	1.0			<0.05		<0.3
I 1000 μC	458	3/4		9.0		3.0	2.4	3.4		3.5	3.1			<0.05		<0.3
	459	6		6.7		3.4	3.8	0.7		2.6	2.7			0.27		2.6
	460	21	14.5	9.5		6.5	<1.7	6.9		10.8	10.8			<0.05		<0.2

(contd)

Table 16 (contd)

Sample[b]	Test No.	Leaching Period,[c] days	Δ Mass / SA, g/m²	Final pH	(NL)$_i$ Cs	Ca	Ba	Al	Mo	Si	B	Zn	Fe	Ni	Mg	Mn
SRL 211*** (IAEA)	461	1/4		8.7		1.5	<1.7	1.9		1.7	1.5			<0.05		<0.2
Control	462	3/4		8.8		3.1	2.5	3.5		3.6	3.2			<0.05		<0.2
	463	6	11.9	9.2		6.6	1.7	7.0		9.3	9.2			<0.05		<0.2
SRL 211*** (IAEA)		3	8.0	9.7		7.6	2.6	9.1		8.5	11.4		0.2			
MCC		7	8.4	9.7		7.1	2.0	10.1		10.2	14.1		0.2			
		14	10.3	9.7		7.8	2.0	9.6		11.2	16.0		0.2			
		28	11.5	9.7		7.8	1.7	10.6		12.6	18.9		0.2			
SRL 131 (IAEA)	464	1		3.9		2.2		<0.3		1.1	2.2			1.2	1.4	1.9
I 1000 μC	465	2		7.1		1.0		2.1		2.2	1.2			<0.4	1.2	0.4
	466	4	4.2	4.3		2.3		1.0		2.3	2.5			1.0	1.9	1.7
SRL 131 (IAEA)	467	1	3.7	8.7		2.9		4.3		4.6	4.9				2.8	
Control																
SRL 13		3	8.1	9.8		1.0		8.7		9.4	12.8					
MCC[b]		7	12.4	9.8		<0.6		11.4		12.9	19.4					

[a] Normalized elemental loss is cumulative for IAEA-type tests.

[b] "I" represents "irradiated."

[c] Leaching period refers to duration of sample immersion in a single solution. For example, the same sample was leached in three different solutions in tests 445, 446, and 447.

[d] MCC test.

[e] International Atomic Energy Agency tests.

2. Weight loss data indicate that irradiation has little effect on 28-day leaching of PNL 76-68 or SRL 211*** glass. For SRL 131 glass after seven days, the weight loss for the irradiated sample is about one-third that for the control sample.

3. Solution analyses indicate that leaching has been retarded in each of the irradiated samples.

The penetration depth due to leaching may be calculated from known leach rates. Typical values for SRL glass are 0.2-0.5 μm/day. For PNL 76-68 glass, the values are about 0.5-1.0 μm/day. Given a damage thickness of about 20 μm, it is clear that only after 28 days of leaching would the damaged region be fully penetrated. Surface analytical techniques (SEM, EDAX, ESCA) will be used to study the depth of the reacted layer as a function of leaching time and glass type. Although the effect of increased dose on leach rate appears to be nominal, complete analyses are not available.

Overall, no increase in the leach rate of waste glasses due to ion beam irradiation is indicated. In fact, a decrease is probable. Interpretation of the results is continuing.

b. Hot-Pressed SYNROC

The leach tests on hot-pressed SYNROC samples have been completed (Table 17). These were done following the MCC-1 procedure [MCC]. In this procedure, there is no provision to treat the Teflon containers to control the effect of the container on the leachate [see STEINDLER-1981B]. In fact, the procedure results in significant amounts of nitrate and fluoride ions in the leachate, causing the pH of the leachate to be buffered. The pH of blank DIW solutions in Teflon containers ranges between 3 and 4. Previous SYNROC leach tests described above have shown leaching of this waste form to be dependent on pH, and so the data should be interpreted accordingly. Relative comparisons of data from this series of experiments are meaningful, but comparisons with data from other series of experiments may not be meaningful. The results have been given to the Materials Science Division of Argonne.

c. Weathering Studies

Weathering studies designed to produce weathered (hydrated) glass samples are continuing. Samples of PNL 76-68 glass, SRL frit 211, and SRL frit 211* are being weathered at 80°C and 90% relative humidity. Study of the weathered samples will allow description of the hydration process. The weathered samples will be subjected to leaching to determine the durability of hydrated glass.

In addition, an experimental plan has been drafted for performing glass hydration experiments at other conditions. The hydrated glasses obtained by weathering will then be characterized by leaching.

Table 17. Leaching Conditions and Results for Hot-Pressed SYNROC Samples

Sample	Sample No.	Time, days	Temp, °C	Initial Mass, g	Δ Mass, g × 10^{-4}	SA, cm^2	Final pH	Final Leachate Vol, mL
HP4	L-436	28	90	0.7031	58	6.79	5.5	53.8
HP4	L-437	28	90	0.7870	71	6.77	5.3	50.4
HP4	L-438	28	90	0.6531	61	6.73	5.4	51.3
HP5	L-439	28	90	1.7833	+20	6.50	9.3	48.3
HP5A	L-440	28	90	0.8087	4	3.91	5.6	36.7
HP1	L-441	28	90	1.6867	+1	7.18	4.0	51.0
HP2	L-442	28	90	2.2897	+2	7.49	4.0	53.1
HP3	L-443	28	90	1.2184	2	6.97	3.1	52.0
Blank	L-444	28	90				3.1	43.5

Sample	Sample No.	Cs		Mg		Si		Ni		Ce		Mo		Al		Fe		Ba		Ti	
		mg/L	(NL)	mg/L	(NL)	mg/L	(NL)	mg/L	(NL)	mg/L	(NL)	mg/L	(NL)	mg/L	(NL)	mg/L	(NL)	mg/L	(NL)	mg/L	(NL)
HP4	L-436	30	432	0.06		10.9		1.40		5.21		23.2	166	0.14		0.81		10.8		<0.05	
HP4	L-437	35	474	0.08		13.3		1.88		6.24		34.9	234	0.19		1.29		14.3		<0.05	
HP4	L-438	40	554	0.07		11.1		3.66		5.19		26.2	180	0.16		2.40		15.4		<0.05	
HP5	L-439	20.7	302	0.05		2.12		1.32		2.39		2.69	18.9	0.16		1.21		6.85		<0.05	
HP5A	L-440	5.8	107	<0.05		2.29		4.74		0.87		8.76	76.1	0.06		1.44		3.30		<0.05	
HP1	L-441	0.46	5.7	<0.05		0.48		0.16		0.35		0.18	1.2	0.16		0.08		0.61		<0.05	
HP2	L-442	0.28	3.7	<0.05		0.34		0.10		0.17		0.21	1.4	0.11		0.10		0.39		<0.05	
HP3	L-443	0.80	13.0	<0.05		0.67		0.21		0.11		0.90	6.2	0.29		0.29		1.29		<0.05	
Blank	L-444	<0.05		<0.05		<0.05		<0.05		<0.05		<0.05		<0.05		<0.05		<0.05		<0.05	

III. BRITTLE FRACTURE STUDIES

(L. J. Jardine, W. J. Mecham, and G. T. Reedy*)

A. Introduction

A property of solid radioactive waste forms that must be known is their resistance to dispersion from mechanical impacts received during normal and accidental conditions of processing, handling, interim storage, and transportation. A brittle fracture methodology is being developed which relates the impact-stress distribution to the lognormal size distribution of the particles generated by impact fracture. The practical application of this fracture model is for prediction of the total fracture-surface area and the mass of particles of respirable sizes produced by impact fractures.

Development and preliminary verification of this model has been provided by laboratory-scale tests of impacts of reference glass specimens and by analyses of data available in the technical literature on impacts of various brittle materials and on impacts of large-scale simulated waste-glass canisters. The validity and utility of this brittle-fracture methodology is being examined for a range of laboratory-scale impact conditions and for various solid waste materials. The experimental results have been used to establish correlations of the impact energy with (1) lognormal size-distribution parameters, (2) fracture surface areas, and (3) material strength properties of brittle-waste packages of various sizes and configurations.

This report summarizes laboratory-scale experimental impact test results not reported previously. No further experimental tests are planned for FY 1982 due to significant budget reductions aimed at terminating the program at the end of FY 1982. FY 1982 work will focus on (1) summarizing the characterization methodologies developed and (2) documenting our program results.

B. Experimental Results

(L. J. Jardine, G. T. Reedy,* and R. L. Malewicki)

1. Surface Areas Produced by Impacts of Simulated Alternative High-Level Waste Forms

A series of impact tests have been performed on specimens of simulated waste SRL 131, Westinghouse alkoxide, PNL 76-68 glasses, SYNROC B, and Pyrex. In each test, a cylindical sample was impacted by dropping a steel bar of about 9.9 kg from a predetermined height that would give the desired input kinetic energy. After impact, fragments were collected using dry techniques, and all fragments $\leq$2 mm were transferred into standard 15-cm^3 BET tubes for surface area measurements.

The measured BET surface areas for three different sizes of specimens of these materials at different total impact energies (or energy densities) are summarized in Table 18. Only fragments passing through 2-mm sieves were put into BET tubes; the fractions of the surface area associated with fragments $\geq$2 mm were not measured. The fractions of surface areas associated with the

*Member of the Analytical Chemistry Laboratory, ANL.

Table 18. Summary of BET-Measured Surface Areas of Pyrex, Simulated Waste Glasses, and SYNROC Ceramics

Specimen			Calculated Impact Energy[a]		BET Surface Area		
Size	ID No.	Material	Density,[b] J/cm^3	Total, J	Measured, m^2	Factor[c]	Corrected to Include >2 mm Particles,[d] m^2
1-in. OD x 1 in.							
	133	Pyrex	1.2	16	0.12	0.82	0.15
	Z92A	SRL 131	1.2	16	0.10	0.82	0.12
	134	Pyrex	2.4	32	0.28	0.91	0.31
	Z89	SRL 131	2.4	32	0.20	0.91	0.22
	135	Pyrex	5	64	0.51	0.95	0.54
	Z88	SRL 131	5	64	0.33	0.95	0.35
	136	Pyrex	10	130	0.78	0.97	0.80
	Z96	Pyrex	10	125	1.02	0.97	1.05
	Z76A	Pyrex	10	125	1.04	0.97	1.07
	Z76B	SRL 131	10	151	0.74	0.97	0.76
	Z92B	SRL 131	10	128	0.60	0.97	0.62
	Z92C	SRL 131	10[e]	121	0.55[e]	0.97[e]	0.57[e]
	Z85	alkoxide	10	130	0.76	0.97	0.78
	Z81	PNL 76-68	10	130	0.67	0.97	0.69
	107AB	SYNROC B	10	146	0.87	0.97	0.90
1 1/2-in. OD x 2 1/2 in.							
	132	Pyrex	0.21	15	----------Did not break----------		
	131	Pyrex	0.43	32	0.33	0.7	0.47

Table 18. (contd)

Specimen			Calculated Impact Energy[a]		BET Surface Area		
Size	ID No.	Material	Density,[b] J/cm^3	Total, J	Measured, m^2	Factor[c]	Corrected to Include ≥2 mm Particles,[d] m^2
	125	Pyrex	1.2	90	0.57	0.82	0.70
	126	Pyrex	1.2	90	0.58	0.82	0.70
	Z102AB	Pyrex	1.2	88	0.76	0.82	0.93
	Z100ABC	SRL 131	1.2	84	0.48	0.82	0.59
	127	Pyrex	2.4	180	1.36	0.9	1.5
	Z102CDE	Pyrex	2.4	177	1.17	0.9	1.3
	Z97AB	SRL 131	2.4	170	0.98	0.9	1.08
1/2-in. OD x 1 in.							
	137	Pyrex	10	32	0.22	0.97	0.23
	138	Pyrex	50	161	0.81	0.99	0.81
	129	Pyrex	100	319	1.45	0.99	1.45

[a]Calculated from height and mass of drop-weight.

[b]Calculated from measured specimen volume and calculated impact energy.

[c]This is the fraction of cumulative surface area for all fragments ≤2 mm, based on lognormal parameters obtained from measured cumulative mass distributions of fragments.

[d]Since only fragments passing a 2-mm sieve were measured in the BET surface area device, the measured BET surface areas were corrected using the fractions calculated from lognormal parameters. This is the best estimate of the surface area of the fracture fragments.

[e]This was an axial impact test; all others were diametral impacts.

fragments <2 mm are shown in Table 18. The missing fractions were determined from the lognormal parameters. These fractions were used to calculate the "corrected" total BET surface areas for all fragments, as shown in the rightmost column of Table 18; the latter surface areas are assumed to best represent the surface areas generated in the impact tests.

Plotted in Fig. 14 are the corrected surface areas for the 1-in. OD by 1-in. size specimens (Table 18). These results show that surface area increases relatively smoothly with increasing impact energy. The results for Pyrex and SRL 131 bound all other measured surface areas. Over the eightfold energy range tested, the surface area increases for SRL 131 glass are ∿20-30% less than those for Pyrex. In previous measurements, respirable particles generated from SRL 131 waste glass were only ∿50-60% of the quantity generated by Pyrex. At the 10 J/cm^3 standard test conditions, the alkoxide and PNL 76-68 waste glasses also generated ∿20-30% less surface area than did Pyrex upon impact (essentially the same as SRL 131 glass). Slightly more surface area may have been generated by the SYNROC B ceramic than by the waste glasses, but less surface area was generated than by Pyrex.

Plotted in Fig. 15 are the corrected BET surface areas for three different sizes of Pyrex specimen as a function of impact energy. There is probably no significant difference between the 2.5-cm OD x 2.5-cm and 3.8-cm OD x 8.9-cm specimens over the impact energy range tested. However, for a given impact energy, the smaller size (1.2-cm OD x 2.5-cm) specimens may generate less surface area than the larger specimens. Further tests are

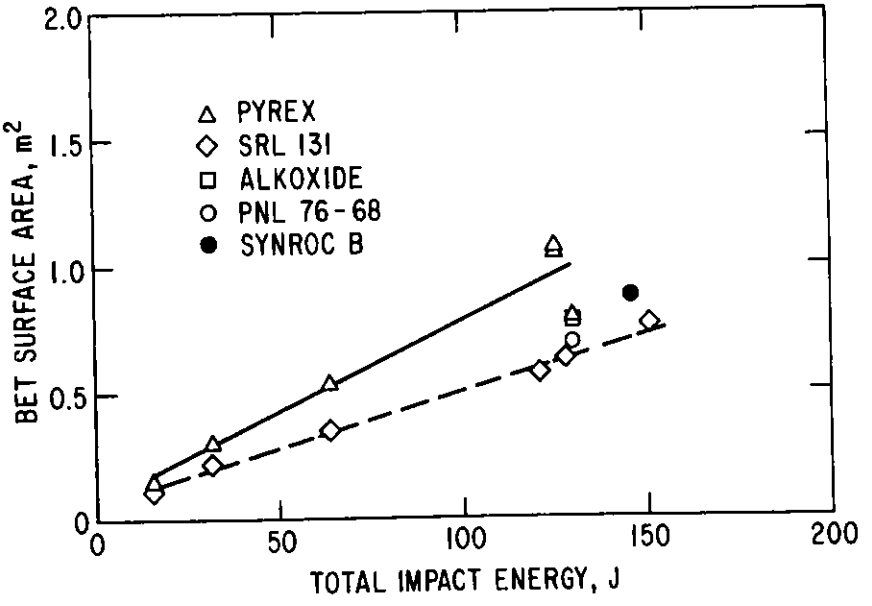

Fig. 14. Measured BET Surface Areas vs. Impact Energy for 1-in. OD x 1-in. Long Specimen of Materials Indicated. There is only one datum point each for the alkoxide PNL 76-68 glasses, and the SYNROC B material.

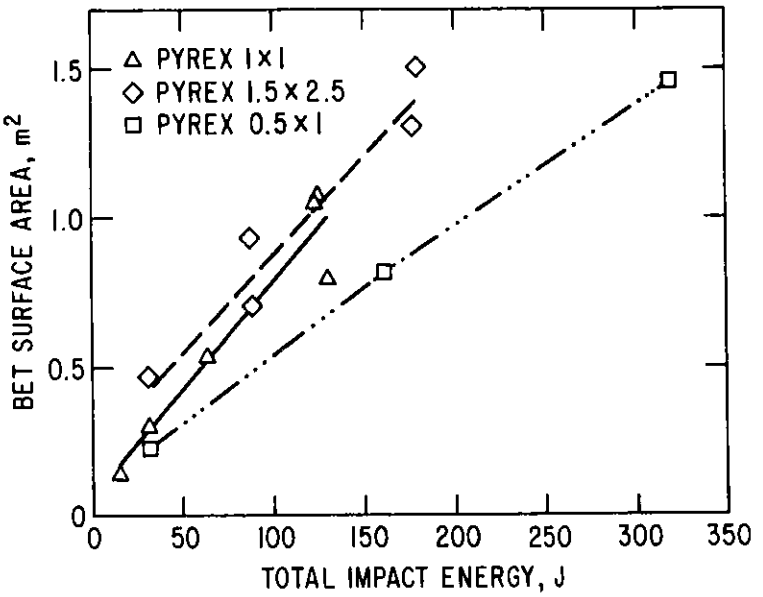

Fig. 15. Measured BET Surface Areas vs. Impact Energy for Pyrex Specimen of Indicated Sizes (specimen dimensions in inches)

needed to establish any significant differences or definite patterns. It is concluded that the specimen sizes do not change the surface area of impact fragments by more than a factor of two.

Figure 16 shows plots of the measured BET surface area for two different sizes of Pyrex and SRL 131 specimens as a function of impact energy. Similarly to the observation for Fig. 14 in relation to 2.5-cm OD x 2.5-cm specimen, it was observed that for a given impact energy, larger 3.8-cm OD x 8.9-cm specimens of SRL 131 glass also produce less surface area than does Pyrex. Further tests are needed to establish definite correlations.

2. Experimental BET Instrument Surface Area "Calibration" Correlations for Range 0.1 m^2 to 4 m^2 Total Surface Area

The objective of these BET measurements was to establish if the Analytical Chemistry Laboratory's Micrometrics Model 2100D BET analyzer could measure samples with total surface areas as low as tenths of a square meter. BET measurements are normally performed on high-specific-surface-area materials and thus on samples with total surface areas of many square meters. The brittle fracture program experiments have generated simulated waste glass and ceramic fragments samples of very low specific surface areas and very low ($\sim$1/2 m^2) total surface areas, which require BET surface area measurements. The performance of the CEN-ACL BET instrument for such samples was still to be evaluated. The measurements described below were undertaken to establish the performance by bounding both the probable accuracy of BET measurements and the precision of BET measurements in the sample size range of 0.1 m^2 to about 3 m^2 total surface area.

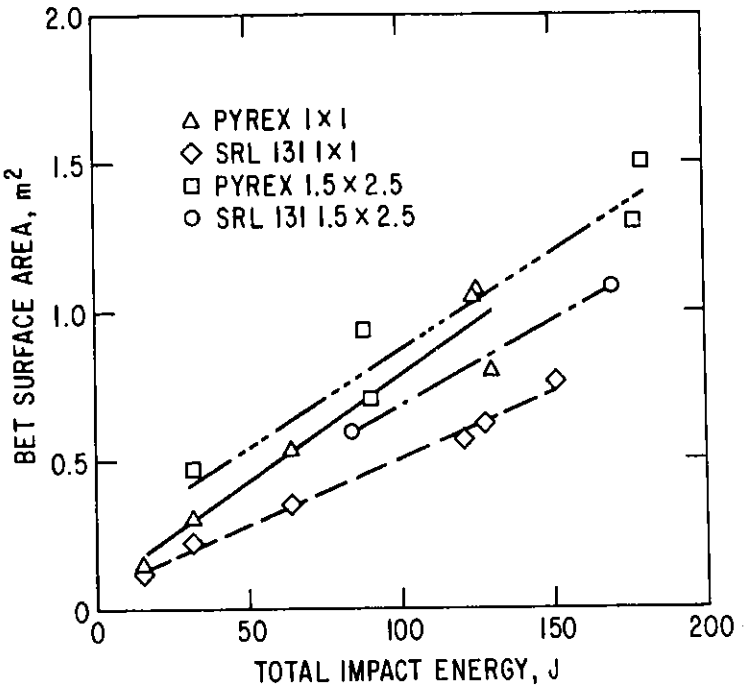

Fig. 16. BET Surface Area as a Function of Total Impact Energy for Two Different Sizes of Pyrex and SRL 131 Glass Specimens (specimen dimensions in inches)

It should be noted that there are no materials for establishing the absolute calibration of BET surface area devices. This is due to the lack of smooth materials that can serve as calibration standards (i.e., the lack of materials with surface roughness on a scale of angstroms, since BET measurements depend on monolayers of krypton gas adsorption). Hence, for our brittle fracture studies, the approach discussed below was defined and used to estimate the accuracy and to determine the precision of BET measurements of samples of $\sim$0.1 m^2 to 4 m^2.

a. Introduction

Materials were sought that could be used as stand-ins for nonexisting calibration standards for the CEN-ACL Micrometrics 2100D BET analyzer. The initial requirements for these materials were that they have shapes whose geometric surface area could be calculated and be of a reasonably high specific surface area such that material with about 0.1 m^2 of surface area could be fit into a 15-cm^3 standard BET measurement tube. The particles also had to be less than about 2-mm diameter so as to fit into the standard BET tubes. Thus, three different types of glasses, each consisting of <120-μm-dia particles of various sphericities were identified and procured--namely, stock No. 299 and stock No. 150 from Duke Scientific Corp. and NBS standard reference material 1003.

Various amounts of these three materials were then used as "quasi standards" for BET measurements. Comparisons of the measured BET surface areas with calculated geometric surface areas, based on measurements of different masses of the materials of assumed specific (geometric) surface areas, allowed correlations of the BET and geometric surface areas to be established.

Two other materials were identified and used to establish the typical precision of the BET device for samples in the operating range of 0.1 m^2 to 4 m^2. One material was a ZnO powder with a well-characterized specific surface area. Glasses were also used to establish the BET measurement precision in two ways: (1) by performing measurements of the same Pyrex fragments at ANL and at an off-site laboratory (Micrometrics) and (2) by performing replicate BET measurements of individual glass samples. Details are presented below.

b. Surface Area Correlations for Glass Monospheres: BET Measured vs. Geometric Calculated

Two sources of single-size glass microspheres, whose BET surface areas could be measured and whose geometric surface areas could be calculated, were obtained from Duke Scientific Corporation. The uniform spheres had a density of 2.45 g/cm^3 and two different diameters, 50.7 ± 1.2 μm (stock #299) and 120 ± 3 μm (stock #150). For these two sizes, specific geometric surface areas were calculated to be 0.052 m^2/g and 0.021 m^2/g, respectively. These values neglect any surface roughness.

Quantities ranging from ∿2 to 19 g of the 50.7-μm glass spheres were measured and transferred into standard BET tubes. The corresponding range of geometric surface areas was ∿0.1 m^2 to ∿1.0 m^2. Table 19 summarizes these values and the corresponding measured BET surface areas. Comparison of these data shows that the BET surface areas were larger than the geometric, being on the average 11 ± 9% larger. These data are also plotted in Fig. 17 and suggest a linear correlation. A solid line, denoted by theory, has also been included which corresponds to the line when the BET surface area equals the geometric surface area. In no cases are the measured BET points smaller than the calculated geometric surface areas. It should be noted that several measurements were made of blanks (i.e., with no material in the BET tube) to establish the BET tube background surface area as 0.02 m^2, which was then subtracted from all the reported measured BET surface areas. Thus, surface areas approaching 0.1 m^2 had a ∿20% correction applied for the BET instrument backgrounds.

Quantities of 120-μm glass spheres ranging from ∿2-1/2 to ∿14 g were also weighed, loaded, and their surface areas measured with the BET device. Because of the small specific surface area and the limited quantities of spheres, the range of the measured geometric surface areas was only 0.05 to 0.3 m^2. Results are given in Table 19 and are also plotted in Fig. 17. The correlation again appears to be linear over the limited range studied. The BET surface areas were always larger (the average being 24 ± 6% larger) than the geometrically calculated areas. SEM examinations of a sample of the microspheres showed them to have minor surface imperfections, which makes plausible the apparently larger BET surface areas than geometric surface areas.

Table 19. Comparison of Measured BET Surface Areas with Calculated Geometric Surface Areas for Glass Microspheres of Uniform Size

Sample		Surface Area		Calculated Deviation,[c] %
ID No.	Mass, g	Calculated,[a] m^2	Measured,[b] m^2	
50.7 ± 1.2 μm spheres				
122-7	1.90	0.098	0.10	0
122-8	2.76	0.14	0.17	22
122-9	3.80	0.20	0.20	0
122-10	5.62	0.29	0.33	14
121-8	8.56	0.45	0.47	5
122-11	13.4	0.70	0.83	19
124-2	19.0	0.99	1.13	14
				11 ± 9 average
120 ± 3 μm spheres				
122-12A	2.44	0.05	0.06	20
122-13	7.47	0.16	0.21	31
120-12B	8.89	0.19	0.24	26
124-1	14.4	0.30	0.36	20
				24 ± 6 average

[a]Calculated areas, assuming spheres of given sizes and a glass density of 2.45 g/cm^3: 50.7-μm spheres have a specific surface area of 0.052 m^2/g and for 120-μm spheres it is 0.021 m^2/g.

[b]Measure with Micrometrics model 2100D BET device using krypton; background of 0.02 m^2 substracted from all runs. Background has been corrected.

[c](Measured - calculated) divided by calculated, times 100.

As shown in Fig. 17, the correlations are nearly linear for both size spheres over the entire measured ranges of 0.1 m^2 to ∿1 m^2. A regression or least squares fit of these data generated the following correlation relations for the two sizes,

$$A_{BET} = 1.16\ A_{Geo} - 0.015 \quad \text{(50.7-μm spheres)}$$

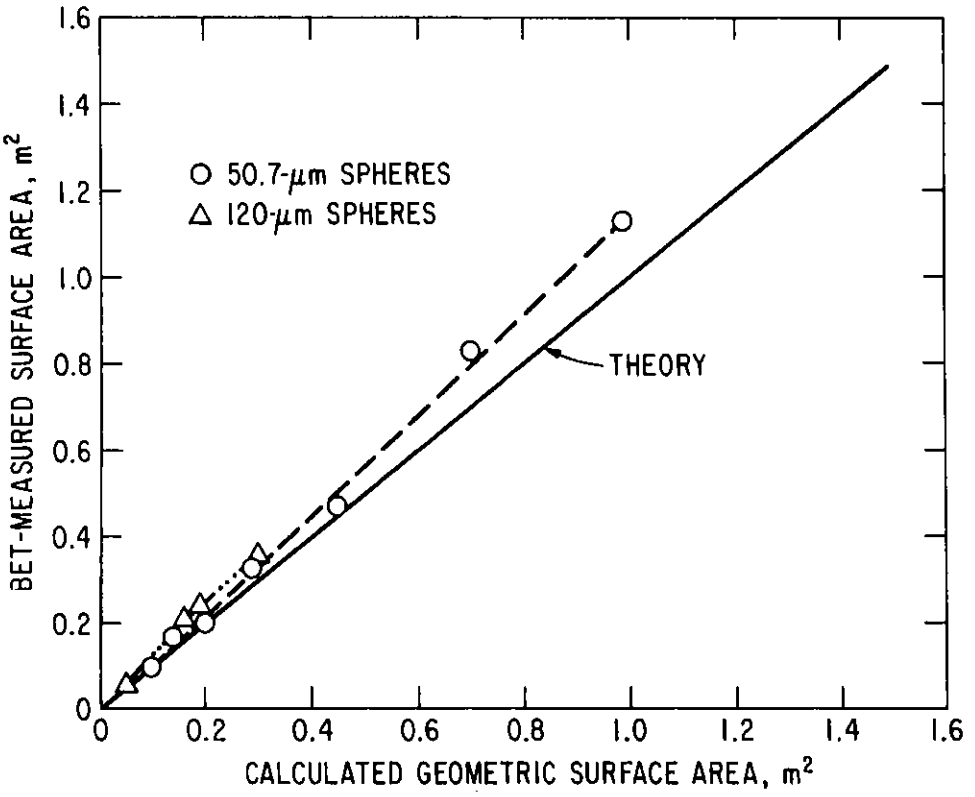

Fig. 17. Correlation of Measured BET Surface Area of Glass Microspheres with Calculated Geometric Surface Area

$$A_{BET} = 1.20\ A_{Geo} + 0.008 \quad \text{(120-μm spheres)}$$

where A_{BET} is the measured BET surface area in m^2, and A_{Geo} is the geometric surface area, neglecting any surface roughness.

It is concluded from these results that the BET surface areas are consistently higher by 10 to 30% than surface areas calculated from geometric factors. A linear correlation was measured over the range of 0.1 m^2 to ∿1 m^2. A surface roughness on the scale of tens of angstroms cannot be estimated. However, as an explanation of these 10-30% deviations, the roughness could exist since the size of krypton atoms is ∿3 Å. Currently, nothing can be stated about the accuracy of these results. No measurements of precision were attempted with this material.

c. Precision of BET Measurements

To establish the precision of the BET measurements over the range of 0.1 to 4 m^2, a source of ZnO (stock #208) having a known (to ±5%) specific surface area of 0.63 ± 0.03 m^2/g was procured from Duke Scientific Corporation. The specific surface area of the ZnO was established to ±5% by

a series of round robin measurements using several types of BET instruments. The ZnO is used for determining the precision of BET measurements, but not their accuracy.

The procedure used to determine BET measurement precision was first, to weigh out different amounts of the ZnO powder of known specific surface area. From the mass of ZnO, the surface area of each sample in the BET tube was determined. Masses were selected to provide samples having 0.06 m^2 to about 4 m^2 total surface area since the objective was to define the precision over this measurement range. More data points were obtained for amounts of ZnO whose surface areas approached the BET instrument background (established in blank runs) of 0.02 m^2.

In Table 20 are given (1) the measured surface areas and (2) the surface areas calculated from the masses of ZnO used and the ZnO specific surface area furnished by the vendor. The same data have been plotted in Fig. 18.

Table 20. Comparison of Measured BET Surface Area with Calculated Geometric Surface Areas for ZnO to Establish Precision

Sample		Surface Area		Calculated
ID	Mass, g	Calculated,[a] m^2	Measured,[b] m^2	Deviation,[c] %
121-2	0.093	0.059	0.05	-17
121-9	0.16	0.10	0.10	0
121-3	0.24	0.15	0.14	-7
121-10	0.32	0.20	0.20	0
121-11	0.49	0.31	0.31	0
122-5	0.79	0.50	0.48	-4
122-6	1.08	0.64	0.65	+2
121-4	1.59	1.0	0.94	-6
-	6.04	3.81 ± 0.18	3.84	+2
				-3 ± 6 average

[a]Calculated surface area based on measured mass and vendor-supplied specific surface area of 0.63 ± 0.03 m^2/g.

[b]Measured with Micrometrics model 2100D BET device, using krypton; background of 0.02 m^2 subtracted from all runs.

[c](Measured - calculated) divided by calculated, times 100.

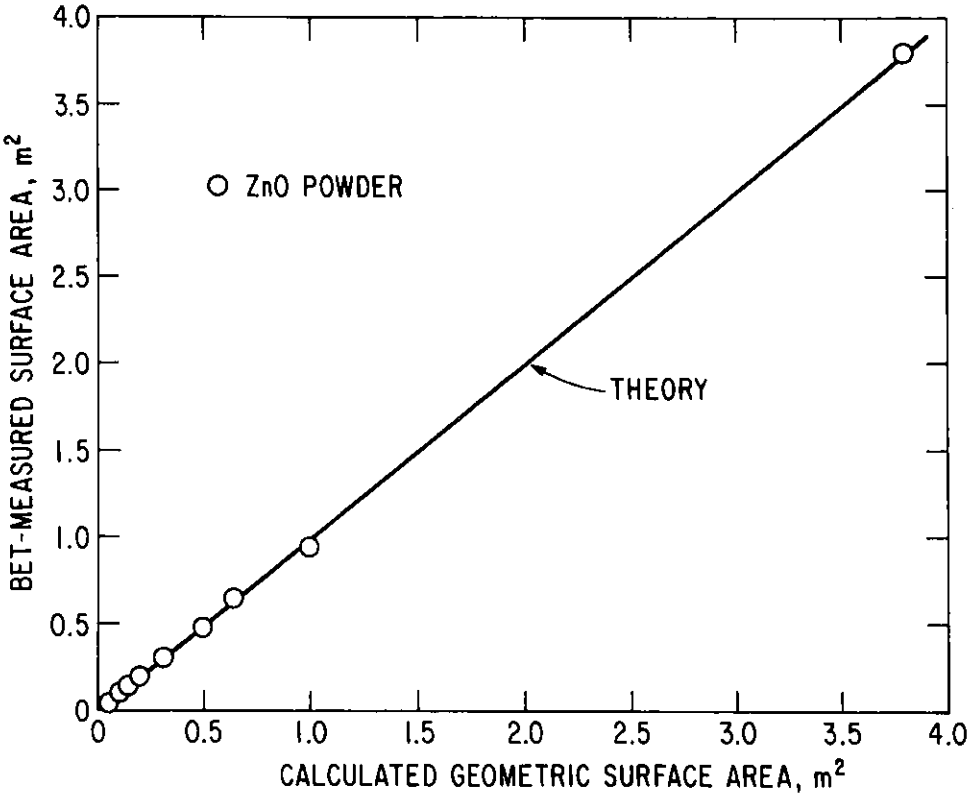

Fig. 18. Correlation of Measured BET Surface Area of Zinc Oxide Powder with Geometric Calculated Surface Area to Establish Precision of BET Measurements

These results show a precision of about ±6% if the single point at 0.05 m^2 surface area is excluded. (This exclusion might be justified since the BET instrument background correction of 0.02 m^2, applied to all points, is a ∿30% correction for this one datum point.) The precision is the same as the given specific surface area uncertainty of ±5%. Hence, it is concluded that BET precision is ±6% when measuring surface areas of ZnO over the range of 0.1 to 4 m^2.

To provide another estimate of the precision of determining BET surface areas, two Pyrex specimens (3.8-cm OD × 6.3 cm long), identified as samples 108-A and 108-B, were each impacted in a separate test with an energy of 181 J (2.4 J/cm^3 energy density) in the sealed drop-weight chamber. The fragments were collected, using dry transfers, and were sieved. Two size fractions collected from specimen 108-A (165.8 g total initial specimen) were a size fraction of <125 μm (labeled 108 A-1) and a size fraction of >125 μm, <500 μm (labeled 108 A-2). These two size fractions were then measured by BET analyses by R. L. Malewicki of our Analytical Chemistry Laboratory, after which they were removed from the CEN-ACL BET tubes and sent off-site to Micrometrics to establish that site's measurements of the BET surface areas of these samples. The two size fractions, labeled 108 B-1 and 108 B-2, from specimen 108-B (158.2 g total initial specimen) were collected and loaded directly into bottles for shipment to Micrometrics for BET analyses.

The results of these measurements are shown in Table 21. The Micrometrics measurements (108 A-1R and 108 A-2R) were done on different sample masses than were those of CEN-ACL (108 A-1 and 108 A-2). The measured specific surface areas and sample masses were used to calculate comparable surface areas (assuming that representative samples were taken), which are shown in the extreme right-hand column of Table 21. The two size fractions agree within ±3% for the larger size fraction and ±12% for the smaller size fraction when the ANL and Micrometric results are compared. This comparison is also a measure of the precision of performing BET measurements at different sites with the same model of BET instrument. However, the uncertainties of obtaining representative samples when the entire sample material has not been measured precludes firm conclusions. The use of either the glasses discussed below (in Section III.B.2.d) or ZnO (described above) gives better, more direct measures of the precision of BET measurement. However, it is encouraging that these two results for Pyrex agree and that the precision is within the same ±6% established for the ZnO measurements.

The Micrometrics BET measurements for specimens 108 B-1 and 108 B-2 also are shown in Table 21. If the two separate 2.4 J/cm^3 impacts and the particle collection methods at the two sites were reproducible, the surface area for run 108 A-1 should agree with that of run 108 B-1, and likewise for runs 108 A-2 and 108 B-2. However, a 20% disagreement is apparent. The disagreement is reduced by perhaps a factor of two if the sum of 108 A-1 and 108 A-2 is compared with 108 B-1 and 108 B-2. This sum type of comparison has less dependence on a good sieving separation but is still dependent on the impact test itself. From these results, it is concluded that the two separate impact tests generated the same surface area within about ±12% for all fragments collected that were smaller than 500 μm.

Estimates of the precision were also made by performing repeated measurements of the same material in the same BET tube, on different days, employing no sample transfers, with the BET operators not informed of the replication. The precision of BET measurements was found to be ±2% for samples with 1 m^2 and 4 m^2 surface areas. Such a precision is claimed by the BET instrument manufacturer. This precision is smaller than ±6% determined with ZnO powder over a much wider range of surface areas--i.e., 0.1 m^2 to 3 m^2. However, the quoted uncertainty in the ZnO specific surface area itself was ±5%, which means that a ±2% precision may be achievable in BET measurements.

d. Other Materials Examined for Surface Area Calibration Correlations

Glass beads (NBS Standard reference material 1003) in the size range 5-30 μm were procured from the National Bureau of Standards (NBS). The microscopically characterized glass beads were intended for calibrating equipment and methods for sizing particles in the range of 5-30 μm. The use of these beads for BET measurements is not recommended by the NBS. However, these beads were studied using BET measurements since they represent a source of glass fragments whose shapes are somewhat geometrically characterized. Of the beads, 96% were stated to be spheres and have an average specific gravity of 2.39 ± 0.01 g/cm^3. The specific surface area based on NBS microscopic measurements was stated to be 0.173 ± 0.005 m^2/g; there were 500,000 to 600,000 particles per milligram. Some of the beads contained gas voids (i.e., were partially hollow) according to the NBS literature.

Table 21. BET Surface Area Results for Pyrex Specimen (3.8-cm OD × 6.3-cm long). Impaction: 181 Joules (2.4 J/cm^3).

Specimen	Site[a]	Sample Measured[b] Mass, g	Specific Surface Area, m^2/g	Surface Area,[c] m^2	Total Specimen Mass, g	Total Specimen Surface Area,[c] m^2	
Size <125 μm							
108 A-1R } d	Micro	2.176	0.21	0.46	2.263	0.48	<0.51±0.03>[d]
108 A-1 } d	ANL	2.249	0.24	0.54	2.263	0.54	Avg
108 B-1	Micro	2.194	0.27	0.59	2.3116	0.62	
Size <500 μm, >125 μm							
108 A-2R } d	Micro	3.180	0.044	0.14	8.291	0.37	<0.36±0.01>[d]
108 A-2 } d	ANL	8.304	0.043	0.36	8.291	0.36	Avg
108 B-2	Micro	2.69	0.041	0.11	7.968	0.33	

[a]The site performing a BET measurement (using krypton) was either Micrometrics (Micro) or CEN-ACL.

[b]For some samples, only a part was measured. The actual sample size and its specific surface area are given. From these, surface area may be calculated.

[c]Includes a background subtraction of 0.01 m^2 from Micrometrics values and a 0.02 m^2 subtraction from ANL values.

[d]The same material from an impacted specimen was measured at two different sites; comparison of the results allows BET precision to be estimated to be ±6% or ±3%.

Eight samples weighing from 0.7 to about 18 g were put into standard BET tubes, and their surface areas measured. The calculated surface areas based on the NBS specific surface area provided ranged from 0.1 m^2 to 3 m^2.

SEM examinations of this material revealed that many spheres were hollow and broken, perhaps as a result of the thermal cycling used in the BET measurements (i.e., heating to outgas and cooling with liquid N_2). These SEM observations are consistent with (1) larger BET surface areas than would be based on the single NBS specific area value and (2) a larger deviation than that determined for the uniform microspheres described in Section III.B.2.a.

These BET data did not allow any conclusions to be made on the accuracy of the BET measurements. A linear correlation was established over the entire measured range of 0.1 m^2 to 3 m^2, but the BET-measured surface areas were consistently about 30-40% larger than the calculated geometric surface areas.

A source of reportedly spherical glass beads of optical glass was procured from Potters Industries. They were type "H" series spheres of sizes <200 mesh or <75 μm (stock No. H-002). The density of the beads was 4.493 g/cm^3. The beads were mechanically sieved into three size fractions of 20-30 μm, 45-53 μm, and 63-75 μm. The corresponding specific surface areas were calculated from average diameters of these three size fractions as 0.054 m^2/g, 0.0276 m^2/g, and 0.0196 m^2/g, respectively.

Different masses of these different fractions of sieved glass beads were then weighed out and loaded into standard BET tubes for surface area measurements. The 20-30 μm spheres were measured to have surface areas ranging from 0.1 m^2 to ∿0.9 m^2. The measured BET surface areas were uniformly larger (an average of 12 ± 3% larger) than the values based on the calculated (geometric) specific surface areas.

In the measurements of various quantities of 45-53 μm spheres, the surface areas ranged from 0.1 m^2 to ∿1.3 m^2; krypton was used for the BET determinations. The results show that the BET surface areas were consistently ∿30% larger than the geometrically calculated surface areas and are uniform over this entire range.

There were only two samples of 63-75 μm fraction beads, one of 0.1 m^2 and one of 0.6 m^2. These limited data gave measured BET surface areas ∿60% larger than the geometrically calculated surface areas.

From microscopic observations, broken and undersize beads were observed in all three size fractions. In a 20-30 μm size fraction sample, ∿8% by number count were either broken or undersized. In the 45-53 μm size fraction sample, ∿28% by number count were either broken or undersized. Such an observation is consistent with the smaller deviation from the calculated surface areas for the 20-30 μm sizes (±12%) than for the 45-53 μm sizes (±30%).

From all of these data, it is concluded that the BET measurements are consistently larger than the geometrically calculated surface areas by 12 to 60%, depending on the size fraction examined. Microscopic examinations show that the smaller size fractions have the smallest number of broken spheres and have measured surface areas with the smallest deviations from geometric surface areas.

3. Characterization of Impact Fragments of SRL 131 Simulated Waste Glass

Fragments of SRL 131 glass from a 10 J/cm^3 standard impact test were characterized using optical microscopy. Micrographs of fragments (Fig. 19) show that smaller particles (<10 μm) definitely are attached to the larger particles. These fragments had been collected from the chamber, using water, and had been wet sieved.

The SRL 131 synthetic waste glass sample was examined in detail to determine if smaller particles (<10 μm) were attached to the larger ones. A sample was anchored to a slide using double-sided tape to immobilize the large particles. A tungsten needle with a tip having a 1-μm radius was used to attempt to detach the small particles visible on the surface of the larger

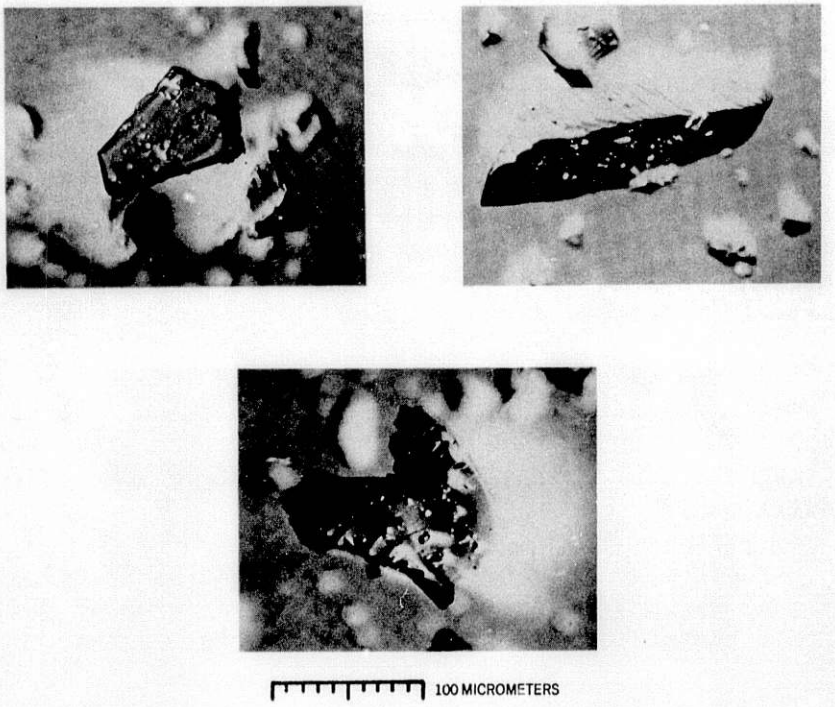

Fig. 19. Fragments of SRL 131 Glass from 10 J/cm^3 Impact Tests Showing Small Particles that Adhere to Larger Fragments

ones. Roughly one-third to one-half of the fines did not detach. This indicates a very strong binding mechanism--probably surface welding or fusion. This attachment was seen preferentially on the flat surfaces of the particles. Stepped surfaces, irregular topography or conchoidal fractures with high surface relief showed little evidence of attachment. Surface fusion (especially with clean, freshly exposed surfaces which result from the grinding of glass) was not uncommon. The adhering particles have a chemistry like that of the large particles, have no precisely defined melt point since glass has a liquid structure at normal temperature, and do not require preferred orientation to effect fusion (as is the case for crystalline materials). Then, too, there is the possibility of locally high temperatures as the particles collide during drop-weight impact. The latter possibility will be examined theoretically.

4. Conclusions

BET surface area measurements were performed on glass samples of reasonably well-characterized geometric shapes and with geometric surface areas of 0.1 m^2 to 4 m^2. The BET surface areas were consistently higher by ∿10 to 30% than the geometrically calculated surface areas, depending upon the material. Smooth linear correlations of BET-measured surface areas with calculated geometric surface areas were observed. The precision of determining BET surface areas in the above range was measured to be ±2 to 6% (i.e., better

than ±6% and perhaps as good as ±2%). The accuracy of performing BET measurements cannot be defined because of the absence of standards. However, the results for the above three materials, based on the suppliers' material characterizations, coupled with our microscopic characterizations of the materials, indicate that the accuracy is probably in the range of ±10 to 20% for the materials tested.

It is concluded that the CEN-ACL Micrometrics 2100D BET device during krypton adsorbate performs BET surface area measurements to a precision of ±2 to 6% on glass samples having total surface areas ranging from 0.1 m^2 to 4 m^2.

C. Methodology Development and Application
(W. J. Mecham)

1. Introduction

Our methodology of characterization of the impact fracture of brittle waste materials has developed the following principal features:

(1) A standard drop-weight impact test of approximately 2.5-cm by 2.5-cm cylindrical specimens with a 10-kg tup [ANL-81-27; p. 25];

(2) Determination of the lognormal particle size parameters, D_g and σ_g, by combining sieving data and Coulter counter data, which are determined by the size distribution of the fracture particulate in the range, 8 μm to 2 mm;

(3) BET measurement of the total surface area of the fracture particulate, which defines the impact strength of the material (J/m^2) and the mean surface/volume shape factor, α, (dimensionless) for the given D_g and σ_g;

(4) Finite-element modeling of the dynamic stresses as a function of time during the compression stage of impact, whereby strain-energy density, mean stress, and impulse are defined as impact-severity parameters which may be correlated with particle-size parameters for various impact conditions and body sizes.

In principle, a complete characterization of the impact fracture of brittle waste materials in accidents could be provided by this approach. That is, from calculations of impact severity parameters for accident conditions, particle size and surface area parameters (evaluated in small-scale tests) could be used to predict accident behavior. Since these correlations are empirical generalizations, experimental confirmation over the range of conditions of practical interest is required to confirm their reliability. Although the results obtained indicate the utility and economy of this approach, additional experimental evidence with larger size specimens is required to establish the reliability of the overall correlations if they are to be applied to accidents.

In this report, standard impact tests of Pyrex and of SRL 131 simulated waste glass are summarized in order to show how the parameters describing particle sizes and shapes vary with impact energy. Our standard impact test

is a diametral impact; axial impacts have also been made for Pyrex and SRL 131 simulated waste glass at the standard energy density of 10 J/cm^3 to allow comparison of particle size distributions.

Particle size distributions from impact tests of SYNROC in Australia have been reported [RAMM]. These data were analyzed lognormally and were compared with data from our tests with similar material. The Australian particle size measurements were made by a method different from that we use; measurements by this alternative method and four other alternative methods have been compared with our Coulter counter measurements for particles smaller than 90 μm.

Dynamic stress modeling, using a finite-increment computer program, has been initiated to examine the effect of impact conditions and body size and shape on the stresses and durations of the compression stages of impact. This method applies to drop-weight testing, free-fall impact testing, and accident cases. From a range of cases, it is calculated that the principal effect (upon impact severity) of increasing the size of the moving mass is to increase the time during which the body remains compressed before it can rebound. These results will be reported later.

2. Summary of Impact-Characterization Parameters of Standard Impact Tests Made on Pyrex and Simulated Waste Glass

Standard drop-weight impact tests have been made on Pyrex and SRL 131 simulated waste glass specimens over a range of energy densities from 1 to 100 J/cm^3. Three different sizes of cylindrical specimens have been used: 3.8-cm OD by 6.2 cm, 2.5-cm OD by 2.5 cm, and 1.3-cm OD by 2.5 cm length. The principal parameters are: (1) the impact energy/fracture surface area correlation; (2) the respirable fraction; (3) the geometric mean of the particle size (D_g); (4) the geometric standard deviation (σ_g); and (5) the mean surface/volume shape factor (α) for the lognormal particle size distribution defined by D_g and σ_g. Plots of these parameters for Pyrex are shown in Figs. 20 through 24; the same parameters for SRL 131 simulated waste glass are shown in Figs. 25 through 29. These graphs are largely self-explanatory, but a few generalizations are given below:

(a) The principal measures of impact strength are the impact energy/surface area ratios (γ_f/ε) and the respirable fraction, as shown in Figs. 20, 21, 25, and 26.

(b) The geometric mean (D_g) is approximately inversely proportional to energy density, and the respirable fraction is approximately directly proportional to energy density.

(c) The dimensionless standard deviation (σ_g) and the dimensionless surface/volume shape factor (α) are nearly invariant when energy density changes.

(d) The energy density can be used to calculate a mean value (over the whole specimen volume) of the elastic stress, σ, that would be generated in a body fully compressed before fracture. This mean stress (in Pascals) is given by

$$\sigma = (W_i/V_o)^{1/2}/(2E)^{1/2}$$

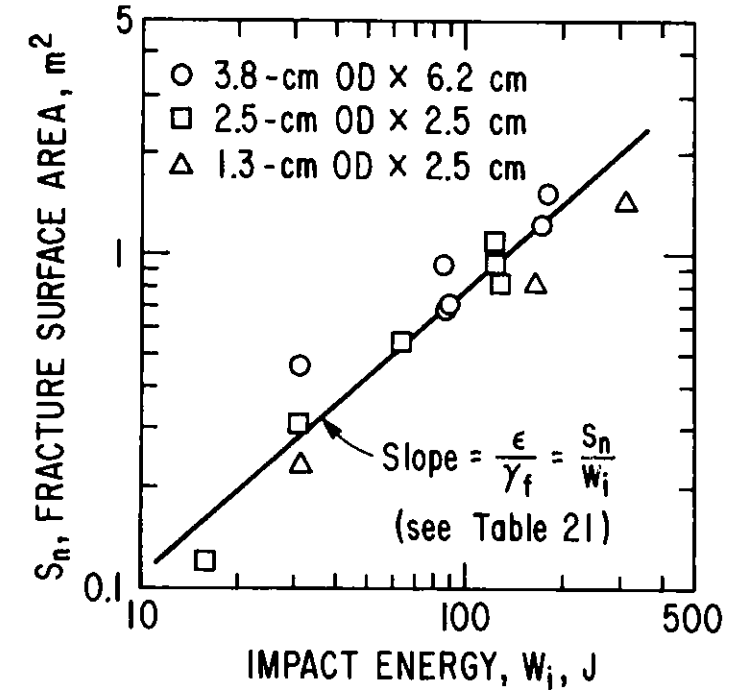

Fig. 20. Pyrex Surface Area vs. Impact Energy for Diametral Impacts. ϵ = energy efficiency. γ_f = impact strength

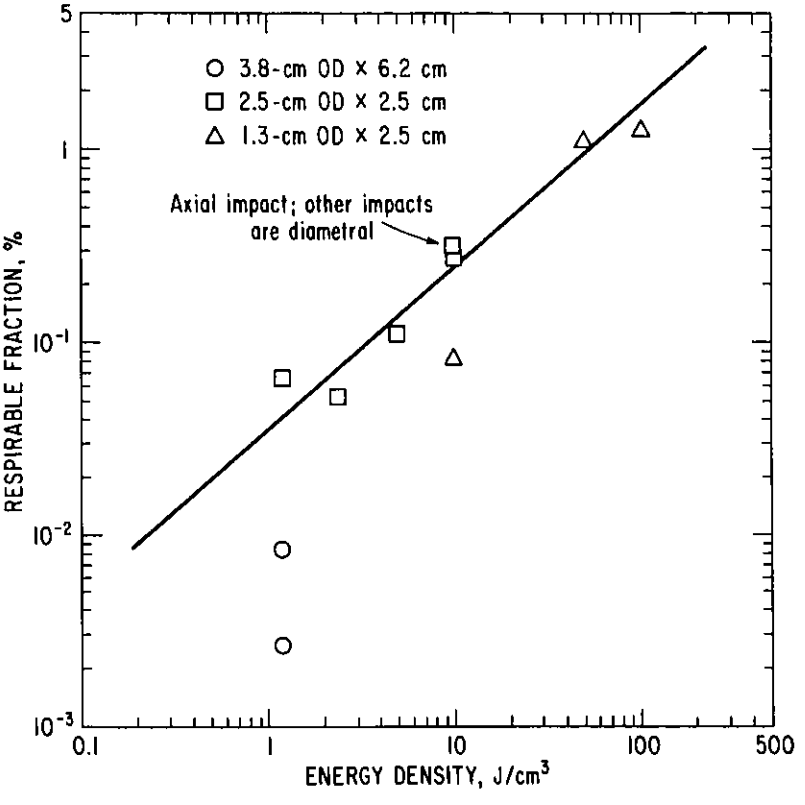

Fig. 21. Pyrex: Respirable Fraction vs. Energy Density

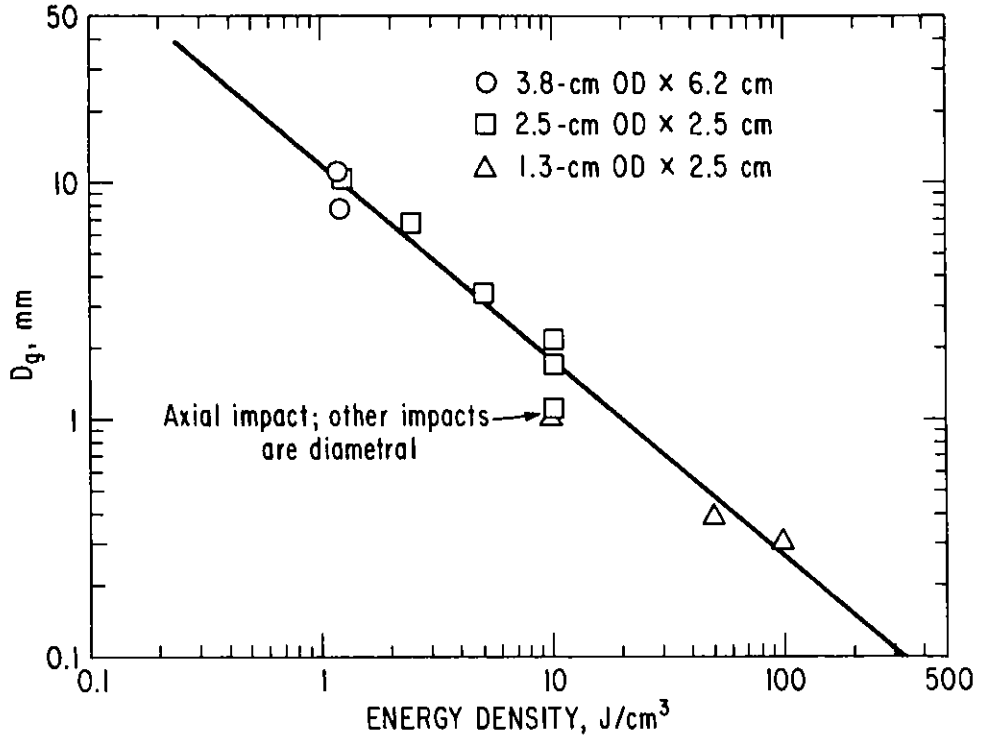

Fig. 22. Pyrex: Geometric Mean of Particle Size, D_g, vs. Energy Density

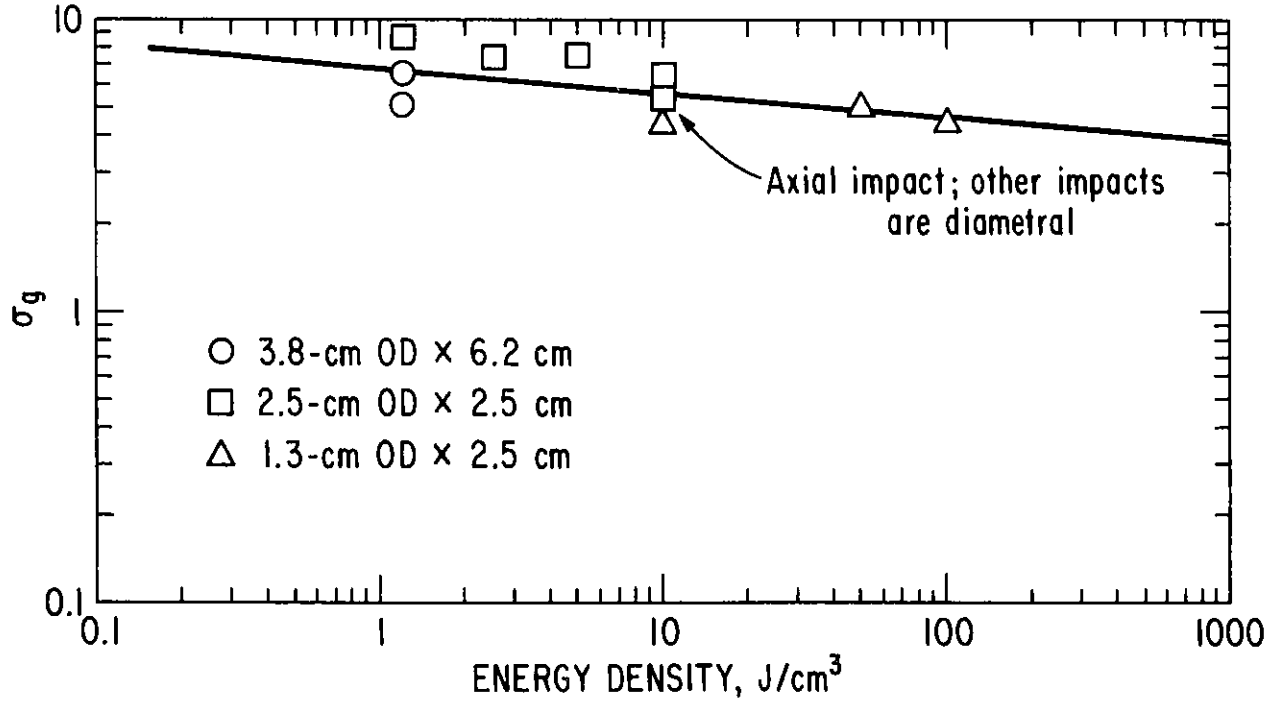

Fig. 23. Pyrex: Geometric Standard Deviation, σ_g, vs. Energy Density

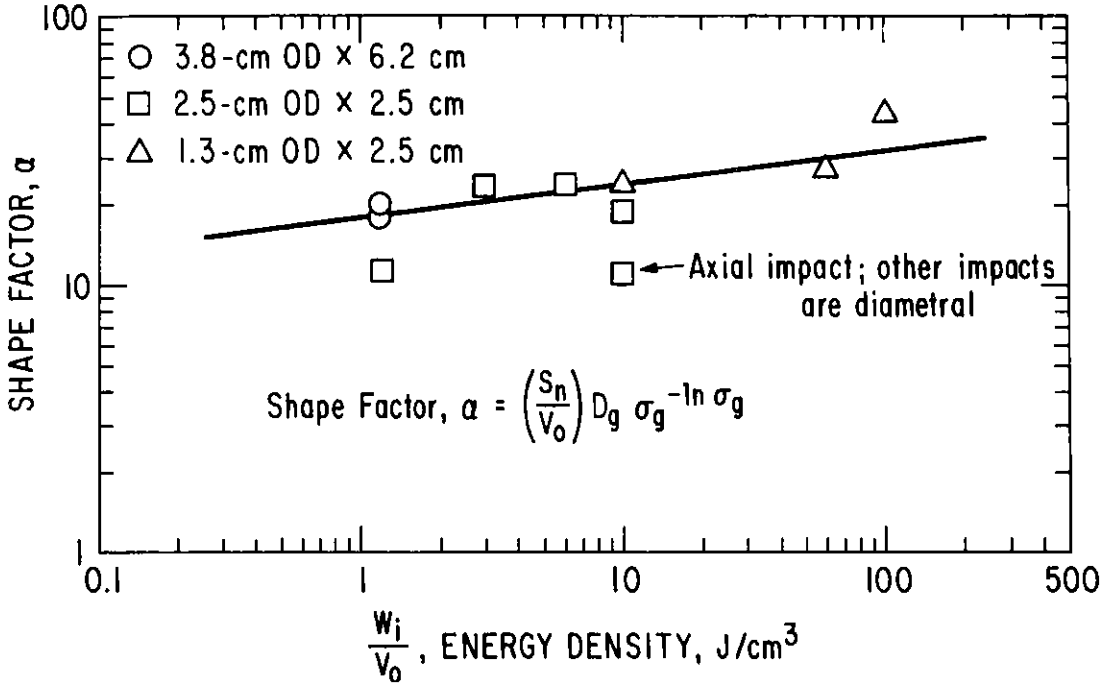

Fig. 24. Pyrex: Mean Surface/Volume Shape Factor vs. Energy Density. V_o = volume of original specimen. σ_g = geometric standard deviation.

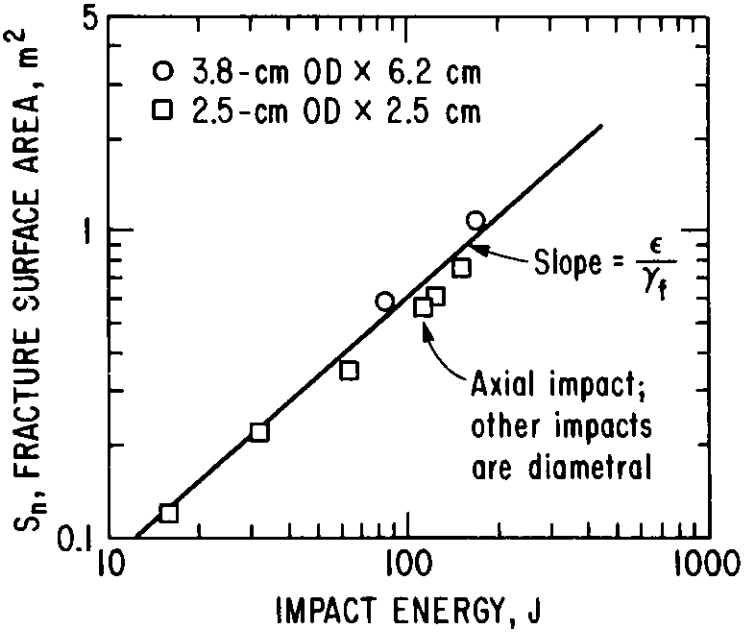

Fig. 25. SRL 131 Simulated Waste Glass: Surface Area vs. Energy Density

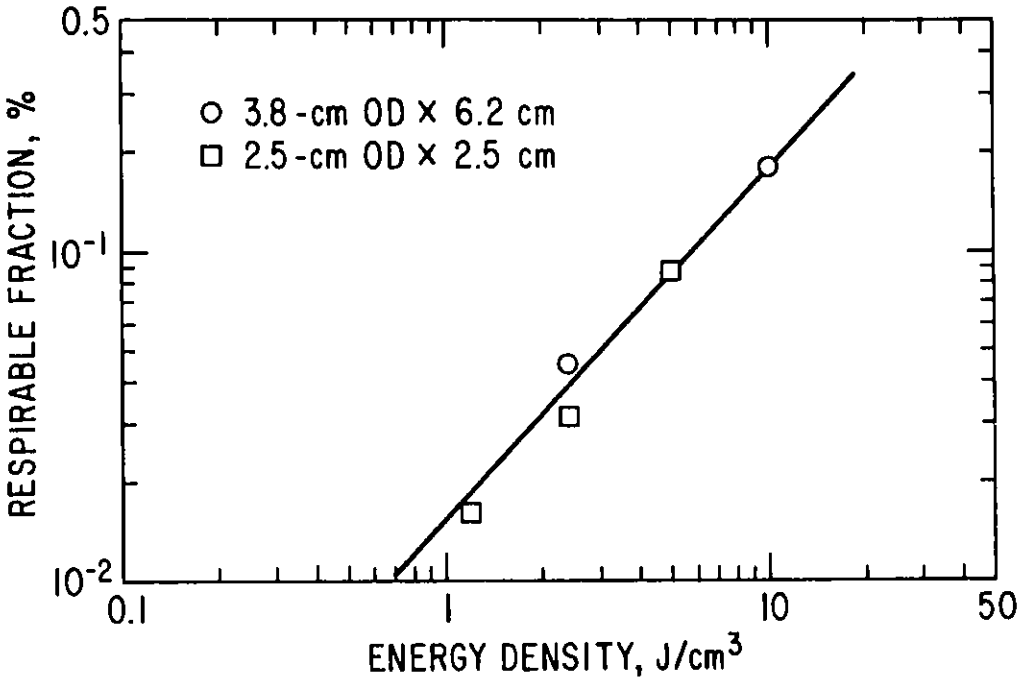

Fig. 26. SRL 131 Simulated Waste Glass: Respirable Fraction vs. Energy Density

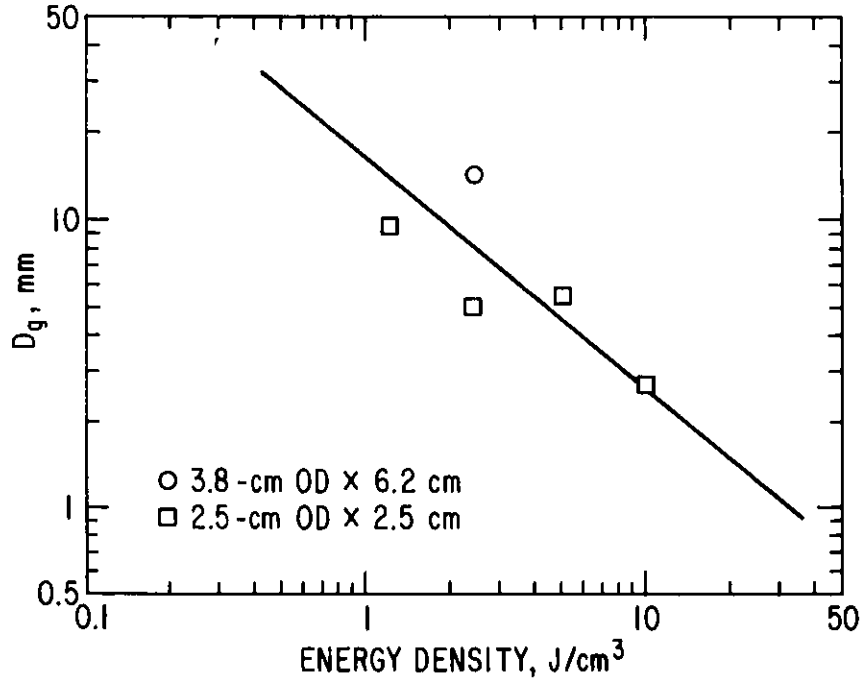

Fig. 27. SRL 131 Simulated Waste Glass: D_g vs. Energy Density

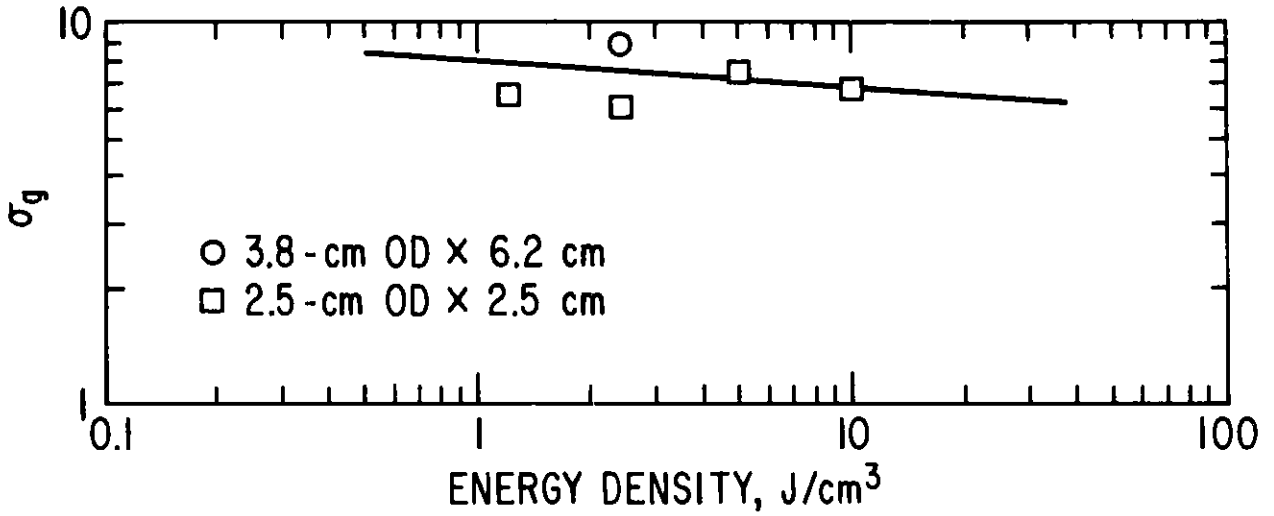

Fig. 28. SRL 131 Simulated Waste Glass: Geometric Standard Deviation, σ_g, vs. Energy Density

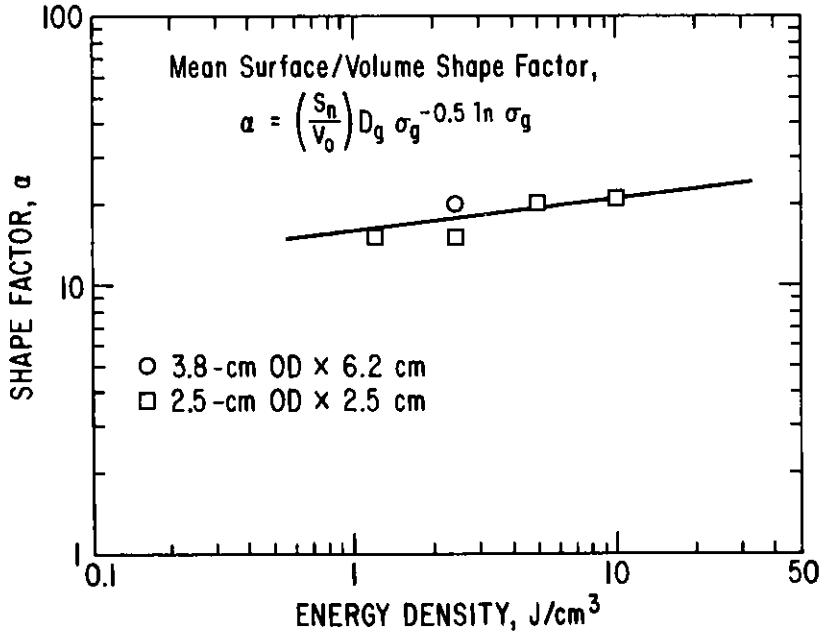

Fig. 29. SRL 131 Simulated Waste Glass: Shape Factor, α, vs. Energy Density

where W_i/V_o is the energy density (in J/m^3) and E is Young's modulus (in Pascals). This mean stress (or the equivalent energy density that is the principal parameter describing impact severity) is the proposed basis for predicting accident effects.

A numerical basis of correlations of impact parameters is shown in Table 22. This table presents global averages for results of the Pyrex and

Table 22. Invariances of Preliminary Correlations of Lognormal Parameters for Fracture Particulates from Drop Weight Impacts over a Range of 1.2 J/cm^3 to 50 J/cm^3 Impact Energy Densities

Parameter Description	Parameter Symbol, unit	Pyrex Tests[a] Mean Value (% Range)	SRL 131 Simulated Waste Glass Tests[b] Mean Value (% Range)
Geometric Standard Deviation	σ_g, none	5.9(+25%-27%)	7.2(+24%-15%)
Product of Geometric Mean and Energy Density	$D_g \frac{W_i}{V_o}$, $\frac{J}{m^2}$	1.6×10^4(+25%-38%)	2.2×10^4(+54%-50%)
Ratio of Respirable Fraction[c] to Energy Density	$\frac{P_v\ (10\ \mu m)}{(W_i/V_o)}$, $\frac{m^3}{J}$	2.0×10^{-10}(+35%-60%)	1.6×10^{-10}(+19%-19%)
Dimensionless Surface/Volume Shape Factor	$\alpha = \frac{a_s}{a_v}$, none	24(+13%-21%)	18(+17%-17%)
Impact Strength	γ_f, $\frac{J}{m^2}$	77[d](assumed)	90[d](+28%-22%)
Energy Efficiency	ϵ, %	56(+40%-29%)[e]	56[e]
Combination Strength Parameter[f]	$\frac{\alpha\ \gamma_f}{\epsilon}$, $\frac{J}{m^2}$	3.3×10^3(+70%-40%)	3.0×10^3(+43%-37%)

[a] 2.4 J/cm^3 to 50 J/cm^3 input energy density.

[b] 1.2 J/cm^3 to 10 J/cm^3 input energy density.

[c] Respirable fraction = P_v (10 μm) = cumulative volume (mass) fraction for all particles smaller than 10 μm.

[d] Assumed for Pyrex, from literature; calculated for waste glass from γ_f and ϵ of Pyrex.

[e] ϵ for Pyrex calculated from an assumed value of γ_f of 77 J/m^2; ϵ for waste glass assumed the same.

[f] Calculated as $(W_i/V_o)D_g\sigma_g^{-0.5}\ln\sigma_g$ from test data.

simulated waste glass tests, together with the extreme range of variation in the tests. Except for the indicated linear correlations of D_g and the respirable fraction with energy density, no attempt was made to provide numerical correlations with energy density. At a given energy density, the variability of the parameters in the table would be smaller than shown. Overall, the variability is usually less than a factor of two, and thus is sufficiently accurate for most accident analyses. However, a demonstration of the scaling laws must be undertaken.

3. Comparison of Various Particle Size Measurements

In order to compare alternative techniques for measuring particle size distributions of particles smaller than 90 μm, identical samples of such particles (obtained for SRL 131 glass specimens that had been impacted in the standard manner) were sent to five different laboratories, and one sample was analyzed with our Coulter counter instrument.

A brief description of the five alternative methods is given below.

1. Micromerograph analyzer used by the Val-Dell Company of Norristown, Pennsylvania. This method is based on Stoke's law of sedimentation velocity in gas. A sample of about 0.1 g is de-agglomerated and allowed to fall through a 3 m column of nitrogen to an electronic servo-balance at the bottom. The relative particle size distribution of the sample is determined from the record of mass accumulation as a function of time. (This method was used for the reported size distribution of the feature particulate of Australian SYNROC, discussed below.)

2. PMS-2000 analysis by Fluid Energy, Inc. of Hatfield, Pennsylvania. This method is based on Stoke's law of sedimentation in liquid and on the measurement of particle concentration by photoextinction. A 10-cm test cell is filled with liquid in which the sample particles are suspended initially in a 0.05% wt concentration. A light beam and associated instrumentation monitors the progress of sedimentation at intervals of one second. A computer program calculates the size distribution and produces a tabular or graph output.

3. HIAC PA-70 analysis by the HIAC/ROYCO Division of the Pacific Scientific Company, Menlo Park, California. This instrument measures the projected area of individual particles as they pass through a light beam. The suspending medium can be an aqueous or organic liquid or a gas; the medium used was water with Ethomeen C-15 dispersant. This is a counting method, like the Coulter counter, but it has a possible advantage in that measurement is not limited to water-insoluble particles as is the Coulter instrument. Both types of counters must cope with the highly irregular shapes of glass particles.

4. Sedigraph analysis by the Micromeritics Instrument Corporation, Norcross, Georgia. This method is based on liquid sedimentation rate, as is the Fluid Energy instrument (method 2 above), except that the Sedigraph uses an X-ray source and a scintillation detector to measure particle concentration in a liquid as a function of time.

5. ELZONE analysis by Particle Data Laboratories, Elmhurst, Illinois. This instrument measures the displacement volume of individual

particles suspended in an aqueous electrolyte as they pass through an orifice. This principle is much like the Coulter counter, except that the ELZONE instrument measures voltage; in the Coulter counter, a current pulse is used. Also, there are some differences in the handling of samples in the two instruments.

The particle size distributions for the sample described, measured by our Coulter counter and the other five instruments, are presented in Tables 23 through 28. Cumulative volume (mass) percent for all particles smaller than a given size is shown normalized to the sample size and also normalized to

Table 23. ANL Coulter Counter Measurement of Particles from Impacted SRL 131 Glass Specimen

Upper D, μm	Sample, cumulative vol %	Cumulative vol %, normalized to V_o
8.0	0.3	1.4×10^{-2}
10.1	0.8	3.7×10^{-2}
12.7	1.9	8.7×10^{-2}
16.0	3.9	0.18
20.2	6.9	0.32
25.4	11.2	0.51
32	17.9	0.82
40	27.4	1.3
51	41.0	1.9
64	58.7	2.7
80	82.0	3.8
102	99.9	4.6

Table 24. PMS 2001 Measurement by Fluid Energy, Inc., of Particles from Impacted SRL 131 Glass Specimen

Upper D, μm	Sample,[a] cumulative vol %	Cumulative vol %, normalized to V_o
5	2.05	0.094
10	4.06	0.19
15	12.8	0.54
20	19.0	0.87
25	26.6	1.22
30	35.3	1.6
40	49.5	2.3
50	63.0	2.9
60	77	3.5
70	88	4.0
80	98.1	4.5
90	100	4.6

[a]As reported by Fluid Energy, Inc.

Table 25. Sedigraph Analysis of Particles from Impacted SRL Glass Specimen at Micromeritics Instrument Corporation

Upper D,[a] μm	Sample,[a] cumulative vol %	Cumulative vol %, normalized to V_o
3.0	0.0	0
5.0	1.0	0.046
10	7.8	0.36
20	21	0.97
30	40	1.8
35	50	2.3
40	60	2.8
50	77	3.5
60	91	4.2
70	97	4.5
80	100	4.6

[a]Read to two significant figures from a clear graph.

Table 26. Micromerograph Analysis of Particles from Impacted SRL Glass Specimen at Val-Dell Co.

Upper D, μm	Sample,[a] cumulative vol %	Cumulative vol %, normalized to V_o
2.4	0	0
4.0	5.6	0.26
6.0	9.0	0.41
10	22	1.0
20	49	2.2
30	68	3.1
40	75	3.4
50	84	3.9
60	89	4.1
80	97	4.5
90	100	4.6

[a]Read from a clear graph to two significant figures.

Table 27. Measurement by ELZONE Method of Particles from Impacted SRL 131 Glass Specimen at Particle Data Laboratories

Upper D,[a] μm	Sample,[a] cumulative vol %	Cumulative vol %, normalized to V_o
4.86	0.1	0.0046
6.61	1.0	0.046
12.25	6.0	0.28
23.57	22	1.0
40.41	50	2.3
64.15	78	3.6
90.73	94	4.3
128.31	99	4.6
181.66	99.9	4.6

[a]Taken from tabular data.

Table 28. HIAC Analysis of Particles from Impacted SRL 131 Glass Specimen at PSA Laboratory

Upper D,[a] μm	Sample,[a] cumulative vol %	Cumulative vol %,[b] normalized to V_o
2.7	0.10	4.6×10^{-3}
3.2	0.28	1.3×10^{-2}
3.8	0.42	1.9×10^{-2}
4.5	0.79	3.6×10^{-2}
5.3	1.32	6.1×10^{-2}
6.2	2.02	9.3×10^{-2}
7.4	3.15	1.4×10^{-1}
8.7	4.79	2.2×10^{-1}
10.2	7.08	3.3×10^{-1}
12.1	10.12	4.7×10^{-1}
14.3	14.04	6.5×10^{-1}
16.3	19.24	9.1×10^{-1}
19.9	26.35	1.2
23.4	33.84	1.6
27.6	43.98	2.0
32.6	54.48	2.5
38.5	66.40	3.0
45.4	78.06	3.6
53.6	88.57	4.1
63.2	95.64	4.4
74.6	99.21	4.6
88.1	99.83	4.6
103.9	100.00	4.6

[a]Transcribed from tabular data.

[b]Renormalization factor: 0.046.

the total mass of the impacted specimen. The cumulative volume percentages for the samples are plotted on linear coordinates in Fig. 30. The cumulative volume percentages normalized to the impact specimen volumes are plotted in Fig. 31. The curve in Fig. 31 is that originally obtained in an impact test (SZ-82, not reported) for these conditions; it represents the particle size distribution defined by the lognormal parameters (D_g = 2.7 mm, σ_g = 6.8; respirable fraction <0.18%) derived from combined Coulter counter and sieving data over the size range, 8 μm to 2 mm. Because impact fragmentation follows the lognormal probability law, the use of lognormal size parameters compensates for insensitivity of the Coulter counter to particles smaller than about 10 μm.

Figure 30 shows that the ELZONE instrument has an insensitivity to particles smaller than 10 μm, similar to (but less pronounced than) the insensitivity for the Coulter counter. Possibly, a Coulter counter with a smaller orifice would measure particles in this size range more accurately.

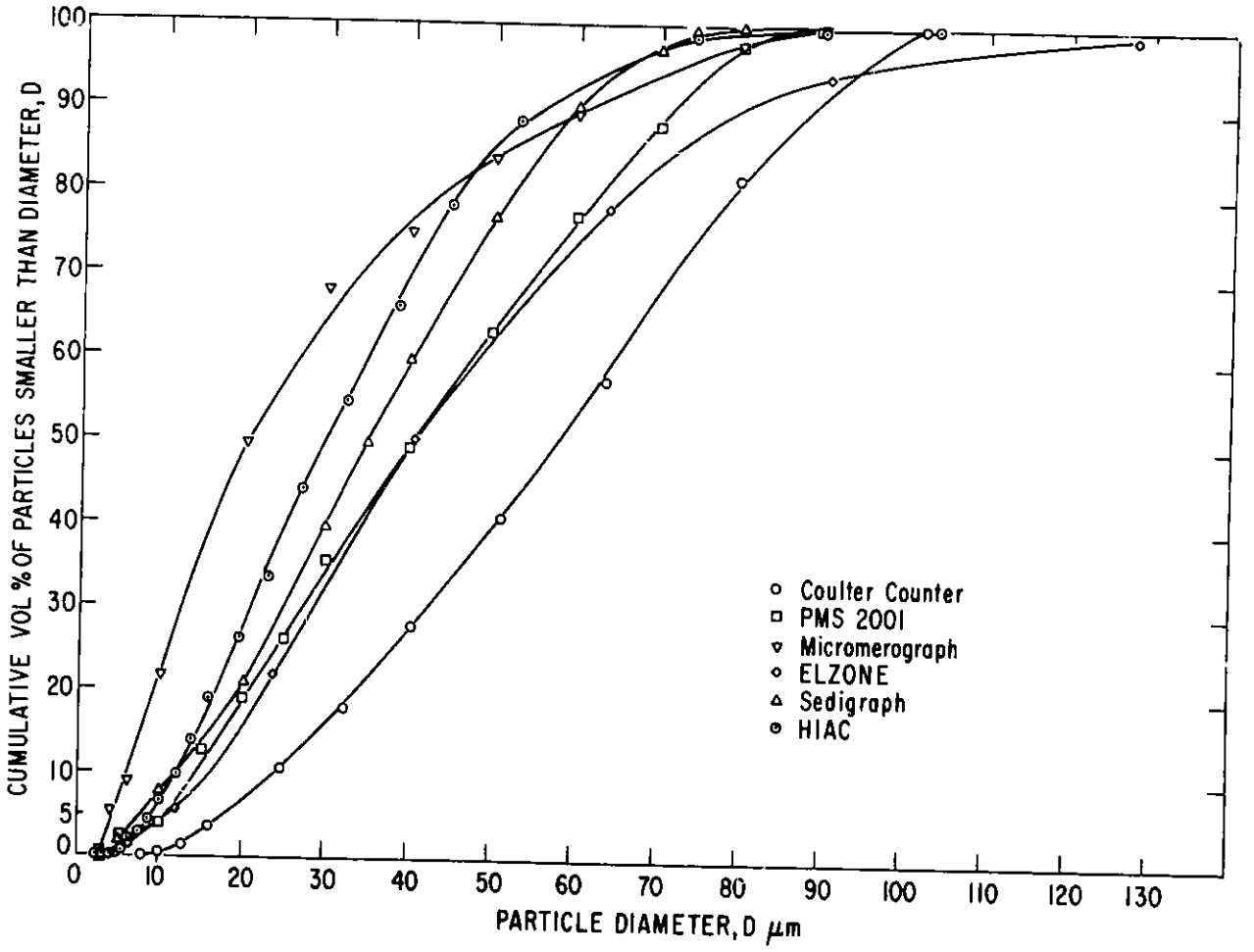

Fig. 30. Comparison of Particle Size Distributions for Six Measurement Methods For Sample Submitted

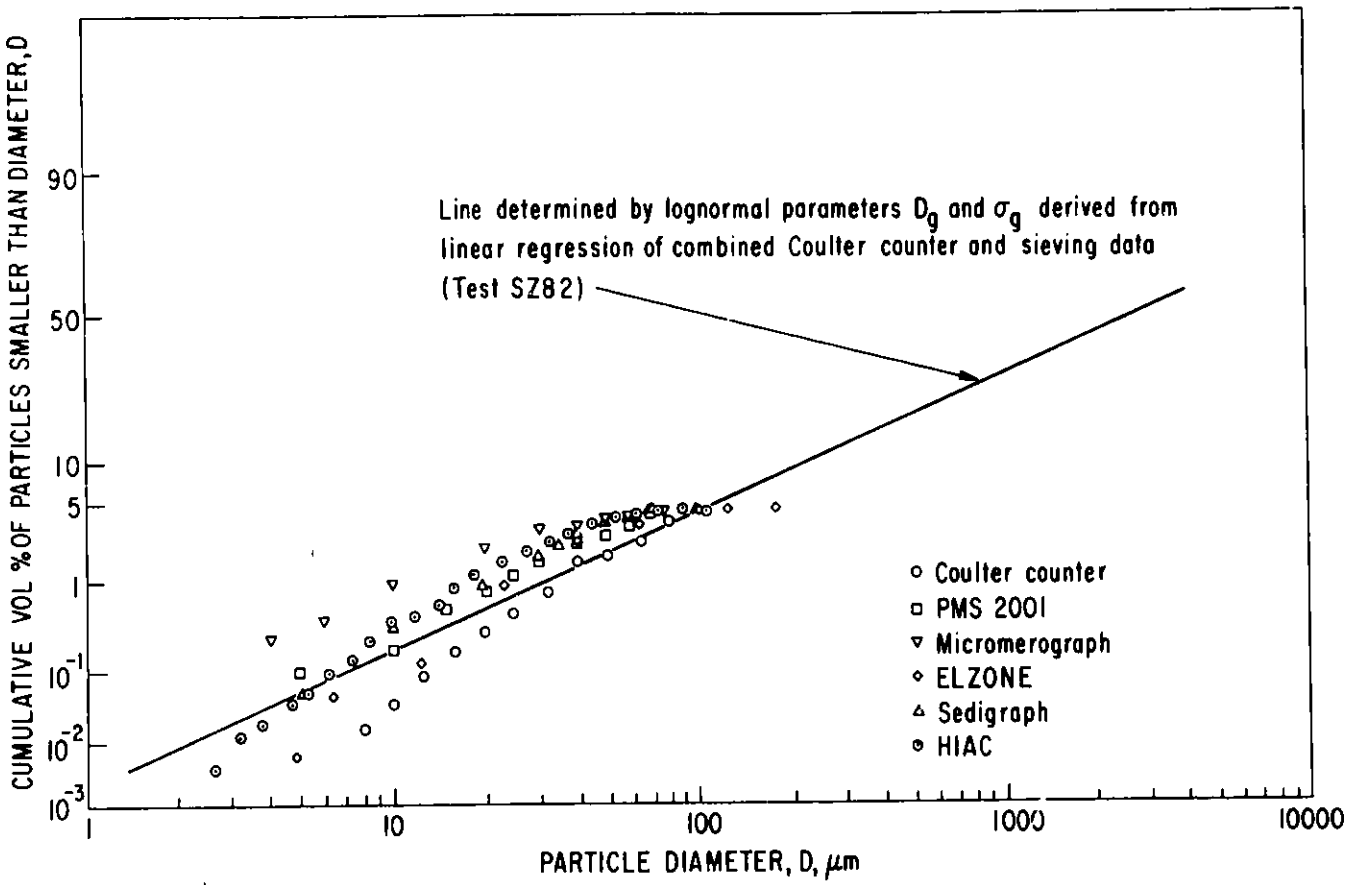

Fig. 31. Particle Size Distributions Determined by Six Measurements Normalized to the Volumes of the Entire Impacted Specimens

In the absence of an absolute standard, the methods whose data points lie close to the lognormal straight line appear to be the most reliable for this size range. These are the ELZONE, PMS 2001, Sedigraph, and HIAC methods, although the HIAC method seems to produce higher values than the other methods for particle sizes above about 50 μm (Fig. 30). Overall, the agreement seems quite reassuring for characterizing particles as irregular in shape as those produced by the impact fracture of glass.

A review was made of the use of electron microscopy for the measurement of submicron particles. This is probably the only way to measure particles as small as 0.01 μm. Possibly, the HIAC counter could be utilized along with imaging from a transmission electron microscope to measure these particle sizes. At the Applied Mathematics Division, an image-analyzing computer, ALICE, is available.

4. Comparison of Axial and Diametral Impacts

In our standard drop-weight impact test, a 2.5-cm-dia by 2.5-cm-long cylindrical specimen is impacted (diametral impact) with a 10-kg striker tup at an energy density of 10 J/cm^3. An axial impact test (PD106A) of a Pyrex specimen was made under the same conditions, and the fracture particulate was

measured in the standard manner by sieving, Coulter counter analysis, and some BET surface-area measurements. To allow comparison, the results are shown in Fig. 32 along with the results of two diametral impacts (PD128C and PDZ80/50-53) of Pyrex specimens.

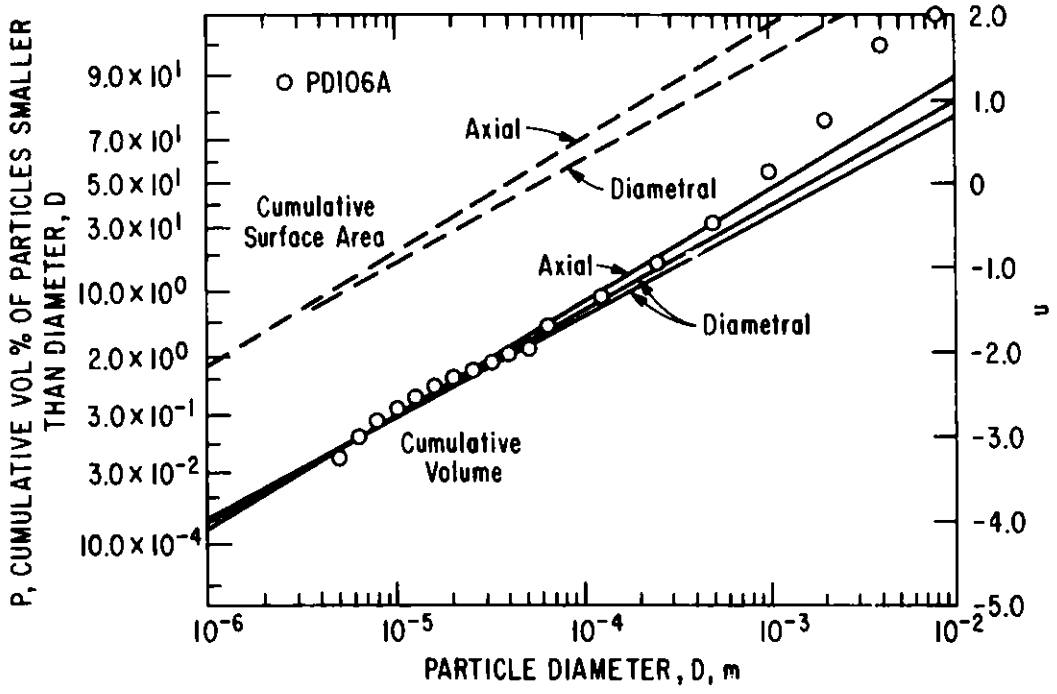

Fig. 32. Cumulative Volume Fractions and Surface Area Fractions for Axial (PD106A) and Diametral (PD128 and PDZ80/50-53) Impacts of 25 mm x 25 mm Pyrex Specimens at 10 J/cm^3.

The parameters in Table 29 are the same as those explained previously. The two diametral impacts agree closely with each other with respect to particle size distribution. This can be seen from the plots of size distributions in Fig. 32. In Table 29, it is seem that the values of σ_g of the replicate diametral impacts agree within 10%, the D_g values within about 25%, and the values of the respirable fraction $P_v(10\ \mu m)$ within about 3%.

The parameters for axial impact and diametral impact tests agree for the respirable fraction, but differ significantly with respect to D_g and σ_g (Table 29). Possibly, the more uniform initial stress distribution in an axially impacted specimen results in smaller σ_g and α, although overall stress averaging keeps the respirable fraction the same. A comparison of the effects of axial and diametral impacts on parameters can also be seen in Figs. 21-25.

Table 29. Particle Parameters for Axial and Diametral 10 J/cm^3 Impacts of 2.5-cm by 2.5-cm Pyrex Specimens

Parameter[a]	Axial (PD106A)	Diametral (PD128C)	Diametral (PDZ80/50-53)
V_n, cm^3	12.9	12.9	12.9
W_i, J	129	129	129
D_g, mm	1.1 ± 37%	2.1 ± 15%	1.6 ± 11%
σ_g	5.6 ± 5%	6.9 ± 3%	6.3 ± 2%
P_v(10 μm), %	0.30 ± 27%	0.28 ± 10%	0.29 ± 8%
S(2 mm), m^2	b	0.78[c]	0.78[c]
P_s(2 mm), %[d]	98	97	98

[a] D_g and σ_g determined for V_n, using all particle size data points between 8 μm and 1000 μm, inclusive.

[b] Pyrex measurement of surface area not available.

[c] BET measurements made on particles from a separate (replicate) impact test.

[d] $P_s(2\text{ mm}) = P(u_v + \ln \sigma_g)$; $u_v = \ln(2\text{ mm}/D_g)/\ln \sigma_g$.

5. Lognormal Size Analysis of the Impact-Fracture Particulate from Australian SYNROC

The impact behavior of SYNROC has been reported by Australian workers [RAMM]. Machined cylinders (12.5 mm by 12.5 mm) were impacted axially at 217 J, using a hardened-steel punch-and-die device of a type previously used by PNL. Particle size measurements were made by sieving (down to 63 μm) and by a Micromerograph instrument.* The particle size distributions for three types of SYNROC (SYN 1, SYN 2, and SYN 3) were presented graphically by the original investigators. These plots were read to two significant figures and we replotted the data on lognormal coordinates (Fig. 33). The parameters are given in Table 30. A better lognormal fit was obtained when the two points representing the largest-size particles, 1 and 2 mm, were excluded from the linear regression. The lognormal analysis was based on eight data points in the range of 5 to 500 μm. From Fig. 33, these data points have a lognormal distribution.

From Table 30, it appears that the size distributions of the fracture particulate from the two sintered specimens agreed very closely, showing no effect of the waste addition. The hot-pressed material (with no waste) had a significantly different fracture behavior, showing a higher impact resistance, as indicated by its value for the parameter, $\alpha\gamma_f/\epsilon$, in Table 30. In our Pyrex test at 100 J/cm^3 (not reported), the value of this parameter

*See Section III.C.3 for a description of the Micromerograph analysis.

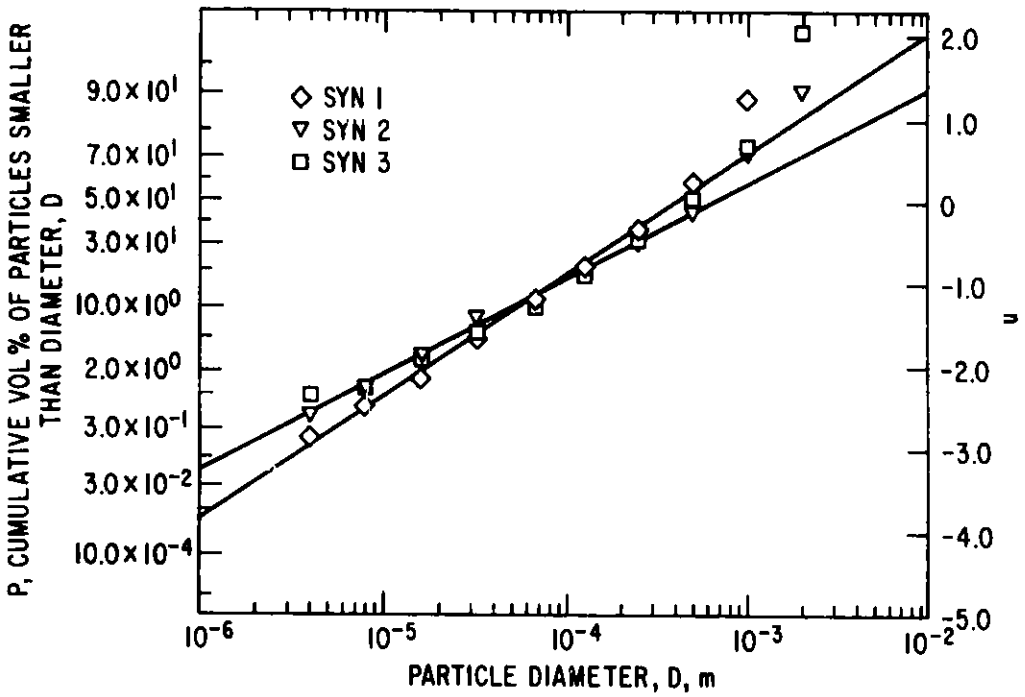

Fig. 33. Cumulative Volume Fractions of Australian SYNROC

Table 30. Lognormal Analysis of Three Types of Australian SYNROC. 12.5-mm x 12.5-mm Cylinders Impacted Axially at 141 J/cm^3

	1250°C Hot Pressed; No Waste Added SYN 1	1300°C Sintered in CO-CO_2; No Waste SYN 2	1300°C Sintered in CO-CO_2; contains 10% waste SYN 3
D_g, mm	0.41(±34%)	0.65(±34%)	0.66(±72%)
σ_g	4.8(±4.2%)	7.3(±5.4%)	7.4(±12%)
P_V(10 μm), %	0.91(±26%)	1.8(±21%)	1.8(±44%)
$\frac{\alpha\gamma_f}{\epsilon}$, $\frac{J}{m^2}$	1.7 x 10^4	1.3 x 10^4	1.3 x 10^4
P_V(10 μm) $\frac{V_o}{W_i}$, $\frac{m^3}{J}$	0.64 x 10^{-10}	1.3 x 10^{-10}	1.3 x 10^{-10}

was 9.3×10^3 J/m^2 and increased with increasing energy density. By extrapolation, it is estimated that the impact strength of SYNROC, as measured by this parameter is about the same as that of Pyrex. A lower value of the respirable fraction correlation parameter (Table 30) indicates greater strength. On this basis, hot-pressed SYNROC is stronger than sintered SYNROC and both are stronger than Pyrex (Table 22). As a first estimate, it appears that sintered SYNROC has about the same strength as SRL 131 simulated waste glass.

6. ANL Impact Tests of SYNROC

Two types of SYNROC were impacted and analyzed by our standard method, and results were compared with similar tests of Pyrex and SRL 131 simulated waste glass. The SYNROC materials were made at Lawrence Livermore Laboratory.

In these tests, 1.3-cm-OD × 1.3-cm cylinders were impacted diametrally at 141 J/cm^3 in a bellows chamber. The chamber was washed out with water after each test to prepare this material for Coulter counter and sieving analysis. The lognormal size distributions are plotted in Fig. 34, and the description of its specimens and the lognormal parameters are given in Table 31.

In conclusion, the range of properties of the Lawrence Livermore Laboratory SYNROC (Table 31) and the Australian SYNROC [RAMM] (Table 30) seems to match closely. Our lognormal analyses give consistent results when compared with standard methods of particle size analysis.

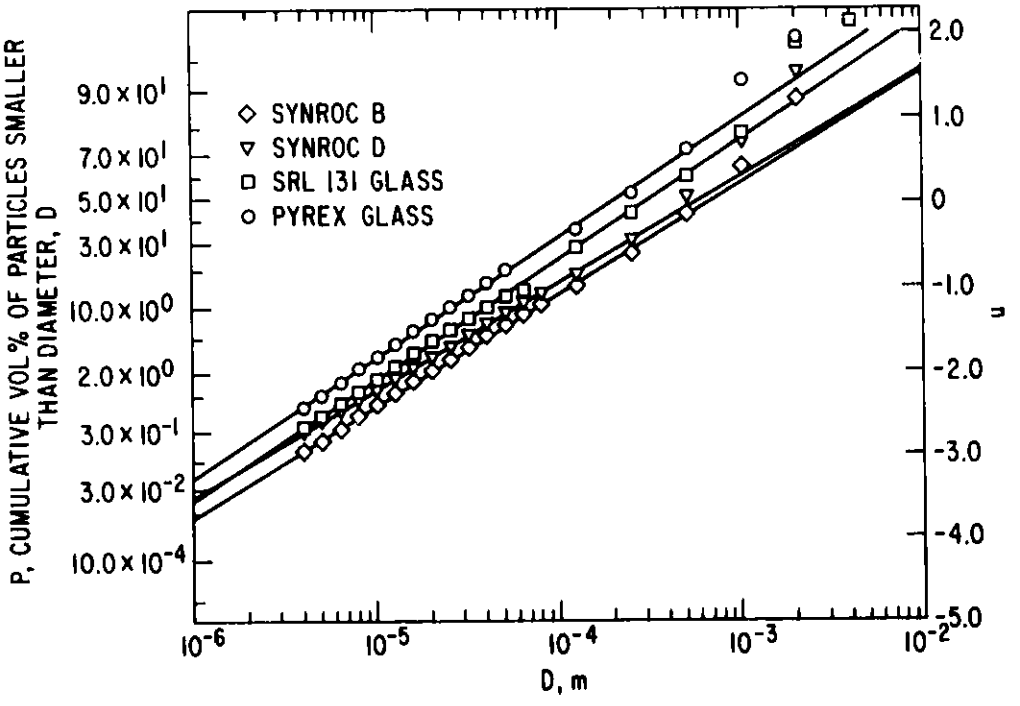

Fig. 34. Diametral Impact of 1.3-cm-OD × 1.3-cm-Long Specimens at 141 J/cm^3 Impact Energy Density of SYNROC, SRL 131 Simulated Waste Glass, and a Pyrex Standard

Table 31. Comparative High-Energy-Density Impact Tests of Four Brittle Materials--Diametral Impacts

Material	Specimen Impacted: Size	Specimen Impacted: Mass, g	Impact Energy,[a] J	Energy Density,[b] J/cm^3	Lognormal Parameters[c]: D_g, mm	Lognormal Parameters[c]: σ_g	Respirable Sizes[d] (<10 μm), wt %[e]
Pyrex	12.65-mm OD × 13.33 mm	3.716	236	141	0.18 ± 0.02	4.7 ± 1	3.2 ± 0.2
SRL 131 Glass[f]	12.78-mm OD × 12.70 mm	4.465	230	141	0.32 ± 0.08	5.2 ± 0.2	1.7 ± 0.3
SYNROC B[g]	12.78-mm OD × 13.96 mm	7.422	253	141	0.59 ± 0.05	5.4 ± 0.1	0.76 ± 0.1
SYNROC D[h]	12.84-mm OD × 13.14 mm	6.693	240	141	0.52 ± 0.03	5.9 ± 0.1	1.2 ± 0.1

[a] Impact energy is maximum available as delivered by dropping a ∿9.9-kg weight onto a sealed chamber from a ∿1.3-m height.

[b] Energy density calculated from the maximum available impact energy and the initial specimen dimensions.

[c] Lognormal parameters of fracture particulates, obtained by computer regression analysis of measured size data. D_g is mass mean diameter and σ_g is geometric standard deviation of measured particle size distribution. Errors are from best fit of data and a regression analysis.

[d] Respirable size is arbitrarily defined for this study as the cumulative amount of all particles smaller than 10 μm diameter, as measured by Coulter counter and mechanical sieving procedures.

[e] Value is obtained from computer analysis of the data from one impacted specimen and is illustrated by data in Fig. 30. The wt % is in reference to the total initial specimen mass.

[f] SRL 131 specimens (28 wt % waste) were core-drilled from an annealed piece of SRL 131 simulated waste glass that had been remelted.

[g] SYNROC B (no waste) was core-drilled from a bulk piece supplied. Density was reported to be 4.2 g/cm^3 (96% T.D.).

[h] SYNROC D (64 wt % waste) was core-drilled from a bulk piece by LLL. Density was reported to be 3.96 g/cm^3 (99% T.D.).

IV. ROCK-WATER INTERACTIONS
(M. G. Seitz and D. L. Bowers)

A. Introduction

Work this quarter was performed in two programs.

Work in the program on nuclear logging consisted of core-flood experiments to test oil-reservoir logging with gamma-emitting radionuclides.

In work performed in the Laboratory Analog Program for the Nuclear Regulatory Commission, bentonite material was tested for possible use in the analog experiments. In addition, laboratory treatments are proposed that will age the repository materials for use in testing the performance of an old repository.

B. Core-Flood Experiments

Experimental work performed this quarter centered on performing core-flood experiments to test whether the oil content of rock can be determined from its gamma signal after a radioactive fluid is injected into the rock. In the proposed method of logging a reservoir, the radioactivity of the reservoir is first measured using a gamma-sensitive probe. The reservoir is then injected with water containing a gamma-emitting radionuclide, and the reservoir is logged again with the probe. Differences in the measured radioactivities can be related to the residual oil saturation of the reservoir.

A program designed to test this concept consists of an experimental series (described in detail below) with two sets of cores, one set having a known residual oil saturation and the other set having zero residual oil saturation. The cores (in rock-core holders) are injected with a water solution containing the gamma-emitting radionuclide, sodium-22, and then the gamma-ray signals from the two sets of cores (detected outside the cores holders) are compared to determine the net signal resulting from the residual oil in the cores. Gamma-ray signals have been measured for many different volumes of radiochemical fluid injected in the cores. The experiments will be duplicated to reduce the effect of different physical and chemical characteristics of the rock cores.

In one experiment, cores of Berea sandstone, 6.830 cm in diameter by 14.605 cm long, were saturated with water (two cores) or oil (two cores) in preparation for the experiments. The cores were immersed in liquid (either water or oil); then the atmosphere was removed from above the liquids by placing the submerged cores in a vacuum jar and evacuating the air from the jar. This expanded the air in the rock pores and allowed it to bubble to the surface.

Next, the cores were allowed to stand submerged at atmospheric pressure for several days. Continued absorption of fluid occurred during the first two days as indicated by lowering of the liquid level above the cores. The vacuum jar above the submerged cores was reevacuated, brought back to atmospheric pressure, and then the cores were removed from the liquid and weighed to determine liquid saturation. Results for the four cores are listed in

Table 32. The porosities calculated by fluid saturation are very close to the 21.0% porosity calculated from the densities of the sandstone (2.098 g/cm^3) and the mineral quartz (2.655 g/cm^3).

Table 32. Liquid Saturations and Calculated Porosities of Four Cores of Berea Sandstone

Description	Weight of Saturating Liquid, g	Calculated Sandstone Porosity,[a] %
	Water Saturation	
Bottom of Column 2	116.64	21.8
Top of Column 3	115.02	21.5
	Oil Saturation	
Top of Column 2	104.01	21.8
Bottom of Column 3	104.85	22.0

[a]The water was assumed to have a density of 1.000 g/cm^3. The density of the oil was measured to be 0.891 g/cm^3. The cores have a geometric volume of 535.1 cm^3 each.

A solution representative of groundwater in a sandstone reservoir was prepared by dissolving chemicals in distilled water and filtering the residue. The solution contained eight elements or compounds at concentrations representative of groundwater from a sandstone oil reservoir. The solution composition is shown in Table 33. A portion of the solution was made radioactive by adding 60.2 μCi of ^{22}Na to 1784 g of solution (3.37 x 10^{-2} μCi/g).

Multichannel analyzers were set up to record radioactive levels and counting times on paper tape; the paper tape is used to create data files in the Argonne computing facilities. Data logging facilities have been set up, using a Digital PDP 11-23 processor with disc storage of data. This facility will be used to record fluid pressures in core-flood experiments. The electronics, scintillation detectors, and hydraulic plumbing have been configured.

Experiments were run with two cores, one with a known residual oil saturation and the other with zero residual oil saturation. The cores were injected with water solution containing the gamma-emitting radionuclide, sodium-22, and the gamma-ray signals (detected outside the core holders) were compared in order to determine the net signal attributable to the residual oil in the cores. The gamma-ray signals were measured following the injection of many different volumes of radiochemical fluid. This fluid was injected at a rate of 0.9 to 5.0 mL/min into cores having a 6.9-cm-dia cross section and 21% porosity.

Table 33. Constituents of the Simulated "Groundwater" Used in the Core-Flood Experiments

	Concentration,[a] mg /L
Na^+	7788
Mg^{2+}	240.8
Sr^{2+}	7.30
Fe^{3+}	22.50
Cl^-	11005
CO_3^{2-}	60.6
SO_4^{2-}	1599
HCO_3^-	615.4
Total	21340[b]

[a]Chemicals were dissolved in distilled water.

[b]This compares with 30220 mg/L total solids in the "average" sandstone reservoir fluid, calculated using about 10 analyses from Dowell, U.S. Geological Survey, Gulf Oil Corp., and the Indiana Geological Survey.

The results indicate a substantial difference in the gamma signals from the cores with and without oil. The maximum gamma-ray signal at the detector for the core with 40% of its pore volume containing oil was 2.00 counts per second, whereas the core containing no oil produced a signal of 3.15 counts per second. Therefore, a 36% reduction in gamma signal was observed in the presence of oil. The gamma-ray signals were independent of fluid injection rate.

These experiments will be repeated to examine the effect of variations in the rock core material. The results will be evaluated to determine whether the resulting signal is substantial enough to overshadow uncertainties in gamma-ray-intensity measurements that are expected under field conditions.

C. Laboratory Analog Experiments

In the laboratory experiments, technical progress included (1) obtaining rock cores from the basalt blocks and (2) testing the engineered barrier for leach properties. In addition, laboratory treatments are proposed for "aging" of repository components for use in analog experiments.

1. Rock Cores

Rock cores were obtained from basalt blocks by coring the rock, then grinding the cylinders to the size required for the core holders. One rock core was tested and was found not to conduct water. The cores, consequently, will be split prior to use in the experiments.

2. Engineered Barrier

Bentonite clay and basalt plus possible additives are suggested as the engineered barrier in the Basalt Waste Isolation Program [TURCOTTE]. Bentonite samples were obtained for the program from American Colloid and from the Minerals Library, University of Missouri, Columbia, MO. The clay was tested to see if it would be a source of fluoride for the water used in the experiments. As part of the screening test, 10 g of clay from American Colloid was leached in 150 mL of stirred, distilled water at ambient temperature for several hours. After mixing, the pH was measured to be 7 (litmus paper). Because F^- is volatile in an acidic media, 75 µL of 12N NaOH was added to prevent loss of the F^- during the following heating step. The resulting pH was measured to be 8. The stirred slurry was then heated to 90 ± 4°C for approximately 17 h, with an occasional addition of water to replace water lost by evaporation. The slurry was cooled and filtered, using Whatman No. 1 filter paper. The filtrate was diluted to 200 mL and submitted for F^- analyses.

The filtrate obtained from the leach test was found to have the constituents shown in Table 34. The bentonite did not add fluorine or chlorine to the water in sufficient quantities to modify the composition of the groundwater used in the basalt laboratory analog experiments. (Water from the Grande Rhonde structure, which is proposed for the waste repository, contains 37 mg/L fluorine and 148 mg/L chlorine.)

Table 34. Analyses[a] of Anions in Solution after Leaching from Bentonite (mg/L)

Fluoride	Chloride	NO_3^-	SO_4^{2-}	PO_4^{3-}
0.95	3.39	6.35	149.9	1.00

[a]Analyst F. Williams; Analysis No. 81-0556-01, 9/11/81, of sample Bent-F.

The quantity of sulfate leached from the bentonite also is not significant, as exemplified by the following comparison. From 10 g of bentonite, 3.0 mg of sulfate was leached. Since an experiment will typically use 0.2 g of bentonite, 60 µg sulfate will be available from the bentonite. With a flow of 1 mL/h in the experiments, this amount of sulfate, released in 24 h, will raise the sulfate level of the water by 3 mg/L, which is not significant in comparison to the ∿114 mg/L sulfate already in solution.

3. Laboratory Aging of Repository Materials

Laboratory treatments of repository materials are proposed that reproduce the major effects of aging of the materials in a nuclear waste repository. By the treatments, materials are to be prepared for use in the Laboratory Analog program that will explore the performance of a 1000-year-old repository.

One objective of the Laboratory Analog program is to assess changes in nuclide migration that would be expected as a result of the aging of nuclear waste, clay backfill, and rock. This will be done by observing migration in materials that have been treated to reflect aging in a waste repository. The treatments selected represent severe cases of aging--that is, the treatments modify those properties of the materials which most strongly affect nuclide migration. Further, the properties will be modified as extensively as they might be under extreme conditions in the repository. Under average natural conditions, much less severe aging than is simulated in the laboratory can be expected.

Aging of the glass waste form, the engineered barrier, and the host rock will occur after emplacement of waste in a nuclear waste repository. The aging will involve many processes, such as devitrification, hydration, dissolution, radionuclide transmutation, radiolysis, radiation damage, and chemical reaction.

The aging depends on the compositions of the materials (waste loading, chemical additives, etc.) and is influenced by open-system variables (groundwater flow, groundwater composition, etc.) which may be buffered by the rock (e.g., the composition of groundwater may be buffered). The aged states of repository material also depend on the size and geometry of breaches of the waste package.

Responding to so many variables, a material may acquire any one of many possible aged states. The generation of three different aged states simultaneously on one waste solid is illustrated in Fig. 35.

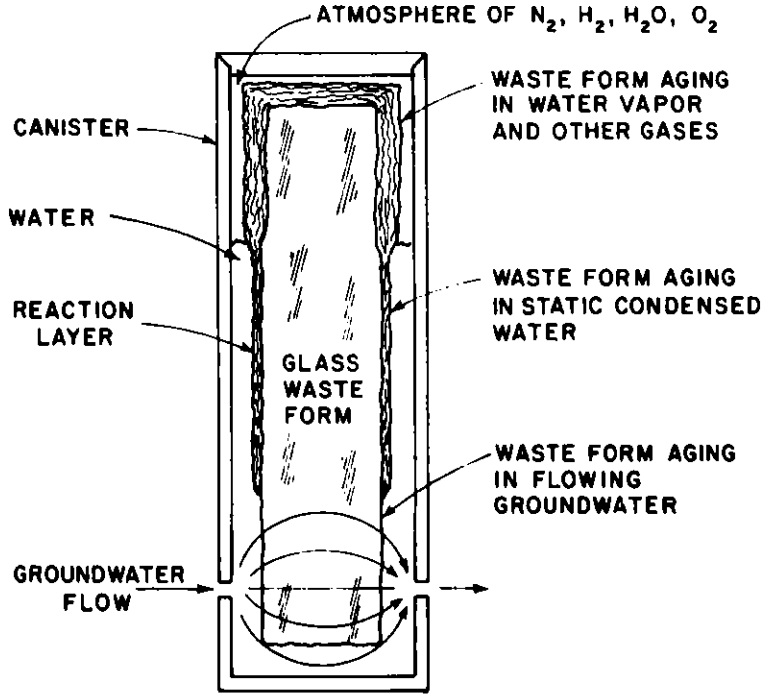

Fig. 35. Waste Solid Undergoing a Variety of Aging Processes

Aging can be characterized by changes in physical and chemical parameters, such as fraction of crystallized solid, weight of water of hydration, moles of dissolved elements, amount of stored energy, and number of interstitial atoms (parameters corresponding to aging processes listed above). In comprehending the possibilities for aging, one might imagine a multidimensional plot with an axis for each important parameter. The change in each variable would be independent, to some degree, of changes in other variables, and so the possible aged states for one age would occupy a space in this multidimensional volume, as discussed below.

To illustrate the "space" of possible aged states, we use the model of a breached canister shown in Fig. 36, in which a small hole in the canister would allow hydration but no loss of cesium from the canister. Two holes in the canister would allow both hydration and the loss of cesium by flowing water. The final state of the waste would depend on the times of formation of the holes and the sizes of the holes. A hypothetical plot of the "space" described by the hydration and mass-loss parameters is illustrated in Fig. 37 for the three periods, 500, 1000, and 2000 y. Another breach model may permit an age "space" for a given period different from that shown in Fig. 37.

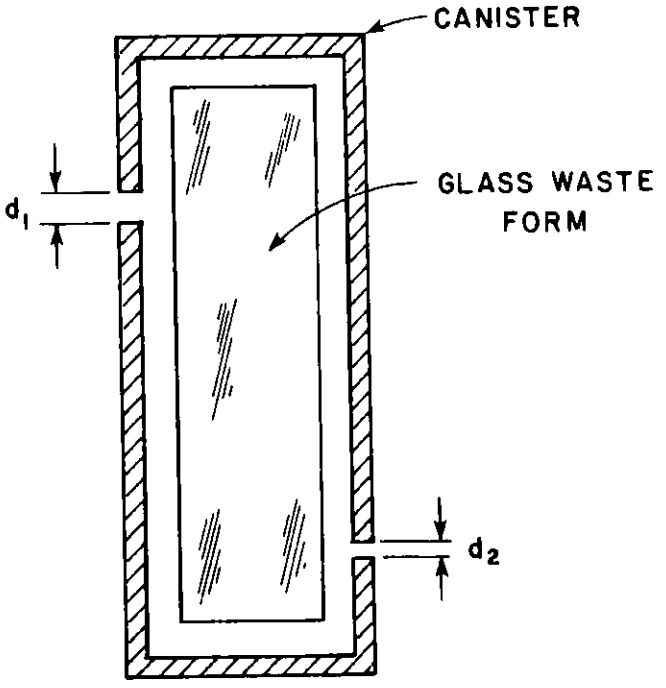

Fig. 36. Model of Canister Breach in which d_1 and d_2 are Gap Widths with $d_1 > d_2$. (The gaps are at different hydraulic pressures. An increase in d_1 would provide an increased supply of groundwater for hydration. An increase in d_2 would provide an increased flow-through of groundwater.)

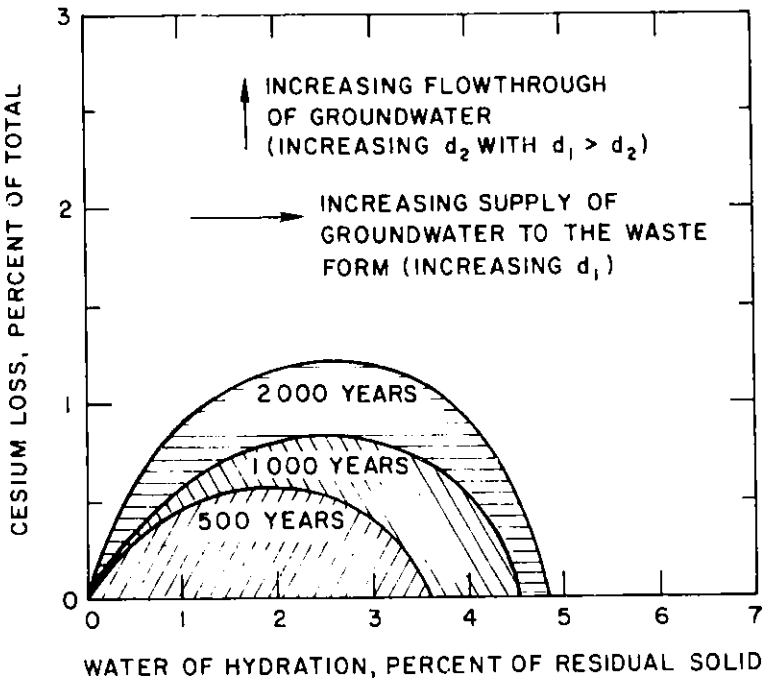

Fig. 37. Hypothetical Relationship of Cesium Loss to Water of Hydration During Aging (see Fig. 36 for the descriptions of d_1 and d_2).

The point of this discussion is that a great variety of aged states are possible for repository materials. Different aged states may exist simultaneously in a repository containing hundreds of waste canisters. The practice in the Laboratory Analog program will be to simulate for each material one aged state at 1000 y and one at 2000 y. The laboratory aging procedures are selected to produce the modifications of waste package behavior that are most significant in terms of nuclide release and migration.

4. Selection of an Aging Process

Aging processes evaluated for their applicability to waste glass are: hydration at elevated temperature, dissolution, devitrification, radiation damage, and leaching. For basalt, aging processes considered are hydration and radiation damage. For bentonite in combination with granulated basalt (under consideration as backfill for waste repository), hydration and recrystallization are being considered as possible aging processes.

a. Waste Glass

Waste glass will age in the hydrous and thermal environments of a waste repository. In the presence of hydrous environment (as either a liquid or a vapor), the dry waste form, which will be hot when waste is first deposited, will react with water to form a hydrous layer on its surface. This layer may grow (age) in the presence of static water, and then, if exposed to

flowing water, lose mass (be leached). Hydration at elevated temperature is, therefore, considered a major aging phenomenon of waste glass and would result, for example, from a breach in the canister during the early thermal period of the repository.

During hydration in the atmosphere, radionuclides would be released from the glass structure but not detached from the waste form. After hydration in the atmosphere and submersion in water, the radionuclides would quickly be dissolved. This rapid accumulation in groundwater may have important consequences to migration (such as saturating readily accessible adsorption sites and allowing the movement of radionuclides).

Devitrification is not expected to be an important phenomenon in the aging of waste. At the maximum design temperatures for the repository (temperatures below 500°C), waste glasses are not expected to devitrify [TURCOTTE]. Furthermore, devitrification in the absence of cracking seems to have little effect on the leach rates of the glasses that are candidate waste forms [WEBER, WALD]. Devitrification may occur during waste processing that precedes storage, however. Because of this possibility, the waste glass will be subjected to heating during the artificial aging treatment to introduce some crystallization.

Radiation damage, primarily from alpha-recoiling nuclei, is not likely to be an important aging mechanism for 1000-year-old waste, but may be important for older waste. The alpha-recoil damage has no effect initially, when the radiation-damaged areas are isolated and do not overlap to form a connecting network. The consequences of the damage on the chemical stability of the glass after a time (when the integrated alpha-recoil density is high) is an area of controversy [HALL, DRAN]. The estimates of elapsed time before alpha-recoil damage may be important range from 2000 y to in excess of $\sim 10^6$ y [DRAN, MENDEL].

Leaching was not selected specifically as an aging process for glass because leaching is already an integral part of the Laboratory Analog experiments. Extensive leaching (hydrothermal alteration) would be expected to produce a waste form that is less chemically active than fresh glass; therefore, except for the loss of radionuclides that would occur during leaching, extensive leaching would not be expected to modify waste form properties in a detrimental way.

The aging process selected for the solid waste in this work is slight devitrification by annealing, followed by hydration in water vapor. Hydration in water vapor is expected to be the most common aging process for solid waste because the durable, essentially leak-free containers (canister and overpack) and clay barrier envisioned in repository designs will exclude most of the water. Some water for hydration may exist in the sealed containers or leak through tiny holes in the barrier. Hydration would be the dominant aging process in a repository built in unsaturated sediments [WINOGRAD].

Factors that affect the hydration of glass are temperature, water vapor, pressure, glass composition, vapor species other than water, and time. The relation of hydration to time and temperature has been studied for obsidian [EWING, TOMBRELLO, FRIEDMAN, ERICSON], reviewed by the NRC [BARKETT], and can be roughly approximated by the relationship,

$$k = Ae^{-E/RT} \quad (1)$$

where k is the amount of hydration [$(\mu m)^2$/1000 y], A is a constant, E is the activation energy of the hydration process (cal/mol), R is the gas constant (cal/mol K), and T is temperature (K).

The thickness, d, of the hydration layer is given by

$$d = (kt)^{1/2} \quad (2)$$

where t is the time in units of 1000 years. These relationships incorporate (in the values selected for A and E) the effects of water vapor pressure and glass composition, both of which are known to affect the amount of hydration. The influences of water vapor pressure and glass composition on hydration are ignored if A and E are treated as constants for all water pressures and glass compositions. In these studies, water is assumed to be the only important vapor species.

To simulate a repository condition using our present understanding, it is necessary to assume that the above relationships are valid, to ignore the effect of water pressure, and to use data obtained for obsidian (which is known not to be valid for waste glasses). When this is done, the value adopted for A is 1×10^{16} $(\mu m)^2$ per 1000 y [TOMBRELLO]; the value adopted for E is 2×10^4 cal/mol [TOMBRELLO].

If the aging conditions in a repository are assumed to be water vapor at a temperature of 100°C for 1000 y, the hydrated layer is estimated to attain a thickness of 150 μm. However, this thickness could vary between 318 and 17 μm/1000 y on the basis of the full range of known values for A and E (A ranging from 1.4×10^{15} to 1.8×10^{16} $(\mu m)^2$ per 1000 y and E ranging from 19,200 to 20,700 cal/mol, as reported by [FRIEDMAN]. Whether the behavior of waste glasses would fall within this range is not known. Given the uncertainty in the thickness of hydration layer, consideration of a more detailed thermal history for a repository does not appear to be warranted.

To simulate the aging process, hydration must be done at elevated temperatures. The data shown in Table 35, column 2, were calculated from Eqs. 1 and 2. It would take 69 days at a temperature of 275°C to obtain a hydrated layer 150 μm thick. The data in column 3 were calculated assuming the hydration layer is removed after it reaches a thickness of 20 μm, exposing a new surface, and that the process begins again.

These calculations were done using all of the information provided by Catholic University as well as updated information obtained over the past two years [BARKETT]. It should be obvious that such calculations are tenuous for obsidian and totally unsupported for waste glasses. To provide adequate simulation criteria for the aging program, it would be necesary to demonstrate that Eq. 1 and 2 are valid for waste glasses and to obtain values for A and E for each glass. Additionally, it is necessary to determine the effect of water vapor pressure on the hydration process and, to be realistic, to determine the effects of condensation and exfoliation on hydrated layers.

Table 35. Calculated Hydration Layer Thicknesses Using $A = 10^{16}$ $\mu m^2/1000$ y and $E = 2 \times 10^4$ cal/mol

	Total Layer Thickness Formed[a] in 1000 years, μm	
Temp, °C	From Eq. 1	Assuming Exfoliation
0	0.2	0.2
25	6	6
75	65	200
100	152	1500
125	380	6700
175	1500	10^5
225	4000	10^8

[a]That is, formed and sloughed off.

b. Basalt

Recent fracture surfaces of Pomona basalt (similar to the rock surrounding a repository) will age in the hydrous and thermal environments of the waste repository. Fracture surfaces will age primarily by reactions with groundwater. Devitrification and radiation damage are not considered factors in the aging of basalt because (1) basalt is already crystallized when formed at temperatures considerably higher than the maximum temperature suggested for a repository and (2) basalt will not be subjected to a significant alpha-recoil dose except at its surface. The near-field gamma flux is probably ineffective in producing structural damage.

Surfaces of the basalt will be subject to alpha-recoil damage from adsorbed actinide nuclides. However, the alpha activity would be too low to destroy adsorption sites or otherwise modify the hydrated surface faster than new surface forms on contact with the groundwater. Therefore, radiation damage would be a secondary aging process for the rock in comparison to hydration. Radiation from rock surfaces can produce radiolysis of groundwater, which might alter migration, but this would not be an aging process.

One way of obtaining aged basalt surfaces is to sample old fissures. This approach has the shortcoming that the length of time and conditions under which the fissures were aged are unknown. Therefore, this approach was not taken.

The aging process selected for basalt in this laboratory work is hydration in liquid water at elevated temperature. The laboratory aging is comparable to that expected to occur naturally in recent fissures that quickly become saturated with groundwater. A great deal of information on the alteration of Pasco Basin basalts by groundwater, meteoritic water, and humidity is presented in several reports [BENSON-1978, 1979/1980, AMES, TEAGUE]. Unfortunately, the specific conditions under which the basalts

were altered are not known. As might be expected from the variety of conditions leading to alteration, there are great differences in alteration products from place to place. These observations substantiate the viewpoint developed near the end of Section IV.C.3 of this report, namely, that many age states of a material are possible and that any age state is a result of the particular conditions to which the material was subjected.

The alteration products generally cited in the references are: smectites, illite (celadonite?), clinoptilolite, mordenite, silica (cristobalite, tridymite, opal, chalcedony, quartz), pyrite, gypsum, calcite, apatite, and halloysite. As a general observation, the groundmass (mostly glass) and pyroxene are seen to alter before plagioclase [BENSON 1979/1980]. Alteration products are very heterogeneous in the flood basalts. Some fractures exhibit no alteration products [BENSON-1978]. Clays in some fractures occur in different-colored layers, with many minerals present. Different vesicles sometimes record different portions of the alteration sequence. These differences are probably due to differences in environment (groundwater flow, groundwater composition, temperature, etc.) rather than to differences in the age of the flow.

There is a generalized sequence of precipitation observed in vesicles: clay, then clinoptilolite with or without silica, then clay. Within vesicles, smectites are observed in the upper portion of the stratigraphic column, and clinoptilolite and silica in the lower portion.

Clinoptilolite is replaced by mordenite at depths greater than 880 m [BENSON-1979/1980]; mordenite is among the most siliceous zeolites, and its formation coincides with the advanced stages of silica diagenesis at lower depths. Because the proposed waste repository is deep, conditions that are expected to produce mordenite will be selected for laboratory aging of basalt.

Several attempts have been made to model the reactions which have occurred [BENSON-1978, 1979/1980]. However, these calculations were limited by a lack of thermodynamic constants, and assumption of low ambient temperature (25°C). Further, the modeled reactions involved extensive plagioclase but little groundmass (primarily glass) alteration [BENSON-1979/1980], contrary to observation. Also, the models predicted the formation of many phases not observed [BENSON-1980]. These calculations, therefore, have not been found to be useful in planning laboratory aging procedures for the basalts.

The approach finally selected for the laboratory modification of basalt surfaces to represent aging is hydrothermal treatment of fresh basalt surfaces. Water formulated to represent the composition of water from the Grande Ronde formation will be used as the hydrothermal fluid. One suggestion [LONG] is to use the highest possible temperature that is within the mordenite/illite stability field.

The thickness of the reaction rim to be produced by the hydrothermal treatment will be estimated based on the 0.5- to 1-cm-thick hydration rims observed on 12-million-year-old basalts of the Pasco Basin.

In making the estimate, the following relationship between hydration rim thickness, d, and time, t, will be considered valid:

$$d = \sqrt{kt}$$

where k is a constant at a given temperature. At the ambient temperature of the Pomona basalt, k is determined to be 8.3×10^{-8} cm^2/y for a rim thickness of 1 cm. The rim thickness expected after 1000 y at ambient temperature would be 91 μm and could be reproduced hydrothermally in the laboratory.

As part of the examination of the effect of the laboratory aging process, we would want to compare adsorption properties of the laboratory-altered surface to adsorption properties of natural rock surfaces obtained from depths greater than 880 m in the basalt flows.

c. Bentonite and Basalt

Bentonite is a hydrous clay formed at low temperature. This clay combined with granulated basalt is now under consideration as the backfill for a waste repository in basalt. Aging of the clay in the presence of water and elevated temperature may produce dehydration and recrystallization with some replacement of exchangeable ions by ions from the water.

Heating of the clay in a dry environment may dehydrate the clay; but the clay is not likely to become dry in this basalt environment. Therefore, treatment of the clay in liquid water at elevated temperature is under consideration as the laboratory process for aging the clay and basalt.

There is no evidence that gamma radiation can affect the aging of clay backfill. However, it is conceivable that intense gamma bombardment of the water-saturated clay could lead to unusual surface reactions on the clay due to radiolysis of the groundwater.

The most substantial fear expressed in the literature regarding aging of the engineered barrier is that the bentonite may alter to illite plus chlorite [SMITH]. However, very little potassium is available in a basaltic system and only a minor amount of illite is found as an alteration product. Therefore, this alteration is unlikely to occur and will not be considered in study of the laboratory aging of the engineered barrier.

Based on work [PUSCH, JACOBSSON] with bentonite, MX-80 Volclay (American Colloid Co.), a sodium bentonite from Wyoming, Swedish workers have inferred that the geologic evidence is that the bentonite will retain its desirable adsorption and swelling properties at 500-m depth in granite. Similarly, no extensive modification of bentonite in basalt is suggested by our current understanding.

Although bentonite may not alter to a nonsmectitic mineral in a basaltic environment, it may be modified to some extent. Temperatures at the interface of the canister and engineered barrier may be as high as 300°C [TAYLOR]. The hydrothermal treatment we propose for the engineered barrier is not expected to change the mineralogy of the clay but should alter its physical/chemical properties in some way. A time-temperature condition based on some reasonable rate curve for mineral recrystallization will be selected for aging of the backfill.

V. TRACE-ELEMENT TRANSPORT IN LITHIC MATERIAL BY FLUID FLOW
(M. G. Seitz and R. A. Couture)

A. Introduction

In previous reports [STEINDLER-1981A, 1981B], we have reported on saline water ($[Cl^-]>0.24M$) which we extracted from granite from 1288 m below the surface in Northern Illinois drill hole UPH-3. The water was removed by displacement with water under pressure ("elution") [STEINDLER-1981A]. This method appears to work well, in contrast to sampling of the groundwater by conventional pumping of a well, which would have been very expensive and probably impossible.

It was shown that the water compositionally resembles brine in sediments of the Illinois Basin [STEINDLER-1981B]. The origin and composition of pore fluids are of great interest, since they may be useful for tracing advection and diffusion of fluids and chemical reactions in the granite.

In this report, we report the compositions of pore fluids obtained from five depths in the granite and from the overlying sandstone. Contact was at 664 m. Samples were obtained by the previously described "elution" technique and by washing of crushed rock. Both organic and inorganic constituents were analyzed, since high concentrations of oil were found at some depths.

B. Experimental Methods

The elution method was the same as that described in the two preceding quarterly reports [STEINDLER-1981A, 1981B] except that the ends of the rock core were lapped flat and finished with No. 400 grit silicon carbide.

In order to obtain some measure of the accessible pore volume in the rocks, porosity measurements were made on several samples from UPH-3. The rocks were evacuated at 90°C over a weekend, after which they were weighed and then immersed in water at 13.7 MPa for 1 h. Next, they were dried externally with acetone and quickly weighed again to determine the gain in weight. The weights were corrected for the effects of air temperature and pressure on buoyancy.

For the analyses of soluble salts, rock samples were crushed and leached briefly with ice water. Subsamples were broken or sliced off the cores, and as much as possible of the outer cylindrical surface was chiseled off to minimize contamination. The samples were then crushed in a steel mortar and pestle to sand-sized particles. This procedure is thought to break open most of the intergranular rock pores but relatively few liquid inclusions (which are sealed within individual crystals and therefore are not part of the groundwater system). The samples were carefully split into aliquots. A 2-g portion of each was washed with benzene, and another subsample of 5-20 g was washed with ice water and filtered with a membrane filter. The benzene was removed from the filtrate by evaporation, and 100 μL of solvent was added; 10 μL of this was injected into a liquid chromatograph.

1. Acknowledgments

All organic analytical work was done by Amrit Boparai. The aqueous leachates were analyzed as follows:

For anions and monovalent cations by ion chromatography by Florence Williams;* for calcium and magnesium by atomic absorption by Irene Fox;* for chloride by titrations by Rex Couture; for alkalinity by titrations by Alice Essling;* and for fluoride by ion-specific electrode by Irene Fox.*

C. Results

A core of approximately 10-cm length from the 840-m depth of drill hole UPH-3 was subjected to "elution" analysis. About 0.21 g of liquid was obtained, of which about two-thirds was a yellow oil. A high concentration of chloride was detected in the aqueous fraction, but no quantitative analysis could be obtained. Pumping was terminated, although oil was still being eluted in undiminished quantities.

An infrared spectrum of the oil showed the presence of H_2O or OH, aliphatic compounds, and small amounts of carbonyl or carbonyl amide compounds. The oil has an index of refraction, n_D, of 1.468 to 1.469. It fluoresces blue-white under ultraviolet (350 nm) light. Gas chromatography showed at least 27 compounds, eluted only above 200°C. Thus, the oil is composed primarily of high-boiling-point paraffins.

The presence of so much oil in the rock almost rules out the possibility that the oil is present due to contamination, especially since the rock is highly impermeable. No oil was used in the preparation of the sample. A sample of FD-2, the drilling fluid used on the hole, was analyzed; the benzene-soluble fraction (reportedly mineral oil) consists of about 176 compounds, all of which were eluted below 200°C. Extraction with water did not appreciably change the chromatogram of the drilling fluid. Thus, the drilling fluid does not appear to have contaminated the rock. We are unaware of any other source of contamination.

Table 36 shows the analyses of the leachate solutions for samples from depths of 553 to 1288 m. There are large cation/anion imbalances, which may be due to the presence of organic ions. The chloride analyses were done by ion chromatography and by titration, and good agreement was obtained except for one sample. A NaCl solution, submitted blind as a standard, demonstrated good analytical accuracy.

Table 37 lists porosities and the estimated chloride concentrations in the pore fluid. The estimates were made by assuming that the pores were filled with aqueous liquid and that the density of the rock (excluding pores) is 2.65 g/mL.

The porosities of the graphite samples correlate with their condition and are in the range reported for granite [BRACE]. However, the porosities presumably apply only to an effective confining pressure (confining pressure

*Analytical Chemistry Laboratory, ANL.

Table 36. Analyses of Leachates from Crushed Rock, UPH-3

Depth, m	Porosity, %	mM									
		Cl^-	alkalinity[a]	SO_4^{2-}	F^-[b]	F^-[c]	Na^+	NH_4^+	Ca^{2+}	Mg^+	K^+
553	17	0.26	0.07	0.027	-	0.014	0.087	0.026	0.022	0.020	0.50
666	3.0	0.33	0.40	0.110	0.149	0.151	0.257	<0.006	0.147	0.136	0.80
670	0.49	0.18	0.10	0.024	<0.003		0.255	0.017	0.045	0.033	0.31
840	0.14	0.32	0.04	0.025	0.151	0.22	0.457	<0.006	0.018	0.004	0.30
1180	0.23	1.26	0.04	0.82	<0.003		1.13	<0.006	0.79	0.003	0.34
1288	0.49	2.72	0.15	<0.021	<0.003		0.72	<0.006	0.41	0.074	<0.003[d]

[a]Alkalinities are in meq/L.
[b]By ion chromatography.
[c]By ion-specific electrode.
[d]Later found to be an analytical error.

Table 37. Estimated Chloride Concentrations in Pore Fluid, UPH-3

Depth, m	Description	Porosity, %	$[Cl^-]$, M
553	Mt. Simon sandstone	17	0.0072
666	Weathered granite with fractures	3.0	0.035
670	Weathered granite with fracture	0.49	0.12
840	Solid granite	0.14	0.68 (2.3)[a]
1180	Solid granite with fracture	0.23	1.4
1288	Granite with microfractures	0.49	2.4

[a]Value in parentheses calculated by assuming 70% of porosity was occupied by oil. The porosity measurement may not be accurate for this sample.

minus pore pressure) of 1 atm, since the pore pressure was approximately equal to the total pressure. At higher confining pressures, the porosities of the granite might be somewhat lower [BRACE], although the porosity of the sandstone would be essentially unchanged.

The chloride concentrations are clearly low in the sandstone and in the weathered granite near the contact. The estimated concentration at 553 m (0.007M) in the sandstone is comparable to that of a nearby well (0.00027M at 302-m depth) [LENA]. At greater depths, the pore water is highly saline. The chloride concentration lies between 0.6M and 2M at 840 m, and exceeds 1M below 840 m.

There are some surprises in the leachate analyses (Table 36). It is possible that the high concentrations of potassium are due to contamination with drilling fluid, which was about 0.02M in KCl [STEINDLER-1981A, pp. 74-85]. However, since the potassium concentrations are much higher than the chloride concentrations in three of the samples, contamination does not seem to be the most likely explanation.

The sulfate and fluoride concentrations are erratic. This suggests inhomogeneity in the rock and dissolution of rock constituents. An appreciable amount (on the order of 1%) of fluorite (CaF_2) is present at 840 m. The fluoride concentrations are enormous in leachates from samples from the 666 m and 840 m depths, which have F/Cl mole ratios of 0.5.

The hexane-soluble organic matter consists mainly of five major compounds and a homologous series of minor components. The major components in the benzene leachates are present in the same ratios as in the oil which was eluted (840 m). Unfortunately, resolution was not adequate to detect more than about ten compounds in the leachates, and qualitative analysis was therefore difficult.

Semiquantitative organic analyses are presented in Table 38. They were derived from the highest peak on each chromatogram, using the eluted oil from the 840 m level core as an external standard. The accuracy in Table 38 is not the best since the chromatograms were run on different days.

Table 38. Oil Content (Approximate) of Rocks from UPH-3

Depth, m	Description	Porosity, %	Oil Content, µL/g of rock	$\frac{\text{Volume Oil}}{\text{Pore Volume}}$, %
553	Mt. Simon sandstone	17	0.19	0.30
666	Weathered granite with fractures	3.0	0.021	0.19
670	Weathered granite with fracture	0.49	0.0055	0.29
840	Solid granite	0.14	0.37	70
1180	Solid granite with fracture	0.23	0.005	0.57
1288	Granite with microfractures	0.49	Not analyzed	

However, the estimate in Table 38 of the oil content at 840 m agrees roughly with the amount obtained by elution in which roughly 0.36 µL of oil per gram of rock was obtained before pumping was stopped.

The oil content decreases with depth, except at 840 m, where oil is a major fraction of the pore volume. At this depth, oil and water were eluted in an approximately 2:1 ratio, in good agreement with Table 38. Nevertheless, because of the high oil content in this sample, its porosity measurement is in question.

D. Discussion

The elution technique gives results which differ considerably from the results of leaching. These results are compared in Table 39. In comparison to elution, leaching appears to increase Ca/Na and Mg/Na and to decrease F/Cl.

Table 39. Comparison of "Elution" and "Leaching" Techniques for Pore Fluid Analysis. Sample from 1288 m, UPH-3. The first two fractions of eluate are shown

	Ca/Na	Mg/Na	K/Na	SO_4/Cl	F/Cl	Br/Cl
Elution	0.053	0.007				
	0.112	0.014	0.022	0.019	0.020	0.0014
Leaching	0.57	0.10	<0.004	<0.024	<0.003	

In general, we would not expect leaching to give very representative numbers. Dilution or concentration can greatly shift equilibria [see SAYLES]. Moreover, liquid inclusions may be opened by crushing [see ROEDDER], and the reactive rock matrix may dissolve [see ROEDDER, p. 37].

The elution samples, on the other hand, were obtained under conditions of more realistic dissolved salt concentrations and with minimal disturbance of the rock structure. Experience has shown that it is possible to get representative samples of pore fluid in sediments by squeezing [see GIESKES, COUTURE], and we think we can reasonably expect to get representative samples by elution. We assume also that the chloride analyses of the leachates are not seriously in error.

The oil and saline water were presumably derived from the overlying sediments. Stratigraphically adjacent sediments of the Illinois Basin contain oil and brine [MEENTS]. The presence of oil in the granite is a clear indication of movement of fluids within the granite and penetration of fluids to substantial depths. However, leaching analysis of the sandstone (Table 37) shows that the overlying sediments now contain fresh water and only trace amounts of oil.

The presence of saline water in the granite (see Table 37) is a clear indication that communication with fresh water in the overlying sediments is limited. The salinity is appreciable (0.1M), even in fractured and weathered granite as little as 6 m below the contact. The salinity is very high in the solid granite at 840-1180 m and in the granite at 1288 m, which was taken from a fracture zone [HAIMSON].

The existence of large dissolved salt gradients is not necessarily indicative of groundwater movement. Possibly, the upward decrease in salinity is due primarily to diffusion, not advection. More data on pore-water compositions and diffusion coefficients can be obtained to resolve the questions.

It appears that leaching and elution may be very useful techniques for sampling of pore fluid for further study of mass transport in impermeable rocks. Relatively simple techniques can be used to provide detailed profiles which could not be obtained otherwise.

VI. LIGHT WATER BREEDER REACTOR PROOF-OF-BREEDING ANALYTICAL SUPPORT PROJECT

(N. M. Levitz, R. E. Brock, T. F. Cannon, G. L. Chapman, P. G. Deeken, J. E. Fagan, D. G. Graczyk, R. R. Heinrich, R. W. Kessie, H. Lautermilch, R. J. Meyer, R. E. Nelson, John Osudar*, J. E. Parks, L. E. Trevorrow, C. G. Wach and I. O. Winsch)

A. Full-Scale Shear (FSS)

(P. G. Deeken, J. F. Fagan, R. E. Nelson, and C. G. Wach)

The full-scale shear (FSS) remains stored in an out-of-cell location until plans for acccommodating the three-year project extension are finalized and approved by DOE. The shear is mostly disassembled, with its component parts stored. The machine base has been enclosed in a nitrogen-filled tent to minimize corrosion of the feed system bearings and ways. The shear hydraulic power unit, control and instrumentation consoles, and computer-interface rack have been placed at the cell operating face, awaiting the shear's in-cell installation.

Some minor work associated with the shear (Cell M-3) containment structure was completed. Of note was a modification of the containment port where the fuel rod enters the cell. A longer lead-in to this port was provided to facilitate the introduction of the fuel rod container into the hot cell.

A mockup rack for storing canned sheared fuel segments in the existing hot cell storage pits was completed. The rack is to be used to store fuel segments and scrap rod plenum sections until disposition.

B. Single-Unit Dissolver (SUD)

(P. G. Deeken, T. F. Cannon, H. Lautermilch, R. E. Brock, I. O. Winsch, and J. E. Parks)

A series of five additional tests (Runs DD-7 to -11) with the SUD was conducted this quarter, using the new external heater system. This series consisted of three segment-dissolution tests (Runs DD-7, -8, and -10) and two blank runs (DD-9 and -11). These tests were intended to demonstrate the overall performance of the SUD and associated systems, particularly the new external heater system. They also are serving the following objectives: (1) to demonstrate complete dissolution and recovery of thoria, (2) to demonstrate recovery of uranium, cesium, and krypton, (3) to evaluate fission-gas sampling procedures, (4) to evaluate cross-contamination for successive dissolutions to determine the extent of contamination from run to run, using uranium, cesium, and zirconium as monitors, (5) to acquire additional corrosion data on tantalum alloy 63,† (6) to acquire further operating experience with computer-aided operations, and (7) to evaluate the solution sampling systems.

---

*Science Applications, Inc., Oak Brook, IL.

†Registered Trademark, Fansteel Corp., North Chicago, IL 60064. Composition: Ta; W, 2.5 wt %; Nb, 0.15 wt %.

The dissolver charge in each segment-dissolution test consisted of Thorex* solution and a dummy sheared segment composed of Zircaloy hulls and pulverized thoria in amounts corresponding to a 36-cm-long (14-in.-long) segment of standard blanket rod (the largest fuel charge expected to be dissolved during EOL operations). Also in the dissolver charge were uranium (NBS 950a, $^{238}U_3O_8$), cesium (about 10 g of $CsNO_3$), and a sample of nonradioactive krypton. The dissolver charge in the blank runs consisted only of Thorex-Al† solution.

The operating procedure used in the segment-dissolution tests consisted of the highly detailed procedure developed for operation of the SUD. This procedure consists of a 4-h primary dissolution at 195°C and 125 psig (861 kPa) and a 3-h secondary dissolution (same conditions), followed by solution blending, weighing, and sampling operations. Minor modifications were made to the procedure to accommodate additional sampling operations required in these tests. In the blank runs, only the secondary dissolution procedure and subsequent steps were used.

Operationally, the SUD and associated systems worked reasonably well throughout the test series. The external heater system performed satisfactorily, in that heatup and cooldown times were acceptable--20 min and 1.3 h, respectively; a problem with balance of heat distribution remains to be resolved. Vigorous boiling was "observed" using an audio accelerometer mounted on the dissolver. Initial use of the computer system was made during execution of several steps in the operating procedure; i.e., during pressurization and leak-testing of vessels. The operating procedure for the SUD appeared to be in good order, with no changes or deviations required. The blend tank (BT) system performed satisfactorily in these tests. However, the BT design is being modified to eliminate remote assembly problems with the lid gasket seal. An all-welded assembly is being fabricated.

Procedures and equipment developed for sampling both the dissolver and the BT were tested in these runs. Square, 1-oz sample vials were selected to establish their utility; no problems arose in remote handling, and overall performance of the sampling system was satisfactory. These vials have been tentatively selected for the storage of dissolver archive samples during (and after) the EOL campaign. A more resilient vial cap of polypropylene is to be tested to evaluate it for improved resistance to radiation and acid since the presently used rigid plastic caps suffered some breakage in drop tests. A plastic coating on the vial itself (applied by dipping) is intended to reduce the breakage problem. A radiation-induced weight change in the protective plastic coating was observed in exploratory tests, but calculations indicate that this change (5-10 mg) does not impact the analytical procedure.

Initial results from Run DD-7 indicate that quantitative dissolution and recovery of the ThO_2 charge were achieved within analytical error limits; workup of the remaining analytical data from these tests is currently in progress. Corrosion results are discussed separately below.

---

*Thorex (13.6M HNO_3, 0.06M HF) is used for the primary dissolution.

†Thorex-Al, containing 0.06M $Al(NO_3)_3$, is used for the secondary dissolution and for the blank runs.

In associated work, the blend tank (BT) balance was removed from Cell K-3, repaired, reinstalled, and recalibrated. A 66-h stability test was performed on the balance and the balance temperature-control system (TCS). The tare value was stable within ±1 g during the test period, and drift within this range correlated with the measured balance temperature drift (which had a cycle time of 24 h). The TCS was operated continuously for 25 days during the recently completed series of SUD tests; operation was completely satisfactory.

As originally designed, the SUD control system includes a number of safety interlocks. These interlocks were incorporated into the logic of the MODICON* Programmable Controller, which was part of the original control system. Subsequent to installation of the SUD, the decision was made to interface the PDP-11/23 computer to the SUD sensors and controls, in parallel with the MODICON system, to obtain experience with the computer system proposed for the Multiple Dissolver System (MDS) in the end-of-life (EOL) campaign. Operating experience during this report period reveals that operation of the SUD via the PDP-11/23 computer is incompatible with the present interlock system. The need for independent, hard-wired interlocks for safe operation of the SUD via the computer has thus been identified and will be incorporated in any future reworking of the SUD controls.

1. Corrosion

The material of construction of the primary vessels of the SUD and the MDS is Fansteel tantalum alloy 63. Another series of corrosion studies, to verify that corrosion of these vessels will not pose a problem during EOL operations, is described below.

A set of twenty tantalum alloy 63 coupons (weighing about 15 g each) was exposed to Thorex-Al at room temperature for a period of 624 h. The coupons maintained a bright surface throughout the exposure; a mean corrosion rate of 2.8×10^{-6} ipy ±33% was calculated from the weight losses. This rate may be compared with a rate of 7×10^{-3} ipy, which was determined for the same alloy in Thorex solution alone. The reduction in corrosion rate observed in the Thorex-Al solution is due to reduction of the concentration of free fluoride in the Thorex-Al solution as a result of the formation of a complex between the fluoride ions and the aluminum salt.

Coupons were also exposed during a dissolution run in the SUD in which a dummy segment of a LWBR blanket rod was dissolved in 3000 mL of Thorex. The usual two-step dissolution process was used: Thorex solution for 4 h at 195°C (125 psig or 861 kPa), followed by Thorex-Al solution for 3 h (same conditions). Coupons were exposed in both the vapor and liquid phases.

The appearance of coupons exposed in the vapor phase did not change; corrosion rates calculated from the weight losses amounted to 1.9×10^{-4} ipy. Coupons exposed in the liquid phase acquired a blue tint and their weights increased by milligram quantities. By emission spectroscopy, tin and zirconium were identified as the principal constituents of the surface layer; these elements stem from the Zircaloy-4 cladding, which dissolves to some extent in Thorex solution.

*Gould, Inc., Andover, MA, Model No. 484.

It was found that 2-h exposure to concentrated hydriodic acid (HI) at 100°C sufficed to remove the surface layer with minimal effect on the tantalum alloy 63, thereby providing a means for decontaminating a tantalum vessel. The coupons were cleaned via this procedure, and coupon weight losses in the overall process (segment dissolution plus HI cleaning) were used to calculate an average corrosion rate for tantalum alloy 63 immersed in the liquid phase; values obtained ranged from 1.6 to 5.4 x 10^{-3} ipy--about the same order as in the room temperature tests. By use of this information, it was concluded that corrosion would not represent a problem during the service life of the vessels.

2. Dissolver Decontamination

Precipitation of the Sn/Zr layer on the tantalum corrosion coupons (see above) was considered to be related to a previously reported problem--surface radioactive contamination of the dissolver used in the earlier pilot-scale work. After the pilot-scale dissolutions of irradiated fuel rod segments [LEVITZ], the dissolver liner and basket were found to be contaminated with ^{125}Sb, which could not be removed with boiling dilute nitric acid. The ^{125}Sb was considered to have formed a solid solution with the SnO_2 which stems from the Zircaloy cladding. Based on literature information, decontamination of the liner and basket by refluxing concentrated HI was attempted. This decontamination step was successful in that the radiation level of the liner and basket was reduced from 1-3.3 R/h to near cell background (100-400 mR/h). The ^{125}Sb activity was found in the HI solution, which was then neutralized, absorbed on clay, and dried preparatory to disposal. Further application of this decontamination scheme will be explored.

C. Multiple Dissolver System (MDS)
(P. G. Deeken, J. E. Parks, and L. E. Trevorrow)

A battery of four dissolvers operating round-the-clock will be used for the EOL campaign. Design of the dissolvers and associated subsystems is being done by the ANL Engineering Division (ANL-ENG). Recent progress on the MDS is highlighted below, by subsystem. The present "stretchout" plan calls for completion of the design in early FY 1984.

Dissolver Assembly

- Tantalum dissolvers (4) procured from Fansteel Corp. were accepted after CEN/ENG review of the accumulated corrosion test data indicated that weld areas are of adequate thickness for intended service.
- New supports which accommodate the external heaters on the dissolver assembly were designed and fabricated.
- Design of the stainless steel (outer) vessel is now about 90% complete.
- The drawing for the dissolver assemblies was started and is about 60% complete.
- Design of the outer heater jacket (the insulation section, which includes air cooling channels) was started and is about 90% complete.

Off-Gas System

- New design requirements by Proof-of-Breeding (POB) staff regarding location and types of fittings are under review by ANL-ENG, for cost and schedule impact.

Blend Tank (BT) and Sample Balances

- New design requirements by POB staff regarding in-cell location for improved accessibility for remote operation and maintenance were reviewed by ANL-ENG, and design changes in layout drawings were made.

Instrumentation and Controls

- Preliminary drawings of heater power and control circuits were completed by ANL-ENG and were forwarded to POB staff for review.

Cell Modifications

- Checking of drawings by ANL-ENG of the alpha enclosure and the in-cell work table is about 90% complete.

- New design requirements from POB staff regarding in-cell air flow are under review by ANL-ENG.

D. Scrap and Waste
(L. E. Trevorrow and R. E. Nelson)

At DOE's request, process options were reexamined and preliminary cost estimates made for the disposition of about 2000 L of liquid analytical residues (dissolver solution) that will be generated in the end-of-life (EOL) Light Water Breeder Reactor Proof-of-Breeding (LWBR-POB) Analytical Support Program at ANL. Two basic concepts were considered: (1) transfer the material as a liquid to another site that has storage facilities and/or conversion equipment for ultimate disposal; or (2) design and build equipment at ANL for converting the liquid to a solid form suitable for shipment, then transfer the material to a site that can store the solid and eventually arrange for its terminal disposal.

To investigate the liquid transfer option: (1) transportation equipment was identified by literature search and extensive discussions with DOE field office and contractor personnel and (2) potential receivers of the waste were contacted to get preliminary cost estimates for processing and disposing of the material. Three shielded shipping cask systems have been identified as being suitable, although some structural modifications and DOE recertification may be needed. One option is the use of specially designed primary and secondary containers that qualify as "Special Form Containers" as defined in the DOE manual.

Potential receivers for the liquid are the Savannah River Plant (SRP), EXXON Nuclear Idaho Co., Inc. (ENICO), and Battelle Pacific Northwest Laboratory (PNL). The TRUST* facility at Oak Ridge National Laboratory (ORNL),

*Thorium Reactor Uranium Storage Tank.

presently storing purified ^{233}uranium-thorium nitrate solution, has no excess capacity and so cannot accept our waste solution. Facility requirements and handling/disposition methods obtained from the other three sites are summarized below; very preliminary cost estimates provided by the contractors are under review.

At SRP, liquid would be neutralized and added to the large volumes of liquid waste presently stored there. Construction of a relatively costly interface system for receipt and transfer of liquid would be required.

At ENICO, liquid would be added to the existing liquid waste storage tanks, the contents of which are fed to a new fluidized-bed calciner. The resulting calcine would be stored in existing underground bins. Introduction of the fluid to the plant would be by two possible routes: (1) electrolytic dissolution of the primary stainless steel vessels to release the fluid and (2) transfer of solution from the primary canister to a "local" canister that would be transferred to the waste tank farm.

At PNL, the liquid would be transferred to existing storage tanks which provide the feed to an operational spray calciner. The powdered calcine would be converted to glass and stored on the Hanford site to await eventual transfer to a federal repository. PNL has not been able to estimate a cost of interim storage at the Rockwell-Hanford site, but it is expected to be a small fraction of the total cost for waste treatment.

Conversion of the liquid to solid by calcination at ANL, followed by transportation to and storage at Rockwell-Hanford (R-H), remains the reference process at ANL, but work on this system has stopped while review by DOE is in progress.

In summary, the original plan of calcining the analytical residues at ANL is still being compared with alternatives involving shipment as liquid to another contractor for processing and storage. The PNL option is preferred to the other two options because facilities exist there now. Actual completion of the task, however, would depend on several critical items: whether the material is classified as TRU waste, schedules for casks, DOE field office approvals, and necessary state and federal approvals regarding transportation of such materials.

The assistance of Joel Haugen (DOE-CH) in reviewing transportation systems and in liaison activities during this period is gratefully acknowledged.

E. Computer System and Data Management

(J. E. Parks, G. L. Chapman, J. Osudar,* and J. E. Fagan)

An integrated computer system is being developed which will serve a number of functions, among them providing automatic data acquisition and data reduction, process monitoring, and some automatic process control. Computer system hardware currently consists of a VAX-11/780† (shared with other users in this Division) and a PDP-11/23.† The latter unit is currently connected only to the FSS and the SUD via standard CAMAC modules. Work on the computer system during the report period is summarized below.

*Contract person from Science Applications, Inc., Oakbrook, IL.

†Products of Digital Equipment Corp., Maynard, Mass.

1. Hardware. Debugging was completed on the interface between the two electronic balances associated with the SUD and the PDP-11/23 computer. Thus, all sensors and controls for the FSS and the SUD have been interfaced to the computer except for those associated with the heaters. These will be interfaced after further testing of the heaters. The FSS sensors and controls have been temporarily disconnected from the computer to permit installation of the FSS in the hot cell.

2. Software. Software developments for the project computer system fall into three areas -- testing of programs already written, programming of new components of the project system, and preparation of programs specifically for the SUD. Satisfactory testing of the program MONITR has continued for two months. MONITR reads each active project sensor once per second, records the data, and compares the result to limiting values in the file Sensor Table (SENTBL). The "Operator Prompt-and-Response" feature has now been tested, using the SUD Operating Procedure, which is now stored in computer memory.

Three additional components of the system were completed during the quarter--SENTBL, SETCRI, and VS. SENTBL is the computer-readable file which contains the current limit values for each active sensor, and also the computer instruction on actions to be taken in the event of an out-of-spec condition. SETCRI (Set Sensor Criteria) is a small program which enters new criteria into SENTBL for each active sensor each time a new step in the operation procedure is initiated. VS (Variable Send-Data) is a program which provides the means for communication between all other programs. For example, when a new step in an operating procedure is initiated by the operator, VS retrieves the text of the new operator instruction from the appropriate file and transfers it to the CRT display program (CONDSP), which displays it. Then, VS retrieves the appropriate sensor criteria from the same file and transfers that data to SETCRI, which enters it into SENTBL. Finally, VS retrieves the control information (open valve No. XXX, etc.) from the same file and transfers it to the control and display program (presently being written) for execution. The program VS has been found to be of general use to many other users of PDP-11 computers and has been widely distributed, both at ANL and nationwide.

Programming related to the SUD is essentially part of the control and display program, CONDSP, noted above. Several additional programs were written, each one executing an additional "control state" for the SUD controls. In addition, software was written to implement several of the color graphic displays of the piping and instrumentation (P&I) diagrams. This color graphics software is approximately 50% complete.

F. Error Analysis
(D. G. Graczyk)

A comprehensive error analysis of all project measurement operations is in preparation. A major portion of this analysis, dealing with the determination of uranium content and isotopic abundances, forms a portion of a report of previous work [LEVITZ]. This report was completed in revised form and submitted to BAPL for review. The approved report has been submitted for publication.

Another portion of the error analysis completed during the report period deals with the effects of air buoyancy on all project weighing determinations. This analysis shows that buoyancy effects are of the same magnitude as the error limits for the weighing of fuel rods and segments and may be ignored in all other cases. Calculational procedures for the affected weight determinations are being developed.

G. Analytical
(R. J. Meyer and R. R. Heinrich)

The dedicated mass spectrometer arrived at ANL in mid-July. Assembly began in late August and on-site testing began in September. A minor problem with voltage "spikes" prevented completion of the acceptance tests. The vendor's engineer will return to complete the testing after installation of an "isolation" transformer. The engineer is currently scheduled to return in mid-November.

Procurement of the gamma/alpha spectrometer system has also been started this quarter. The main features of this unit are an automatic sample changer with a capacity for 26 samples, a high-purity germanium detector with state-of-the-art resolution for 10% relative efficiency, and a hybrid multichannel analyzer/computer system involving a PDP-11/23 and the divisional user-shared VAX-11/780 system.

H. Miscellaneous

Cleanout of Cell A-5 was started, with completion scheduled for the first quarter of FY 1982. The cell had housed the pilot-scale shear and dissolver, which had been used successfully in the demonstration of the process scheme [LEVITZ] with irradiated test fuel sections. The cleanout efforts to date have involved the removal of out-of-cell piping, controls, and cables, and the remote disassembly of the shear system. In time, the cell will be converted to an analytical cell for the workup of samples generated in the EOL campaign.

As requested by DOE, an updated schedule and cost summary, based on the present 3-y stretchout of the program (EOL campaign in CY 1986, cell cleanout by end CY 1988) was provided for review.

A paper entitled "Chemical and Radiometric Analysis of Segments Sheared from an Irradiated LWBR Fuel Rod Section" [GRACZYK] was presented at the 25th Conference on Analytical Chemistry in Energy Technology, Gatlinburg, Tenn., October 6-8, 1981.

The summary paper, "Precision Measurement and Shearing of Fuel Rods for Destructive Analysis" [FAGAN], submitted to the American Nuclear Society for presentation at its winter meeting, was accepted.

REFERENCES

Ames

L. L. Ames, Hanford Basalt Flow Mineralogy, PNL-2847 (1980).

Barkatt

A. Barkatt, Review of Chemical Stability of Glasses: Dissolution Mechanisms, Test Evaluations, and Applications to Radioactive Waste Fixation, Final Report, NRC Contract No. 04-78-25 (1980).

Bates-1982A

J. K. Bates, L. J. Jardine, K. F. Flynn, and M. J. Steindler, The Application of Neutron Activation Analysis to Leach Rate Determinations, Argonne National Laboratory Report 81-34 (February 1982).

Bates-1982B

J. K. Bates, L. J. Jardine, and M. J. Steindler, The Use of Radioactive Tracers in Measuring Leach Rates from Simulated Nuclear Waste Glasses, Argonne National Laboratory Report ANL-82-10 (in preparation).

Benson-1978

L. V. Benson et al., Basalt Alteration and Basalt-Waste Interaction in the Pasco Basin of Washington State, LBL-8532 (1978).

Benson-1979/1980

L. V. Benson and L. S. Teague, A Study of Rock-Water-Nuclear Waste Interactions in the Pasco Basin, Washington, LBL-9677 (1979);
L. V. Benson, C. L. Carnahan, and M. Che, A Study of Rock-Water-Nuclear Waste Interactions in the Pasco Basin, Washington, Part II. Preliminary Equilibrium-Step Simulations of Basalt Diagenesis, LBL-9677 (1980).

Brace

W. F. Brace, A. S. Orange, and T. R. Madden, The Effect of Pressure on the Electrical Resistivity of Water-Saturated Crystalline Rocks, J. Geophys. Res. 70, 5669-5678 (1965).

Couture

R. A. Couture, R. S. Miller, and J. M. Gieskes, Interstitial Water and Mineralogical Studies, Leg 41, Initial Reports of the Deep Sea Drilling Project, Vol. 41, Y. Lancelot and E. Seibold, Eds., Washington, U.S. Government Printing Office (1977).

Cunningham

J. Cunningham, J. Phys. Chem. 65, 628 (1961).

Dran

J. C. Dran, M. Maurette, and J. C. Petit, Radioactive Waste Storage Materials: Their α-Recoil Aging, Science, 1518-1519 (1980).

Ericson

J. E. Ericson, Prehistoric Exchange Systems in California: The Results of Obsidian Dating and Tracing, Thesis, UCLA (1977).

Ewing
R. C. Ewing and R. F. Haakes, Naturally Occurring Glasses: Analyses for Radioactive Waste Forms, PNL-2776 (1979).

Fagan
J. Fagan et al., Precision Measurement and Shearing of Fuel Rods for Destructive Analyses, accepted for presentation at the winter 1981 meeting, American Nuclear Society.

Friedman
I. Friedman and W. Long, Hydration Rate of Obsidian, Science 191, 347 (1976).

Gieskes
J. Gieskes, Chemistry of Interstitial Waters of Marine Sediments, Annu. Rev. Earth Planet. Sci. 3, 433-453 (1975).

Graczyk
D. G. Graczyk et al., Chemical and Radiometric Analysis of Segments Sheared from an Irradiated LWBR Fuel Rod Section, presented at 25th Conference on Analytical Chemistry in Energy Technology, Gatlinburg, Tenn., October 6-8, 1981.

Haimson
Bezalel Haimson, University of Wisconsin, Fracture log of UPH-3, personal communication (1981).

Hall
A. R. Hall, J. T. Dalton, B. Hudson, and J. A. C. Marples, Development and Radiation Stability of Glasses for Highly Radioactive Wastes, in Management of Radioactive Wastes from the Nuclear Fuel Cycle (International Atomic Energy Agency, Vienna), Vol. 2, pp. 3-14 (1976).

Hochanadel
C. J. Hochanadel, Rad. Res. 16(3), 286 (1962).

Jacobsson
A. Jacobsson et al., Egenskaper hos Bentonitbaserate Buffertmaterial (Properties of Bentonite-Based Buffer Material), KBS-TR-32 (1978).

Johnson
E. R. Johnson, The Radiation Induced Decomposition of Inorganic Molecular Ions, Gordon and Breach, Science Publishers, Inc., New York (1970).

Jones
A. R. Jones and R. L. Durfee, Radiat. Res. 15, 546 (1961).

LENA
Unpublished analysis, for well owned by Lena, Illinois.

Kaucic
S. Kaucic and A. G. Maddock, Trans. Faraday Soc. 65, 1083 (1969).

Levitz

N. M. Levitz, J. E. Parks, I. O. Winsch, R. J. Meyer, D. G. Graczyk, G. Tomlinson and P. G. Deeken, Report of the Shearing, Dissolution, and Analysis of GRIP-II Rod 79-453, Argonne National Laboratory Report ANL-80-88 (October 1981).

Long

P. Long, Rockwell Hanford, Telephone conversation with R. Couture (August 21, 1981).

MCC

Material Characterization Center, MCC-1 Static Leach Test, draft (August 1980).

Mecham

W. J. Mecham, et al., in Scientific Basis for Nuclear Waste Management, Clyde J. M. Northrup, Jr., Ed., pp. 307-314, Plenum Press, New York (1980).

Meents

W. F. Meents, A. H. Bell, O. W. Rees, and W. G. Tilbury, Illinois Oil-Field Brines: Their Geologic Occurrence and Chemical Composition, Ill. Petroleum, No. 66, Illinois State Geological Survey, Urbana, IL (1952).

Mendel

J. E. Mendel, W. A. Ross, F. P. Roberts, R. P. Turcotte, Y. B. Katayama, and J. H. Westsik, Jr., Thermal and Radiation Effects on Borosilicate Waste Glasses, Management of Radioactive Wastes from the Nuclear Fuel Cycle (International Atomic Energy Agency, Vienna), Vol. 2, pp. 49-61 (1966).

PNL

J. E. Mendel et al., A State-of-the-Art Review of Materials Properties of Nuclear Waste Forms, Pacific Northwest Laboratory Report PNL-3802 (1981).

Pusch

R. Pusch, Highly Compacted Na Bentonite as Buffer Substance, KBS-TR-74 (1978).

Ramm

E. J. Ramm and J. J. Ferenczy, Impact Behavior of SYNROC, J. Aus. Ceram. Soc. 16(2) (1980).

Roedder

Edwin Roedder, Composition of Fluid Inclusions, U.S. Geological Survey Prof. Paper 440-JJ (1972).

Sayles

F. L. Sayles and P. C. Mangelsdorf, Jr., The Equilibration of Clay Minerals with Seawater: Exchange Reactions, Geochim. Cosmochim. Acta 41, 951-960 (1977).

Shinn
M. B. Shinn, Ind. Eng. Chem. (Anal. Ed.) 13, 33 (1941).

Smith
M. J. Smith et al., Engineered Barrier Development for a Nuclear Waste Repository Located in Basalt: An Integration of Current Knowledge, RHO-BWI-ST-7 (1980).

SRL
Savannah River Laboratory, Waste Management Technical Progress Report, January-March, 1980, DP-80-125-1, p. 39 (September 1980); Waste Management Program Technical Progress Report, April-June 1980, DP-80-125-2 (December 1980).

Steindler-1980
M. J. Steindler et al., Chemical Engineering Division Fuel Cycle Programs Quarterly Progress Report, Oct-Dec 1980, Argonne National Laboratory Report ANL 81-13 (July 1981).

Steindler-1981A
M. J. Steindler et al., Chemical Engineering Division Fuel Cycle Programs Quarterly Progress Report, Jan-Mar 1981, Argonne National Laboratory Report ANL 81-35 (October 1981).

Steindler-1981B
M. J. Steindler et al., Chemical Engineering Division Fuel Cycle Programs Quarterly Progress Report, Apr-Jun 1981, Argonne National Laboratory Report ANL 81-53 (January 1982).

Taylor
C. L. Taylor, G. J. Anttonen, et al., Borehold Plugging of Man-Made Accesses to a Basalt Repository, RHO-BWI-C-49 (1979).

Teague
L. S. Teague, Secondary Minerals Found in Cores DS2 A1 and DS2 A2 Taken from the Grande Ronde Basalt Formation, Pasco Basin, Washington, LBL-10387 (1980).

Tingey
G. L. Tingey and W. D. Felix, Radiolytic Gas Generation from Calcined Nuclear Waste, BNWL-2381 (August 1977).

Tombrello
T. A. Tombrello, Weathering of Natural Glasses, in High-Level Radioactive Solid Waste Forms, Proc. Conf. Denver, Colorado, 1978, NUREG-CP-0005.

Turcotte
R. P. Turcotte, J. W. Wald, and R. P. May, Devitrification of Nuclear Waste Glasses, Scientific Basis for Nuclear Waste Management, Vol 2, C. J. Northrup, Jr., Ed., Plenum Press (1980).

Wald

J. W. Wald and J. H. Westsik, Jr., Devitrification and Leaching Effects in HLW Glass - Comparison of Simulated and Fully Radioactive Waste Glass, Proceedings of the International Symposium on Ceramics in Nuclear Waste Management, CONF-790420, Technical Information Center, Oak Ridge, TN (1979).

Weber

W. J. Weber, R. P. Turcotte, L. R. Bunnell, F. P. Roberts, and J. H. Westsik, Jr., Radiation Effects in Vitreous and Devitrified Simulated Waste Glass, Proceedings of the International Symposium on Ceramics in Nuclear Waste Management, CONF-790420, Technical Information Center, Oak Ridge, TN (1979).

Winograd

I. J. Winograd, Radioactive Waste Disposal in Thick Unsaturated Zones, Science 212, 1457-1564 (1981).

WNYNSCS

Western New York Nuclear Services Center Study, Vol. 2, Companion Report TDI-28905-3.